

Experimental investigation into the effect of stress
on dissolution and growth of very soluble
brittle salts in aqueous solution

Dissertation zur Erlangung des Grades
"Doktor der Naturwissenschaften"

am Fachbereich Geowissenschaften
der Johannes Gutenberg-Universität in Mainz

Jacques Morel, geboren am 21.09.1974 in Quimper

Mainz, September 2000

Erklärung

Ich versichere hiermit, die vorliegende Arbeit selbständig und nur unter Verwendung der angegebenen Quellen und Hilfsmittel verfaßt zu haben.

Mainz, September 2000

Jacques Morel

Datum der Prüfung: 8 novembre 2000

Abstract

The study of dissolution and growth processes at a solid-fluid interface under non-hydrostatic stresses is essential for the understanding of the deformation mechanisms that are active in the Earth's crust. Among these, pressure solution is the most important ductile deformation mechanism at diagenetic to low to medium-grade metamorphic conditions. However, it is still poorly understood which mechanical, physical or chemical potential energy gradients drive pressure solution. Commonly, pressure solution is assumed to be driven either by differences in crystal plastic strain energy, or by differences in grain boundary surface normal stress. Differences in elastic strain energy are thought to be much too small to play any significant role and are for this reason commonly neglected as a possible driving force for pressure solution. However, recent experimental as well as theoretical investigations have shown that elastic strain may in fact strongly influence the dissolution and growth mechanisms of crystals in solution. As deformation mechanisms occurring in the Earth's crust mostly take place while the rocks are elastically strained, it is very important to improve our understanding of the effect of the elastic strain and define the role it may have during deformation by pressure solution in rocks. This thesis reports on an experimental investigation into the effect of mechanical compressive stress on the dissolution and growth of single crystals of different very soluble elastic/brittle salts in aqueous solution. These salts were chosen as analogues for rock-forming minerals such as quartz or calcite. The effect of stress on the surface dissolution microstructures was studied on potassium alum single crystals. Dissolution grooves, 20-40 μm wide, 10-40 μm deep and about 20-80 μm apart from each other, developed in the highest stressed regions of the crystals, and disappeared as soon as the stress was taken off. The grooves were oriented parallel to low index crystallographic directions, and sub-perpendicular to the local maximum compressive stress trajectories. The size of the dissolution grooves depended on the local surface stress, the surface energy and the degree of undersaturation of the aqueous solution. The microstructural evolution of the crystal surface was found to be in good agreement with theoretical predictions based on the model of Heidug & Leroy (1994) and Leroy & Heidug (1994). The effect of stress on the dissolution rate was investigated on sodium chlorate single crystals. The stressed crystals dissolved faster than the crystals left stress-free. The experimentally observed increase in the dissolution rate of the stressed crystals was one to two orders of magnitude stronger than theoretically predicted on the basis of the increased dissolution driving force due to the increase in the bulk stored elastic energy. The dissolution rate increased linearly with the stress and the increase was larger with increasing degree of undersaturation. Finally, the effect of the stress on crystal growth was studied using potassium alum and potassium dihydrogen phosphate single crystals. The growth rate of $\{100\}$ and $\{110\}$ faces of potassium alum was strongly decreased on the application of stress, by an amount much larger than theoretically predicted on the basis of the decreased crystal growth driving force due to the increase in the bulk stored elastic energy. For all these results, the roughness of the crystal surface played a key role, by inducing a non-homogeneous stress distribution on the crystal surface. The results show that elastic strain may play a significant role during pressure solution, and

that elastic strain gradients may eventually cause significant deformation in the upper crust. Hence, elastic strain should be taken into account while defining microphysical deformation models.

Kurzfassung

Das Studium der Auflösungs- und Wachstumsprozesse an Feststoff-Flüssigkeits-Grenzflächen unter nicht-hydrostatischen Beanspruchungen ist wesentlich für das Verständnis von Deformationsprozessen, die in der Erde ablaufen. Unter diesen genannten Prozessen gehört die Drucklösung zu den wichtigsten duktilen Deformationsprozessen, von der Diagenese bishin zur niedrig- bis mittelgradigen metamorphen Bedingungen. Bisher ist allerdings wenig darüber bekannt, welche mechanischen, physikalischen oder chemischen Potentialenergie-Gradienten die Drucklösung steuern. I.a. wird angenommen, daß die Drucklösung durch Unterschiede kristallplastischer Verformungsenergien oder aber durch Unterschiede der Normalbeanspruchung an Korngrenzen gesteuert wird. Unterschiede der elastischen Verformungsenergien werden dabei allerdings als zu gering erachtet, um einen signifikanten Beitrag zu leisten. Aus diesem Grund werden sie als mögliche treibende Kräfte für die Drucklösung vernachlässigt. Andererseits haben neue experimentelle und theoretische Untersuchungen gezeigt, daß die elastische Verformung in der Tat einen starken Einfluß auf Lösungs- und Wachstumsmechanismen von Kristallen in einer Lösung haben kann. Da die in der Erdkruste vorherrschenden Deformationsmechanismen überwiegend im elastischen Verformungsbereich der Gesteine ablaufen, ist es sehr wichtig, das Verständnis für die Effekte, die die elastische Verformung verursacht, zu erweitern, und ihre Rolle während der Deformation durch Drucklösung zu definieren. Die vorliegende Arbeit beschäftigt sich mit Experimenten, bei denen der Effekt der mechanisch kompressiven Beanspruchung auf Lösungs- und Wachstumsprozesse von Einzelkristallen unterschiedlicher, sehr gut löslicher, elastisch/spröder Salze untersucht wurde. Diese Salze wurden als Analoga gesteinsbildender Minerale wie Quarz und Calcit ausgewählt. Der Einfluß von Stress auf die Ausbildung der Oberflächenmikrostrukturen in einer untersättigten Lösung wurde an Kaliumalaun untersucht.

Lösungsrillen (20 – 40 µm breit, 10 – 40 µm tief und 20 – 80 µm Abstand) entwickelten sich in den Bereichen, in denen die Beanspruchung im Kristall am größten war. Sie verschwanden wieder, sobald der Kristall entlastet wurde. Diese Rillen entwickelten sich parallel zu niedrig indizierten kristallographischen Richtungen und subperpendikular zu den Trajektorien, die der maximalen, lokalen kompressiven Beanspruchung entsprachen. Die Größe der Lösungsrillen hing von der lokalen Oberflächenbeanspruchung, der Oberflächenenergie und dem Untersättigungsgrad der wässrigen Lösung ab. Die mikrostrukturelle Entwicklung der Kristalloberflächen stimmte gut mit den theoretischen Vorhersagen überein, die auf den Modellen von Heidug & Leroy (1994) und Leroy & Heidug (1994) basieren. Der Einfluß der Beanspruchung auf die Auflösungsrate wurde an Natriumchlorat-Einzelkristallen untersucht. Dabei wurde herausgefunden, daß sich gestresste Kristalle schneller lösen als Kristalle, auf die keine Beanspruchung einwirkt. Der experimentell beobachtete Anstieg der Auflösungsrate der gestressten Kristalle war ein bis zwei Größenordnungen höher als theoretisch erwartet. Die Auflösungsrate stieg linear mit dem Stress an, und der Anstieg war um so größer, je stärker die Lösung untersättigt

war. Außerdem wurde der Effekt der Beanspruchung auf das Kristallwachstum an Kaliumalaun- und Kaliumdihydrogenphosphat-Einkristallen untersucht. Die Wachstumsrate der Flächen $\{100\}$ und $\{110\}$ von Kaliumalaun war bei Beanspruchung stark reduziert. Für all diese Ergebnisse spielte die Oberflächenrauigkeit der Kristalle eine Schlüsselrolle, indem sie eine nicht-homogene Stressverteilung auf der Kristalloberfläche verursachte. Die Resultate zeigen, daß die elastische Verformung eine signifikante Rolle während der Drucklösung spielen kann, und eine signifikante Deformation in der oberen Kruste verursachen kann, bei Beanspruchungen, die geringer sind, als gemeinhin angenommen wird. Somit folgt, daß die elastische Beanspruchung berücksichtigt werden muß, wenn mikrophysikalische Deformationsmodelle entwickelt werden sollen.

Table of contents.

Chapter 1. The concept of pressure solution.

1.1) Introduction	12
1.2) History of research into pressure solution	14
1.3) Investigation of the driving force for pressure solution	15
1.3.1) The film diffusion model	15
1.3.2) The undercutting model	15
1.4) Experiments on pressure solution	16
1.4.1) Experiments on NaCl	16
1.4.2) Experiments on elastic/brittle salts	17
1.5) Investigation of the effect of elastic strain on growth and dissolution	18
1.5.1) Experimental approach	18
1.5.2) Theoretical approach	19
1.5.2.1) Starting conditions	19
1.5.2.2) Application of stress	20
1.5.2.3) Effect of small disturbances on the surface	21
1.5.2.4) Alternative models	22

Chapter 1. Figures	24
Chapter 2. Experimental procedures.	
2.1) Materials used	26
2.1.1) Potassium alum	26
2.1.2) Sodium chlorate	27
2.2) Samples preparation	27
2.2.1) Potassium alum	27
2.2.2) Sodium chlorate	28
2.2.3) Aqueous solution	28
2.3) Experimental set-up and procedures	29
2.3.1) Description of the apparatus	29
2.3.2) Experimental procedure	29
2.4) Estimation of the stress around the hole	30
2.5) In-situ experiments	31
Chapter 2. Figures	32
Chapter 3. Effect of stress on surface microstructures.	
3.1) Description of the dissolution features	39
3.1.1) Stress-free crystals	39
3.1.2) Stressed crystals	39

3.1.2.1) Localisation and orientation of the grooves	40
3.1.2.2) Structure and shape of the grooves	41
3.2) Mechanism of formation of the grooves	41
3.2.1) Stability of stress-free crystal surfaces	41
3.2.1.1) Influence of the surface energy	41
3.2.1.2) Periodic bond chains	42
3.2.2) Stability of stressed crystal surfaces	43
3.2.2.1) Influence of the stress distribution on the surface	43
3.2.2.2) Relation between A-type grooves and PBC-directions	44
3.2.2.3) Formation of a dissolution groove network	44
3.2.2.4) Role of stress trajectories	45
3.2.3) Could crystal plastic strain play a role?	45
3.2.4) Influence of stirring	46
3.3) In-situ experiments	46
3.3.1) Experimental procedures	47
3.3.2) Experimental observations	47
3.3.3) Discussion of in-situ results	48
3.4) Theoretical approach	49
3.4.1) Estimation of the equilibrium configuration	50
3.4.2) Influence of small variations in the parameters	51
3.4.3) Relation between stress and A-type groove size	51
3.5) Conclusion	52

Chapter 3. Tables and figures	54
Chapter 4. Dissolution rate of sodium chlorate.	
4.1) Experimental procedures	77
4.2) Results	77
4.3) Discussion	78
4.4) Conclusion	81
Chapter 4. Tables and figures	82
Chapter 5. Effect of stress on growth processes.	
5.1) Starting materials sample preparation	88
5.1.1) Potassium dihydrogen phosphate	88
5.1.2) Potassium alum	89
5.1.3) Preparation of the aqueous solutions	89
5.2) Experimental procedures	90
5.3) Results	90
5.4) Discussion	91
5.5) Conclusion	92

Chapter 5. Tables and figures	94
Chapter 6. Summary and conclusions.	101
References	105
Appendix 1	114
Lebenslauf	

Chapter 1 The concept of pressure solution.

1.1) Introduction.

The study of the evolution of a solid-fluid interface under non-hydrostatic stresses is essential for the comprehension of the deformation mechanisms that occur in the Earth's crust. Among these, pressure solution is the most important ductile deformation mechanism in the crust at diagenetic to low to medium-grade metamorphic conditions (Tada & Siever, 1989; Passchier & Trouw, 1996; Den Brok, 1998). It involves the dissolution of material at places of high stress in rocks, its diffusion through an adjacent fluid phase at grain boundaries or in the pores, and its precipitation at places of lower stress. Pressure solution is important as a deformation and as a compaction mechanism, and may lead to a continuous modification in rock porosity, especially during diagenesis (Sprunt & Nur, 1977a; Tada & Siever, 1989). Unfortunately, the mechanism of pressure solution is still poorly understood and its influence on the strength of the upper crust difficult to quantify (Passchier & Trouw, 1996). This is a problem since pressure solution could cause significant ductile deformation in the upper crust at much lower stresses than commonly thought (Gratier & Guiguet, 1986), and the commonly accepted idea that the upper 10-15 km of the crust behave brittly (Mohr-Coulomb behaviour) could be wrong. Pressure solution could strongly affect crustal strength by allowing fault slip at shear stresses well below the dry fault strength. The healing process of faults could also be affected by pressure solution since the presence of clay minerals or micas in natural rocks has been shown to enhance pressure solution (Schwarz & Stöckhert, 1996; Rutter & Wanten, 2000). Many examples of pressure solution phenomena such as distorted fossils, indented pebbles, or stylolites (e.g. Guzzetta, 1984) can be found in natural rocks. Pressure solution finds implications not only in structural geology and other geosciences such as seismology, but is also of great interest for applied research for the oil and gas industry, and its importance in the stability of porous media involves applications to hydrology and for example to nuclear waste storage. It is thus of prime importance to know which thermodynamic forces can drive pressure solution.

Pressure solution is commonly assumed to be driven either by differences in grain boundary surface normal stress (Paterson, 1973; Lehner, 1995), or by differences in crystal plastic strain energy (Bosworth, 1981; Tada and Siever, 1989; Spiers & Brzesowsky, 1993). Two main models have been proposed to describe the dissolution precipitation processes occurring at grain boundaries. The first model considers the existence at grain boundaries of a thin fluid film, either continuous or with a "island-channel"-like structure, through which the dissolved material diffuses towards less stressed regions of the grains (e.g. Weyl, 1959; Rutter, 1976; Spiers & Schutjens, 1990; Gratz, 1991). This process is assumed to be driven by differences in grain boundary surface normal stress. The second model considers free-face dissolution around the grain contact driven by crystal plastic deformation (Tada & Siever, 1986) or brittle

deformation at the grain contact (Ostapenko, 1968, 1975). In none of the models, however, differences in elastic strain energy have been considered as a potential driving force for pressure solution. Theoretically, the potential energy drop associated with differences in elastic strain energy is two to three orders of magnitude smaller than the one due to differences in crystal plastic strain energy, or the one due to differences in grain boundary surface normal stress (Paterson, 1973; Shimizu, 1995). Recent experimental (e.g. Ristic et al. 1997a & b) as well as theoretical work (e.g. Heidug & Leroy, 1994; Leroy & Heidug, 1994) shows, however, that elastic strain energy may have a much larger influence than commonly thought. The geometry of the solid-fluid interface and the crystallographic orientation of the solid also appear to be essential parameters.

This thesis presents experimental evidence that mechanically induced compressive elastic strain may strongly affect the dissolution process of elastic/brittle salts, when no grain boundary surface normal stress and no crystal plastic strain are present. The experimental results are compared with theoretical predictions. In this first chapter, a brief historical and theoretical overview of the concept of pressure solution is given. The two main models describing pressure solution are presented, and the use of elastic/brittle salts as rock analogue materials is justified. Finally, the model of Heidug & Leroy (1994) and Leroy & Heidug (1994), that will be used as a theoretical support for our experimental observations, is described.

The second chapter describes the experimental set-up and the two materials mostly used in this work, i.e. potassium alum (K-alum) and sodium chlorate. The preparation of the crystal samples and the experimental procedures are explained in detail.

The third and fourth chapters present the results obtained on the influence of mechanically applied compressive stress on the behaviour of the single crystals in undersaturated solution. The effect of stress on the microstructures of the crystal surface of K-alum is presented in the third chapter. The stress-induced dissolution features observed are described in detail and their origin related to the crystallography of K-alum and to the stress distribution in the samples. The development of these structures is studied experimentally and compared with theoretical models and mechanical considerations. The effect of stress on the kinetics of dissolution of sodium chlorate is studied in the fourth chapter. The observed increase in dissolution rate due to the stress is compared with theoretical calculations on the bulk stored elastic strain energy. The cause of this increased dissolution rate is discussed and related to the results obtained in the third chapter.

Some results obtained on the effect of stress on the growth of K-alum and potassium dihydrogen phosphate (KDP) single crystals in solution are presented in a fifth chapter. Finally, the results are summarised and conclusions are drawn in the sixth and last chapter of this work.

1.2) History of research into pressure solution.

Pressure solution is a process during which stressed parts of a solid in contact with a saturated solution dissolve, the dissolved material diffuses along the solid-fluid interface and precipitates at other parts of the solid that are not or less stressed. Considering this definition, we can probably attribute the first formulation of pressure solution to Thompson (1862), who noted that applying stress to both a solid and a fluid phase in contact with each other had not the same effect that applying stress only on the solid phase. Sorby (1863) was the first to apply Thompson's observation to geological problems, attributing indentation pits seen at contacts between pebbles to pressure solution. The non-hydrostatic thermodynamic theory developed by Gibbs (1878) gave the mathematical tools necessary for a first quantitative approach in the interpretation of experimental and field observations. Following these steps, Riecke (1912) explained that if in a closed system two crystals were placed in contact with a saturated solution and one of them was stressed, this system would not be in equilibrium any more and the stressed crystal would start to dissolve, while the stress-free crystal would start to grow. From this idea he concluded that if a crystal was stressed only locally, the material dissolving there could precipitate again at other, stress-free places, of the same crystal.

Russel (1935) showed for the first time with experiments carried out on ammonium-alum, that a single crystal locally stressed with an indenter and in contact with a saturated alum solution, dissolved in the immediate vicinity of the indenter, while it grew at other places. Unfortunately, he did not specify the material used for the indenter and his results used as a proof of a pressure solution mechanism may in reality be due to a chemical reaction between the crystal and the indenter. Den Brok & Melisa (1999, 2000) have shown, with the same kind of experiments also carried out on alum (potassium alum), that the indentation is driven by an oxidation reaction between the metal indenter and the weakly acid alum solution. The first observation of true, i.e. stress-driven pressure solution may probably be attributed to Correns (1949). This author showed, also using alum, that single crystals placed under differential stress in a slightly oversaturated solution dissolved in the direction of maximum stress and grew perpendicular to it, thus developing a crystal growth preferred orientation. This observation was taken as a possible proof for the development of schistosity observed in nature. The mechanism of crystallographic preferred orientation development was studied by Kamb (1959), who pointed out the importance of crystal mechanical anisotropy. All crystallographic directions do not behave similarly when stressed. Applying the thermodynamics of non-hydrostatically stressed solids to pressure solution, Kamb (1959) also explained that a solid aggregate under differential stress could never satisfy equilibrium with an interstitial pore fluid. According to him, solution mass transfer from highly stressed regions of the solid to less stressed regions would lead to a permanent modification of the geometry of the system and hence to a permanent redistribution of the stress. It appeared then that the use of non-equilibrium thermodynamics was necessary for the description of pressure solution phenomena. This was first done by Lehner & Bataille (1984/1985).

1.3) Investigation of the driving force for pressure solution.

Despite an increasing interest of researchers, the mechanism of pressure solution is still poorly understood, and the driving forces controlling it are not well identified. Two different models have been proposed to describe the mechanisms driving pressure solution in a wet solid polycrystalline aggregate (Weyl, 1959).

1.3.1) The film diffusion model.

In this model, an interfacial fluid film is assumed to be present at each grain boundary of the aggregate. These films are interconnected. Pressure solution is assumed to be driven by differences in surface normal stress through the grain boundaries. The material that dissolves at places of high normal stress migrates through the fluid film towards places of lower normal stress. The fluid film is considered either as continuous (Weyl, 1959; Rutter, 1976; Robin, 1978; Rutter, 1983; Fig. 1.1), or as an "island-channel" structure (Raj & Chyung, 1981; Raj, 1982; Spiers & Schutjens, 1990). This structure is formed by "islands" of grain to grain contacts (dry or with a very thin fluid layer) separated by "channels" containing free fluid under hydrostatic pressure (Fig. 1.1). The structure is described as dynamically stable, i.e. the islands and the channels change continuously their position but their number and size stays on average the same. Gratz (1991) developed a pressure solution model assuming a static island-channel boundary structure, the channels being localised at microcracks that develop perpendicular to the grain boundary (see also Den Brok, 1998).

Several mathematical equations have been proposed to calculate the rate of deformation of such a solid matrix by pressure solution, depending on the model used to describe the grain boundary (see for example Den Brok, 1992 for a review). However, the deformation rates predicted by these different theories stays much lower than typical deformation rates measured for natural rocks (Den Brok, 1998).

1.3.2) The undercutting model.

The second model assumes that free-face dissolution around a grain to grain contact, driven by differences in crystal plastic strain energy (Tada & Siever, 1986) or by chemical reactions between grains of different composition and the fluid with which they are in contact (Den Brok & Melisa, 2000) leads to a time-dependent decrease in the contact area, what causes an increase of the stress at the grain to grain contact. This increased stress causes crystal plastic deformation to occur at the contact region (Tada & Siever, 1986, Fig. 1.2), or brittle cataclastic deformation of the contact region (Ostapenko, 1968, 1975). Pressure solution rate at the grain to grain contact is increased until the contact region finally collapses.

1.4) Experiments on pressure solution.

The goal of experimental work on pressure solution is to get results that will be able to help in the understanding of pressure solution in nature. The conditions of pressure, temperature and over all the timescale with which pressure solution takes place in the Earth's crust makes that laboratory experiments on geological material are difficult to carry out. Reports on such experiments on rock forming minerals include e.g. Schutjens (1991), Elias & Hajash (1992), Rutter & Wanten (2000) for pressure solution experiments on quartz sand, Engelder (1982) on calcite, and De Meer & Spiers (1995, 1999) on gypsum. Experiments are for this reason mostly performed on rock analogue materials. These materials, which are characterised by a high solubility and fast kinetics of growth/dissolution at room temperature and atmospheric pressure, allow to get quantitative results in a quite short time.

1.4.1) Experiments on NaCl.

Among rock analogue materials, sodium chloride (halite, NaCl) was the most often used in pressure solution studies. NaCl is intensively studied to understand the behaviour of natural rocksalt, e.g. for the behaviour of salt domes and for the use of salt aggregates as back-fill in holes in salt domes for the storage of nuclear waste (Spiers et al., 1986). Its fast kinetics of growth and dissolution gives the opportunity with this material to get experimental results in a relatively short laboratory timescale. Results on NaCl are therefore used as analogue for the deformation of rock-forming minerals such as quartz or calcite. Hence, NaCl has become one of the most used material for the study of pressure solution phenomena. Different kind of experiments have been carried out on this material with this aim to find out which of the above models gives the best description of natural observations.

Indentation experiments have been carried out by Tada & Siever (1986), Hickman & Evans (1991), Gratier (1993) and Martin et al. (1999). In this kind of experiments, a single crystal of halite in aqueous solution is stressed locally with either an indenter of quartz (Tada & Siever, 1986; Hickman & Evans, 1991; Martin et al., 1999), of stainless steel (Gratier, 1993), or with another halite single crystal (Hickman & Evans, 1991; Martin et al., 1999) and the mechanisms of dissolution at the contact area and at its periphery are studied. Tada & Siever (1986) found in their experiments that pressure solution took place by free-face dissolution around the indenter, combined with plastic deformation under the indenter (see above). Gratier (1993) showed that the mechanisms driving pressure solution could depend on the experimental conditions. When the solution was saturated, he found that pressure solution was controlled by differences in surface normal stress at the contact between the crystal and the indenter. Pressure solution took in that case place by fluid-film diffusion and its rate depended on the indenter diameter. When the solution was slightly undersaturated, however, pressure solution took place by free-face dissolution around the indenter together with crystal plastic deformation under the indenter, as found by Tada & Siever (1986), and the indentation rate was independent of the indenter diameter. Hickman & Evans (1991)

showed that pressure solution may depend also on the nature of the contact between the crystal and the indenter. When two halite lenses were pressed together in saturated solution, no pressure solution was observed (at least not at a measurably rate), while when a silica lens was pressed against a halite lens, pressure solution was observed. According to Hickman & Evans (1991), pressure solution took place by fluid-film diffusion. Such an influence of the nature of the grain to grain contact have been observed on natural rocks, and may particularly be due to the presence of phyllosilicates (Schwarz & Stöckhert, 1996; Rutter & Wanten 2000). This result shows the importance of the chemistry of the system on pressure solution rate, and may suggest an influence of mineral surface energy, on which depends the fluid wetting angle. The experiments from Tada & Siever (1986), Hickman & Evans (1991) and Gratier (1993) were carried out with high stress values, conditions under which crystal plastic mechanisms may strongly influence the pressure solution process. Martin et al. (1999), however, used much lower stress to avoid crystal plastic deformation. They found that the convergence rate between the halite crystal and the other crystal was not constant but showed some periods of acceleration. They suggested that these variations in rate could be caused by an episodic modification of the interface structure, like a dynamically stable "island-channel" structure.

Free-face dissolution induced by crystal plastic strain was also observed by Bosworth (1981) on single crystals of NaCl in undersaturated solution. In his case, rectangular crystal slabs with a cylindrical hole drilled in their middle were pre-stressed in air under uniaxial load perpendicular to the axis of the hole, and then placed in undersaturated solution, without load. As a result of the non-homogeneous plastic strain distribution around the hole, he observed that crystal regions that had undergone crystal plastic deformation dissolved faster. Dissolution enhanced by a non-homogeneous plastic strain distribution around a centrally drilled hole was also observed by Sprunt & Nur (1977b) on halite crystals and on samples of other materials (quartzite, granite, calcite and others) with the same geometry as used by Bosworth (1981) uniaxially loaded in solution, although for some of the other materials mechanisms different than plastic deformation may have occurred.

Many pressure solution experiments have also been carried out on NaCl aggregates (e.g. Urai et al., 1986; Spiers & Schutjens, 1990; Spiers & Brzesowsky, 1993). In that case, for bulk stresses low enough to avoid crystal plasticity, the deformation rate of a salt aggregate by pressure solution is found to be inversely proportional to the cube of the grain size. These experiments yielded observations of pressure solution features such as grain-to-grain indentation and contact truncation, and made the existence of "island-channel"-like grain boundaries during the pressure solution process very likely.

1.4.2) Experiments on elastic/brittle salts.

As rock deformation by pressure solution in the Earth's upper crust generally takes place under conditions where plastic deformation plays no role, it may be questioned whether NaCl, which can deform plastically very easily, is a good material to be used as analogue material for the study of pressure solution. Den Brok et al. (1999a) have demonstrated, using sodium chlorate, that plasticity does not seem to have a

determinant role in pressure solution. These authors showed that sodium chlorate cannot deform by crystal plastic mechanisms at room P-T conditions. However, they found that wet compacted sodium chlorate aggregates deform similarly to NaCl aggregates under the same conditions. According to them, the use of NaCl as analogue material for pressure solution experiments seems therefore justified, in spite of its crystal plastic behaviour. However, the same authors showed that microstructural effects such as grain boundary migration and rate dependent cataclastic behaviour, could occur in wet sodium chlorate as well (Den Brok et al., 1998; Den Brok et al., 1999b). As this material is extremely brittle, it seems likely that these processes were driven by gradients in elastic strain energy. The interpretation of deformation microstructures observed in crustal rocks should thus be made carefully.

1.5) Investigation of the effect of elastic strain on growth and dissolution.

1.5.1) Experimental approach.

The results obtained by Den Brok et al. (1998, 1999a & b) show that differences in elastic strain may play a key role in pressure solution phenomena. Yet these differences in elastic strain energy are commonly assumed not to play a significant role as a driving force for deformation by pressure solution (e.g., Paterson, 1973; Shimizu, 1995; Gal and Nur, 1998). It can easily be shown that, theoretically, the potential energy drop associated with differences in normal stress or differences in crystal plastic strain is two to three orders of magnitude larger than the potential energy drop associated with differences in elastic strain energy at otherwise identical stresses (Paterson, 1973; Shimizu, 1995). However, it has been recently demonstrated that elastic strain can affect the growth and dissolution rates of crystals in solution much stronger than theoretically predicted. Ristić et al. (1997a) have shown that elastic strain in sodium chlorate single crystals induced by synchrotron radiation affects the thermodynamic equilibrium between the crystals and the solution. They found that in a slightly oversaturated sodium chlorate solution, non-irradiated parts of the crystals were growing while simultaneously irradiated parts were dissolving. Furthermore, Ristić et al. (1997b) showed that mechanically induced tensile elastic strain during the growth of potassium alum crystals strongly affects their growth rate. The growth of some particular crystal faces could even be stopped. They found that the application of a tensile stress of 0.1 MPa, corresponding to an increase of $6.2 \times 10^{-5} \text{ J.mol}^{-1}$ in chemical potential, leads to a decrease in the growth rate from $2.2 \mu\text{m.min}^{-1}$ to $1.8 \mu\text{m.min}^{-1}$. The original growth rate could be recovered in two ways: 1) by removing the stress; 2) by increasing, while keeping the crystal under stress, the degree of undersaturation by an amount corresponding to an increase of 7.2 J.mol^{-1} in chemical potential. This means that two driving forces that theoretically differ by five orders of magnitude have the same effect on the growth rate. According to the authors, this would mean that the elastic strain would most probably affect the way in which growth centres develop and propagate.

The recent progress in the formulation of non-equilibrium thermodynamics has led to a different theoretical conception of the pressure solution phenomenon, and allows now a better definition of the role of elastic strain as a potential driving force for pressure solution. We will now describe the model of Heidug & Leroy (1994) and Leroy & Heidug (1994).

1.5.2) Theoretical approach: the "perturbation" theory.

This theory states that if, on an initially smooth interface between a saturated fluid and an elastically stressed solid, a sinusoidal perturbation appears, the chance for it to grow or decay depends on physical parameters such as elastic strain, surface energy and local curvature. We describe here the model of Heidug & Leroy (1994) and Leroy & Heidug (1994). All the equations used in this paragraph were taken from the above mentioned publications.

1.5.2.1) Starting conditions.

Let us consider a fluid-filled cylindrical pore of radius r embedded in an infinite elastic and isotropic matrix. The cavity is opened and connected to an ambient saturated fluid, so that under non-equilibrium conditions, mass transfer is allowed to take place between the pore and the bulk fluid. The thermodynamic driving force X for solid-fluid phase transformation is given by equation (1.1):

$$X = \Psi^s + \frac{p}{\rho^s} - \frac{\gamma}{R\rho^s} - \mu^f$$

where Ψ^s is the Helmholtz free energy of the solid at the interface, p is the fluid pressure, ρ^s is the solid mass density at the interface, γ is the surface tension and μ^f is the solute chemical potential in the fluid.

In this model, the kinetics of growth-dissolution of the solid-fluid interface are assumed to be controlled by surface reactions, i.e. that diffusion of material away from the interface is fast enough to avoid any accumulation of material and change in solute concentration. The chemical potential of the fluid is thus considered as constant in the cavity and equal to μ_0 . It is also assumed that there are no nucleation barriers for growth or dissolution at the interface.

The flux at which the solid-fluid interface may move is derived from the driving force as (equation 1.2):

$$J_n = LX$$

where $L \geq 0$ is a phenomenological proportionality coefficient.

1.5.2.2) Application of stress.

Consider now this matrix subjected to a hydrostatic stress σ_∞ at infinity that will in general be different from the pore fluid pressure p . The assumption is made that the matrix undergoes a plain strain mode of deformation. The application of this stress increases the Helmholtz free energy ψ^s of the matrix and modifies its mass density ρ^s . The cavity is no more in equilibrium and the solid-fluid interface moves. Let us suppose first that the evolution of the pore geometry is homothetic, i.e. the pore grows or shrinks but keeps the same cylindrical geometry. In that case, the rate at which the solid-fluid interface moves is given by equation (1.3):

$$\dot{R} = \frac{L}{\rho^2} \left\{ \left[p - \frac{\gamma}{R} - \mu_0 \rho + \frac{1+\nu}{E} \cdot \frac{\rho}{\rho_0} (\tilde{\sigma}^2 + (1-2\nu)\sigma_\infty^2) \right] \cdot \left[1 + \frac{1+\nu}{E} (\tilde{\sigma} + (2\nu-1)\sigma_\infty) \right] \right\}$$

where ρ_0 is the solid mass density in the stress-free state, ν is the Poisson ratio, E is the Young's modulus and

$$\tilde{\sigma} = \sigma_\infty + p - \frac{\gamma}{R}$$

is the effective stress.

The solid-fluid interface moves until an equilibrium radius is reached for

$$\dot{R} = 0$$

In real situations, however, this equilibrium will not be stable. Structural defects or impurities in the matrix at the solid-fluid interface will cause variations in the surface tension around the pore and the formation of small disturbances on the interface. These disturbances lead to a new stress distribution around the hole.

1.5.2.3) Effect of small disturbances on the surface.

Starting from the equilibrium configuration described above, we consider now that small circumferential perturbations, independent of the position along the axis of the cylindrical cavity, are present on the interface. This kind of perturbations dominates when the normal stress at the interface is close to the fluid pressure (longitudinal perturbations along the axis of the cylindrical cavity dominate when the hoop stress at the interface is close to the fluid pressure). These circumferential disturbances are characterised by a "wavenumber" ξ , and can be described for $\xi \geq 0$ as sinusoidal perturbations of wavelength $2\pi/\xi$ around the cylindrical cavity (Fig. 1.3). $\xi = 0$ is the homothetic mode of deformation, $\xi=1$ corresponds to a shape-preserving translation and is not considered in this model.

This perturbation in the geometry of the interface causes a new distribution of stress, strain and surface tension around the cavity. The pore is no more in equilibrium and, again, the interface moves. Depending on the stress, surface tension and curvature, the perturbation grows or shrinks, at a rate λ_ξ given, if $\xi = 0$, by equation (1.4a)

$$\lambda_\xi = \frac{L}{R\rho^2} \cdot \frac{\gamma}{R}$$

and if $\xi \geq 2$, by equation (1.4b)

$$\lambda_\xi = \frac{L}{R\rho^2} \left\{ -\frac{\gamma}{R}(\xi^2 - 1) + 4 \cdot \frac{\tilde{\sigma}^2}{G}(1 - \nu)(\xi - 1) \right\}$$

where $G=E/2(1+\nu)$ is the elastic shear modulus of the matrix.

The opposite effect of stress, that tends to increase the growth rate of the perturbation, and of the surface tension, that tends to decrease it and thus stabilise the surface roughness, is clear to see in equation (1.4b).

For a given loading situation, a wavenumber ξ corresponding to the fastest growth rate λ_ξ will be dominant and will determine the geometrical evolution of the interface, and thus of the thermodynamic equilibrium configuration. This dominant growth mode is

found by differentiating the equation (1.4b) with respect to ξ , and is obtained for (equation 1.5):

$$\xi = 2 \left((1 - \nu) \cdot \frac{\tilde{\sigma}^2 R}{G\gamma} \right)$$

This wavenumber defines the equilibrium wavelength of the sinusoidal perturbation of the surface. The equilibrium will be stable over a range of stresses given by equation (1.6):

$$(2\xi - 1)^2 \cdot \frac{a}{2} \leq \tilde{\sigma} \leq (2\xi + 1)^2 \cdot \frac{a}{2}$$

with

$$a = \left(\frac{G}{1-\nu} \cdot \frac{\gamma}{R} \right)^2$$

In this range of stress, the perturbation grows in amplitude, but keeps the same wavelength. By increasing the effective stress, however, the circumferential perturbation grows with always higher wavenumber ξ , until the original pore breaks up in ξ smaller pores of the same length.

1.5.2.4) Alternative models.

A variation to the model of Heidug & Leroy (1994) and Leroy & Heidug (1994) has been proposed by Gal et al. (1998), based on a calculation method used by Srolovitz (1989). In this model an initially flat solid-fluid interface is subjected to lateral stress, and the evolution of a sinusoidal perturbation of the surface is investigated. The results are comparable to those obtained by Heidug & Leroy (1994) and Leroy & Heidug (1994), but restricted to one mode of deformation. Under a given loading situation, the perturbation will grow unstably if its wavelength is larger than a critical wavelength. Otherwise it will be smoothed out.

The theoretical model of Heidug & Leroy (1994) and Leroy & Heidug (1994) gives the opportunity to quantify the effect of elastic strain on the stability of a solid/fluid interface. It is thus of prime importance for the study of pressure solution phenomena,

particularly for the study of the "island-channel" model, although particular conditions occurring at grain boundaries, such as solid-solid surface tension effects or long-range intermolecular forces are not considered. An experimental investigation on the effect of elastic strain on free-face dissolution (and growth) of elastic/brittle salt single crystals will help to test this theoretical model.

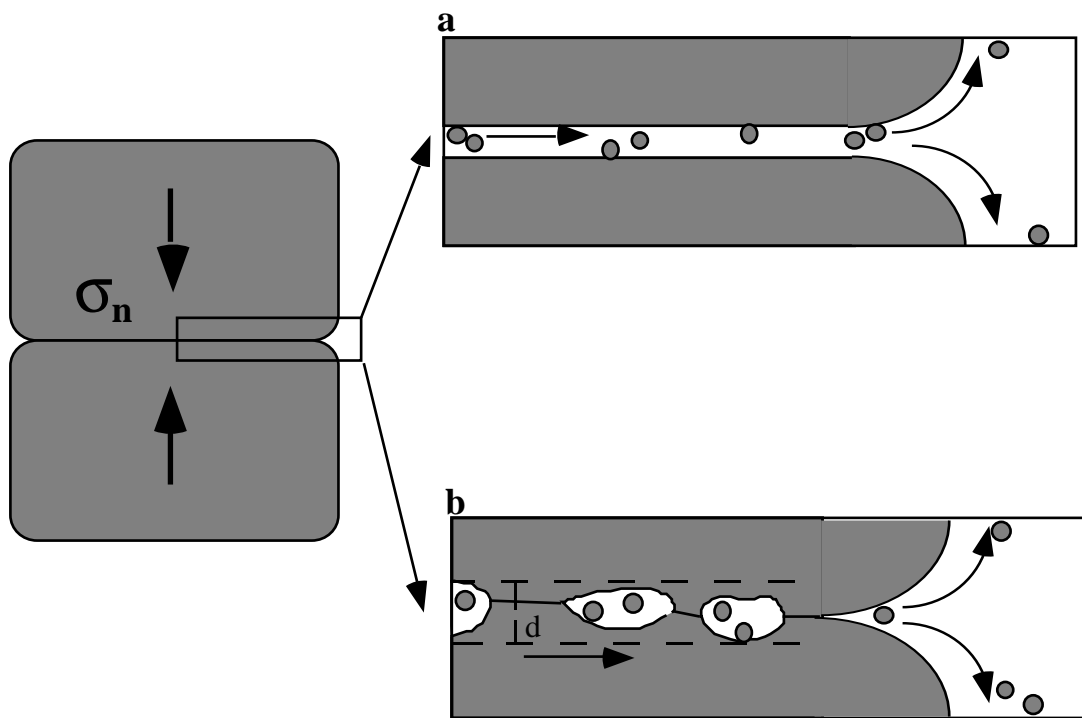


Fig. 1.1 The grain boundary structure according to two different diffusion controlled pressure solution models. a) Dissolved material diffuses along a continuous nanometer-scale structured, high viscosity water film (e.g. Rutter, 1976). b) Dissolved material diffuses through a dynamically stable island-channel structure. The boundary thickness d is assumed to be up to several hundreds of nanometers wide (e.g. Spiers & Schutjens 1990).

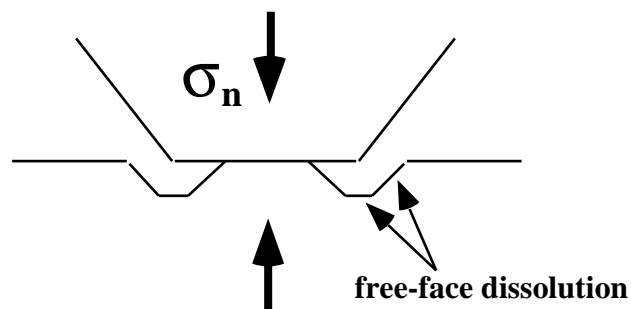


Fig. 1.2 Schematic drawing illustrating assumed grain-to-grain contact structure in the undercutting model. Free-face dissolution is assumed to occur around the contact point between the two grains. The contact area decreases with time and the resulting increase in the stress may lead to crystal plastic deformation of the contact zone and eventually to a (catastrophic) collapse.

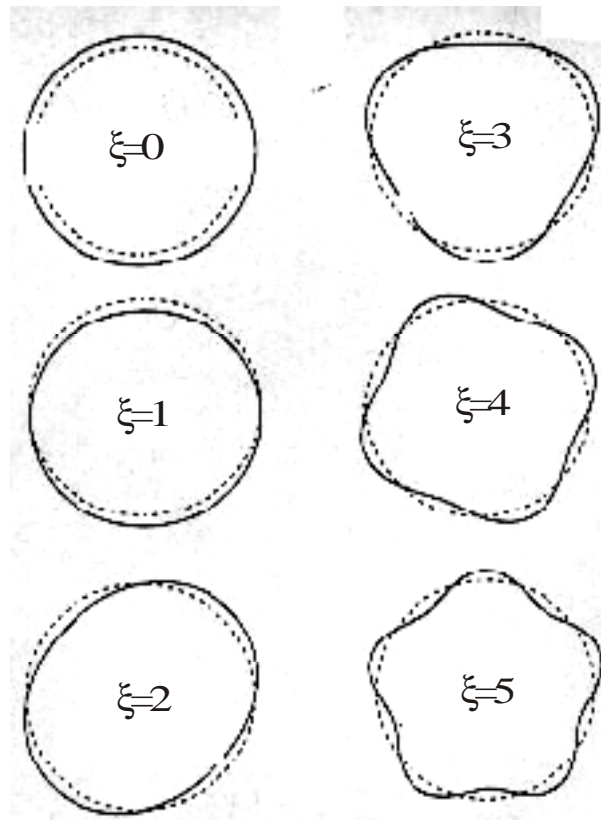


Fig. 1.3 Schematic representation of circumferential perturbations of wavenumber ξ on the surface of a circular pore (after Leroy & Heidug, 1994).

Chapter 2 Experimental procedures.

In this chapter, the choice of the materials used in this thesis is discussed and their most important properties described. The methods for the preparation of the samples and the experimental procedures to test the model of Heidug & Leroy (1994) and Leroy & Heidug (1994) on the evolution of a cylindrical cavity in a crystal stressed in solution are explained in detail.

2.1) Materials used.

As we are interested in the effect of elastic deformation, it was necessary to use crystals that can not deform by crystal plastic mechanisms at room P-T conditions. To get quantitative results in a relatively short time, it was necessary to choose materials with relatively fast kinetics of growth and dissolution. Finally, the crystals should not possess a very significant mechanical anisotropy, so that the isotropic approximation could be made for the calculation of the elastic strain distribution in the samples. For these reasons, potassium alum (K-alum) and sodium chlorate were chosen as rock analogue materials.

2.1.1) Potassium alum.

Potassium alum ($\text{KAl}[\text{SO}_4]_2 \cdot 12\text{H}_2\text{O}$) is a cubic salt, and belongs to the space group T^h_6 . It has a solubility of 0.3 mol.l^{-1} water at 25°C (Van der Hoek et al., 1983; Ullmann Handbook, 1986). Crystals have an octahedral habit typically bounded by $\{111\}$, $\{100\}$ and $\{110\}$ faces (Fig. 2.1). However, the relative importance of these faces and thus the morphology of potassium alum crystals depends on the crystal growth procedures and on the degree of oversaturation at which they are grown (Buckley, 1958). When the degree of oversaturation is high and the diffusion of material from the bulk solution towards the crystal surface is fast, faces with high growth rates such as $\{110\}$ and $\{100\}$, disappear quickly and only $\{111\}$ faces remain, forming bi-pyramidal crystals. Secondary faces such as $\{112\}$ or $\{221\}$ are less often observed, because of their very high growth rates (Wilke, 1988). Crystals used in this work were prepared by cutting commercially available larger single crystals (from ALVA GmbH, Germany). The method of preparation will be described later.

The structure of alum has been extensively described by Lipson (1935) and Lipson and Beevers (1935). The particularity of alum is that each trivalent cation (for K-alum) and

each monovalent cation (for K-alum) is surrounded by six water molecules. According to these authors, such an arrangement around a potassium cation is rare in other materials. It has to be noted that a different sort of potassium alum, with only eleven water molecules, can be found in nature. This variety is called kalinite. It has a monoclinic symmetry and a fibrous habit. Little is known about the properties of this material.

Elasticity parameters and elastic moduli of potassium alum can be found in the literature (e.g. Haussühl, 1961). The Young's modulus E , calculated from the elastic moduli, is 18.63 GPa.

To test whether potassium alum crystals could deform plastically under room P-T conditions, an experiment was performed as follows: a dried crystal sample about $6 \times 2 \times 2$ mm in size with faces parallel two by two was placed 20 hours under a stress of 15 MPa, and then 7 hours under 27 MPa. The length of the sample was measured after both stages. No deformation up to 0.1% strain, the resolution of the measurement, was measured.

2.1.2) Sodium chlorate.

Sodium chlorate (NaClO_3) is a cubic salt, and belongs to the space group $P2_13$. It has a solubility of 9.4 mol.l^{-1} water at 25°C (Ristic et al., 1993; Gmelins Handbuch, 1970). Crystals commonly are rectangular slabs bounded by the prismatic $\{100\}$ faces (Fig. 2.2). Secondary faces such as $\{110\}$, $\{120\}$ or $\{140\}$ are less commonly developed on macrocrystals, because of their higher growth rates, and mostly form only at very low degrees of oversaturation (Kitamura et al., 1982). These faces, however, are of great importance for the study of the chirality of sodium chlorate, which reflects dissymmetrical arrangement of atoms in the crystal structure (Szurgot, 1995).

Elasticity parameters were published for example by Viswanathan (1966). The Young's modulus is $E = 43.67 \text{ GPa}$.

It has been shown by Den Brok et al. (1999a) that sodium chlorate can not deform plastically at room P-T conditions in air under stresses up to 21 MPa. Above this value it breaks brittly.

2.2) Sample preparation.

2.2.1) Potassium-alum

Rectangular crystal slabs were cut from commercially available larger single crystals (from ALVA GmbH, Germany) about $70 \times 50 \times 50$ mm in size. This operation was

carried out with a diamond cutting machine (Isomet, Buehler) and using volatile oil (Shell S4919) as a lubricant. A 2 ± 0.05 mm diameter hole was drilled in the middle of the largest sample crystal face with a twist drill, also using volatile oil as a lubricant. Once under stress, the well known variation of the state of stress around the hole in the crystal (Jaeger, 1969; Timoshenko & Goodier, 1970) allows a reasonable correlation between the amount of elastic strain and the dissolution rate. This geometry has already been used by several authors (Sprunt & Nur, 1977b; Bosworth, 1981). After drilling the hole, the side faces of the crystals were polished using polishing paper (mesh sizes 600, 800, 1000 and 1200), again with volatile oil as a lubricant to finally get right-angled samples about $4 \times 6 \times 10$ mm in size (Fig. 2.3).

The exact crystallographic orientation of the samples was determined after the experiments by examination of the fluid inclusions, which had a negative crystal shape. All samples were oriented to within $\pm 10^\circ$ to either $\{111\}$, $\{110\}$ or $\{100\}$ crystallographic faces. The crystallographic orientation of each sample is given in Table 3.1 in Chapter 3.

2.2.2) Sodium chlorate

Sodium chlorate crystals were grown by slow evaporation of an originally saturated aqueous sodium chlorate solution at room temperature. Crystals about $20 \times 15 \times 5$ mm in size were grown in a few days. The drilling of the 2 ± 0.05 mm diameter hole and the polishing of the crystal faces were carried out following the same procedures as described above, to finally get right-angled samples of about $2 \times 8 \times 12$ mm in size (Fig. 2.3). The faces of the samples were close to the original $\{100\}$ crystallographic faces (to within a few degrees).

2.2.3) Aqueous solutions.

Saturated aqueous solutions of K-alum and sodium chlorate were prepared by dissolving a slight excess quantity of small crystals (K-alum from Merck 101047 "zur analyse", sodium chlorate from Merck 106420 "rein") for a saturation at room temperature in distilled water. The conductivity of the distilled water was 0.054 mS.cm^{-1} . Solutions were heated for 2-24 hours at about 50°C until all the material had dissolved. K-alum should not be heated above 64.5°C , because above that temperature it loses 9 water molecules (Gmelins Handbuch, 1970). The solution was then cooled down to room temperature in the experimental vessel, and small crystals were submerged in it to absorb the oversaturation. The solution was left under these conditions for a few days. Saturation was assumed to be reached when either no change in the size of the small crystals was observed, or when no change in their weight was measured after having taken them out of the solution.

2.3) Experimental set-up and procedures.

2.3.1) Description of the apparatus.

An overview of the experimental set-up is presented and drawn schematically in Fig. 2.4. More detailed drawings of the different parts of the apparatus are given in Appendix 1. The apparatus was composed of two 110 mm high Plexiglas cylinders. The inner cylinder was 100 mm and the outer cylinder was 180 mm in diameter. Both cylinders were fitted in an upper and a lower, 15 mm thick stainless, Vanadium-steel plate. Vanadium steel was needed because normal stainless steel would "rust" in the weakly acid potassium alum solution. The whole was closed using screws with O-rings. The inner cylinder was filled with the aqueous solution. Circulation of oil between both cylinders gave the possibility to control the temperature of the solution. This was achieved using a Haake DC5 temperature controller together with a computer program allowing the decrease or increase of the oil temperature in a given time. However, most of the experiments carried out in this work were done at room temperature, in a room in which the temperature was controlled to within 0.1 to 0.2°C.

The top of the solution vessel was covered with an aluminium plate to prevent evaporation.

The apparatus was designed such that two samples could be used for each experiment. Each of the samples stood on a lower, 10 mm diameter piston. The crystal were kept between this lower piston and an upper, 10 mm diameter piston (all the pistons were made from Vanadium-steel), that rested on it through an opening drilled in the aluminium plate. Two more openings were drilled in this upper plate, one of which allowed the introduction of a thermosensor to measure the temperature of the solution, and another that allowed the addition of distilled water to the solution.

The aqueous solution was continuously stirred with a dual-blade paddle fixed to the upper aluminium plate and running at about 100 rotations per minute.

2.3.2) Experimental procedures.

In each experiment, the vessel was first filled with the aqueous solution. Once the saturation was reached (after a few days), two crystals prepared with the same crystallographic orientation were put in the vessel. Large crystals (more than 8 mm wide and 4 mm thick) were put in the solution before closing the vessel. Small crystals were stuck under the upper pistons using UHU glue and put into the solution once the vessel closed.

The vessel was placed in a loading frame, in which load could be applied with a variable weight consisting of a tank filled with water. The stress, in the range 1-5 MPa (load in kg divided by sample cross section), was applied on one of the crystals through

the upper piston, perpendicular to the axis of the central hole drilled through the crystals. The loading was carried out at a rate of about $25 \text{ kg}\cdot\text{hr}^{-1}$ within 1-10 minutes. The other crystal was left stress-free (the weight of the piston corresponded to a stress of only 0.03 MPa and was therefore neglected). Fat was used to minimise any friction between the piston and the upper plate. The stress on the stressed crystal was measured with a 2 kN, 10 mm diameter and 7 mm high load sensor (Burster, typ 8416) placed between the press and the piston (see Fig. 2.4). Displacement of the piston on the stressed crystal was measured with a LVDT displacement sensor (typ HT400 Schlumberger with a Schlumberger OD4 transducer conditioner). The length of the samples was systematically measured before and after each experiment with a precision of 0.1% strain, using a micrometer screw.

Once the crystals were in the vessel in the saturated solution and the one of them under stress, the solution was diluted quasi instantaneously by adding small amounts of distilled water through the opening in the upper plate. The resulting degree of undersaturation was not measured, but calculated in degree Celsius using the empirical formula:

$$C_0 = e^{0.034336T} \quad (2.1)$$

for K-alum (Van der Hoek et al., 1983; Ullmann Handbook, 1986), and

$$C_0 = e^{0.0091557T} \quad (2.2)$$

for sodium chlorate (Ristić et al., 1993; Gmelins Handbuch, 1970), where C_0 is the saturation concentration ($\text{g}\cdot\text{l}^{-1}$ water) at temperature T ($^{\circ}\text{C}$). Fig. 2.5 shows the very good agreement between these equations and solubility values published in the literature.

Experiment duration ranged between a few hours and a week. After each experiment, the crystals were removed from the solution and immediately dried using a cleaning tissue. Micrographs of both stressed and stress-free holes were taken before and after each experiment under an optical microscope.

2.4) Estimation of the stress around the hole.

The stress distribution around a hole drilled in an infinite isotropic plate submitted to uniaxial compression is well known (Jaeger, 1969; Timoshenko & Goodier, 1970). Under condition of plain strain and if no shear stresses are present, the normal stress at

the periphery of the hole is equal to the pressure in the hole. In our experiments, the aqueous solution in the hole is connected with the bulk solution and is at the atmospheric pressure, which is negligible with respect to the applied load on the crystal. The hoop stress at the periphery of the hole drilled through an infinitely large sample varies from a tension equal to minus the bulk applied stress above and below the hole to a compression equal to three times the bulk applied stress on the sides left and right of the hole (Fig. 2.6).

For a finite plate such as in our case with a centrally drilled hole, it can be shown using finite differences computer programs such as FLAC (Fast Lagrangian Analysis of Continua) that the stress on both compressive sides of the hole reaches higher values. A typical example of stress contours obtained using FLAC is shown on Fig. 2.7. The stress on both compressive sides at the periphery of the hole reaches five times the bulk applied stress. The tensional regions above and below the hole (hatched regions) are found to spread over a much smaller area.

In our case, the polishing of the crystal faces for the preparation of the samples led generally to an undesired asymmetry between both sides of the holes, that was slightly different for each crystal. For this reason, the stress was calculated on both crystal sections on the compressive sides of the hole (load over side cross section), and the average between both sides taken as the estimation of the hoop stress at the periphery on both sides of the hole. The estimation error depended on the asymmetry of the sample. All of the stress values reported in Table 3.1 in Chapter 3 correspond to the conditions of stress at the beginning of the experiments.

2.5) In-situ experiments.

Some experiments were carried out in-situ, i.e. under an optical microscope, in a see-through vessel placed on a horizontal microscope. This vessel consisted of a 1.1 mm thin U-shaped piston made of Ertalon, held and glued with UV-loctite (loctite 350) between two 50 mm high, 50 mm wide and 1.6 mm thick glass plates (Den Brok et al., 1998, 1999b). Crystals used for these experiments had a thickness of about 1 mm. Saturated solution was filled in the vessel with the help of a syringe. The stress was applied on the crystal with a dead weight through a 1 mm thick stainless Vanadium-steel piston. The microscope was coupled to a TK-1070E JVC digital colour video camera connected to a computer, providing the possibility to film the experiment under microscope, using NIH-image software. Experiments were carried out at room temperature.

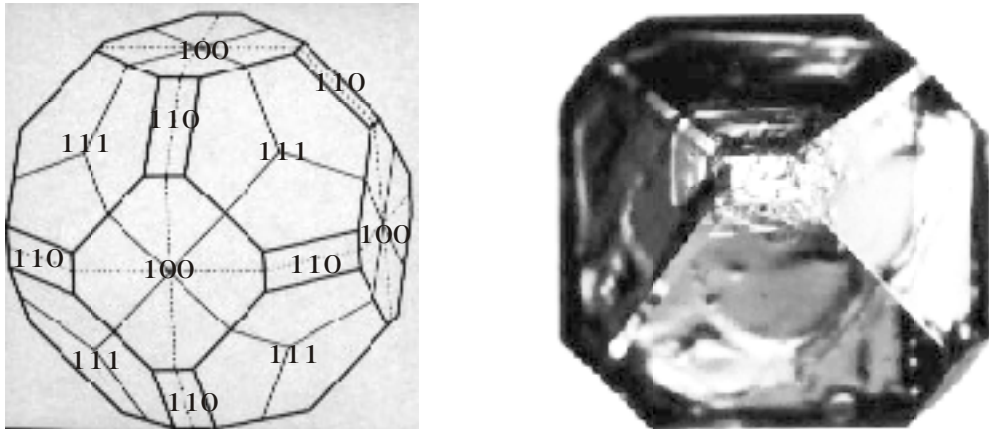


Fig. 2.1 (a) Typical habit of a K-alum crystal according to Schubnikov & Brunowsky (1931), showing the three principal crystallographic faces $\{111\}$, $\{110\}$ and $\{100\}$. (b) K-alum crystal grown by slow evaporation of a saturated aqueous K-alum solution at room temperature. The size of the different crystal faces depends on the growth conditions. The crystal is about 3 x 3 x 3 mm and was grown in one day.

1mm



Fig. 2.2 Sodium chlorate crystal such as used in the experiments. The crystal was grown at room temperature by slow evaporation of a saturated aqueous sodium chlorate solution. The crystal is bounded by {100} faces.

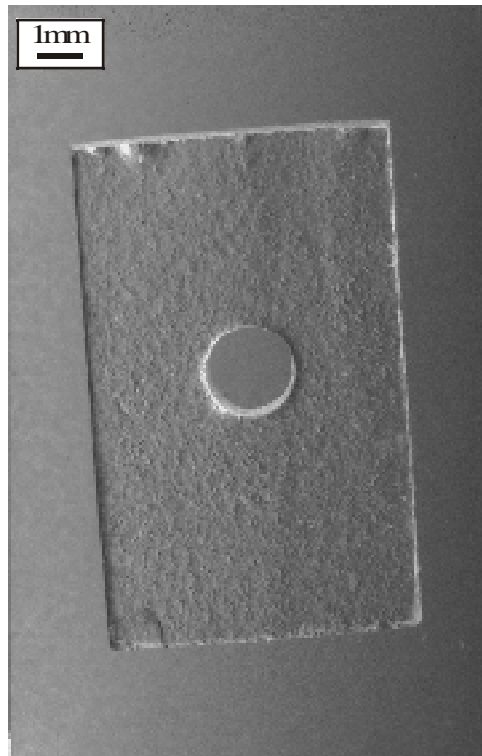


Fig. 2.3 Optical micrograph showing typical geometry of the samples before experiment. The stress is applied vertically, parallel to the sample long-axis and perpendicular to the axis of the hole.

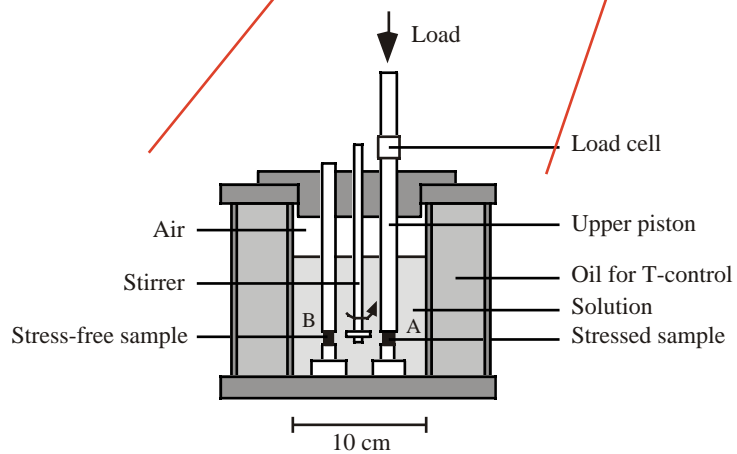
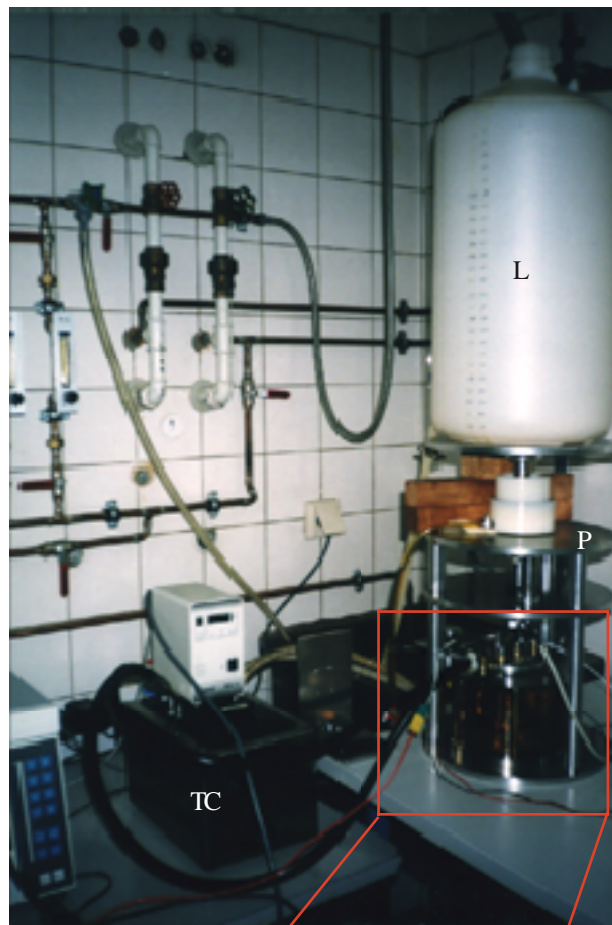


Fig. 2.4. Experimental set up used. The cylindrical vessel is placed under a press (P), and the stress applied on one of the two crystals with a tank filled with water (L). The loading rate can be controlled by accurately controlling the rate at which the tank is filled with water. The temperature of the solution in the vessel is controlled by circulating oil kept at constant temperature with the help of the temperature controller (TC). The two possible positions for the crystals are noted as A and B.

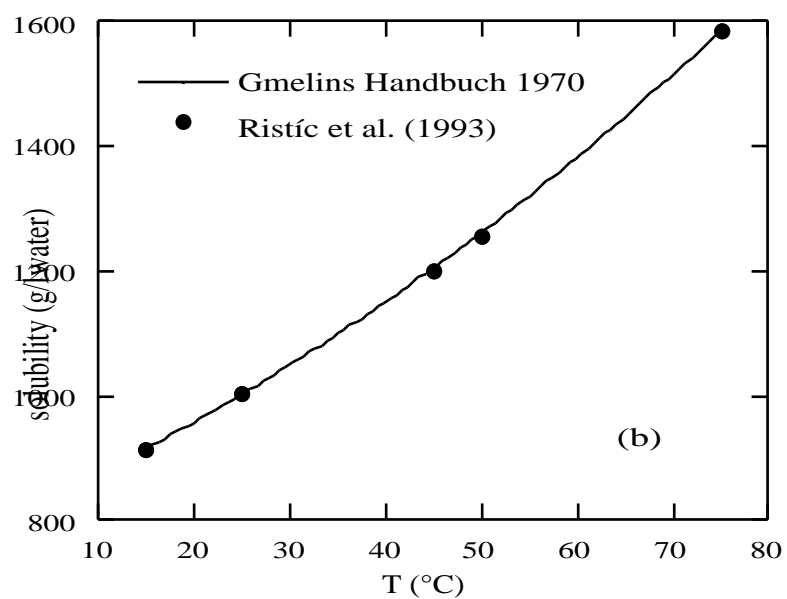
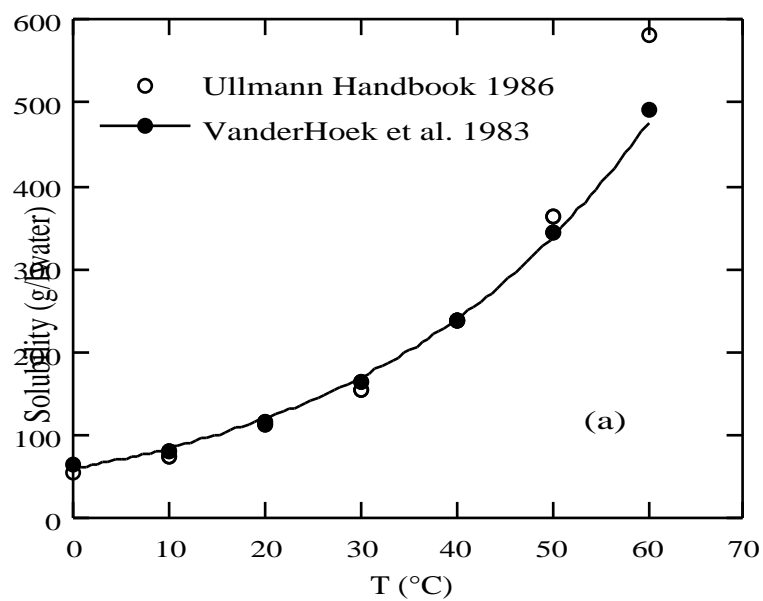


Fig. 2.5 Solubility data of potassium alum (a) and sodium chlorate (b). The curves correspond to the equations given in the text.

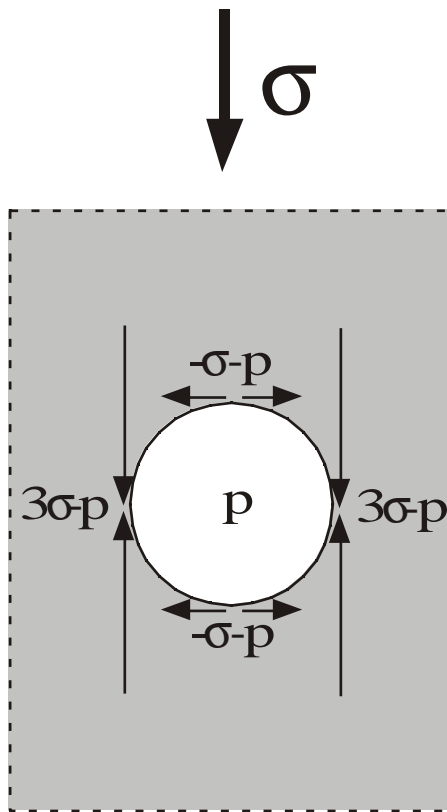


Fig. 2.6 Schematic representation of the stress distribution around a hole drilled in an infinite isotropic plate. The pressure in the hole is noted as p .

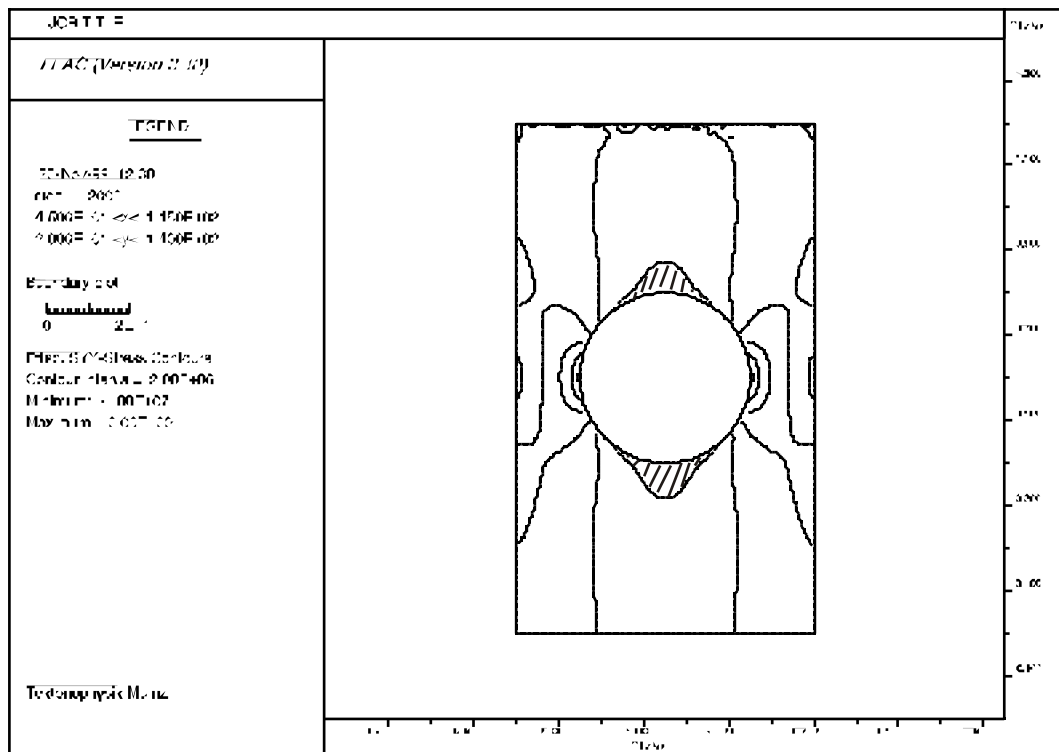


Fig. 2.7 Example of stress contours obtained with FLAC. The geometry of the sample corresponds to sample 50KAD2 at the end of the experiment. The stress contour interval is 2 MPa. With a bulk stress of 2 MPa applied vertically on the top of the crystal, the stress on both compressive sides of the hole reaches 10 MPa. Tension regions above and below the hole are hatched.

Chapter 3 Effect of stress on surface microstructures.

In this section, the experimental results on the effect of stress on the microstructures of free surfaces of crystals held in undersaturated aqueous solution are presented and discussed. After a detailed description of the surface microstructures, the origin of their formation is discussed in the framework of existing physical models on the evolution of stressed solid-fluid interfaces.

3.1) Description of the dissolution features.

After each experiment, both stressed and stress-free crystals were taken out of the solution and immediately dried using a cleaning tissue. A first visual assessment of the crystals could reveal differences in surface structure between stressed and stress-free crystals. While the surface of the stress-free crystals appeared smooth and unaltered, the surface of the stressed crystals was characterised by the presence of fine grooves on both sides of the hole.

3.1.1) Stress-free crystals.

A detailed microscopic examination of the surface of stress-free crystals using an optical microscope revealed the presence of fine etch grooves. These grooves could only be seen at high magnification ($\times 400$). They occurred in bundles at apparently arbitrary localities all over the surface. The grooves were roughly parallel to each other and built an anastomosing pattern (Fig. 3.1). Individual groups of grooves had different orientations on the same crystal surface. These orientations were always parallel to crystallographic low index directions. The grooves were typically 1-3 μm wide, 1-2 μm deep, and separated from each other by 3-10 μm .

3.1.2) Stressed crystals.

On the faces of crystals dissolved under stress, large as well as small grooves were observed under the microscope. The small grooves were identical to those observed on

stress-free samples, but now appeared to occur on the entire surface. They were all oriented in the same direction, at an angle to the bulk applied stress direction ranging from 0 to 40°. Our attention, however, was caught by the much bigger dissolution grooves that had developed on both sides of the hole (Fig. 3.2). They were equally spaced and parallel to each other. They were typically 20-70 µm wide, 10-40µm deep and 20-70 µm apart, i.e. about ten times bigger in size than the grooves observed on stress-free crystals (Fig. 3.3).

In the following, the term "A-type grooves" will be used to characterise the dissolution macrofeatures observed on the stressed crystals, while the structures observed on stress-free crystals will be called "B-type grooves".

3.1.2.1) Localisation and orientation of the grooves.

A-type grooves developed in all cases on both right and left sides of the hole. These grooves were also present in the hole (Fig. 3.4), but not always over the entire length of the hole. A-type grooves developed often only on one face (one 10 × 6 mm face) of the crystals. Stressed crystals, that fractured during the loading operation or just at the beginning of the experiment, typically showed A-type grooves far away from the hole, sometimes covering the entire crystal surface on one side of the fracture (Fig. 3.5). A-type grooves never developed above or below the hole, even in the cases where they propagated everywhere else on the crystal surface (Fig. 3.6). The grooves were also often observed on the small side faces of the crystals (10 × 4 mm faces).

A-type grooves appeared mostly as straight structures. They were either linear (see for example Fig. 3.2), or showed a regular "zig-zag" pattern (Fig. 3.7). While the orientation of B-type grooves made an angle up to 40° with the direction of the bulk applied stress, A-type grooves were always perpendicular (to within a few degrees) to the bulk applied stress. However, A-type grooves appeared sometimes curved, especially in the vicinity of the hole (Fig. 3.8). This curved orientation of the grooves followed in that case the perpendicular to the local curved stress trajectories. The orientation of the A-type grooves, the orientation of the 10 × 6 mm crystal face and the direction of the bulk applied stress for all the experiments are given in Table 3.1. These orientations were determined with the help of the crystallographic facets of negative crystal fluid inclusions.

Some experiments carried out at high stress (bulk stress 3.9-4.2 MPa, Table 3.1), at the limit of the crystal brittle failure strength, have shown that A-type grooves could also develop under these high stress conditions in directions that were not perpendicular to the bulk applied stress or to the local stress trajectories. They sometimes even appeared to have developed roughly parallel to the direction of the applied stress. This situation led to the formation of a dissolution groove network (Fig. 3.9).

3.1.2.2) Structure and shape of the grooves.

A-type grooves looked like alignments of etch pits. In every case, for straight as well as for curved grooves, dissolution from these individual etch pits occurred along low index crystallographic directions, and formed small crystallographic facets (see for example Fig. 3.3). The shape of the A-type grooves could be observed best in side view, at the periphery of the holes, where they appeared in cross section as 10-40 μm deep teeth (Fig 3. 10 and 3.11). In Fig. 3.11 it can be seen that the teeth are formed by crystallographic facets. Size and shape of the A-type grooves are given for all the experiments in Table 3.1.

3.2) Mechanism of formation of the grooves.

A comparison of the microstructure of the surface of a stress-free crystal (Fig. 3.1) with the microstructure observed on the surface of a stressed surface (Fig. 3.3) suggests a strong influence of the stress on their formation. How are these dissolution grooves initiated and why are they about ten times larger in size on both sides of the hole of the stressed crystals in comparison to the stress-free crystal?

3.2.1) Stability of stress-free crystal surfaces.

3.2.1.1) Influence of the surface energy.

The stability of a solid-fluid interface depends on the thermodynamic state of both phases in contact with each other, each of them being characterised by a chemical potential. In equilibrium situation, both chemical potentials are equal. At temperature T_0 , a stress-free crystal with no internal strain (i.e. free of structural defects) is in equilibrium with an aqueous solution saturated at temperature T_0 . In the experiments considered here, however, a stress-free crystal is not in equilibrium with the aqueous solution for two reasons. Firstly, the aqueous solution is intentionally undersaturated, i.e., its concentration is lower than it should be for a saturation at temperature T_0 . This means that the chemical potential of the fluid is higher than that of the crystal, and that the crystal will dissolve, to bring material in the solution to reach the saturation concentration. Secondly, the faces of the samples are not exactly parallel to low index, stable crystallographic planes (see Chapter 2). This means that the crystals can lower their surface energy by faceting. A faceted surface has indeed a lower surface energy and, hence, is more stable (e.g. Herring, 1951). For this reason, once in the undersaturated solution, the crystals loose some material by dissolving along low index crystallographic faces, e.g. for K-alum the $\{111\}$, $\{110\}$ and $\{100\}$ faces (Fig. 3.12).

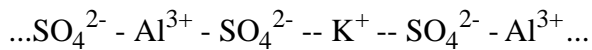
Observation after experiment under the microscope of fluid inclusions with negative crystal shape shows that the fine B-type etch grooves observed on the surface of stress-free crystals (Fig. 3.1) are aligned along crystallographic directions, mostly $\langle 110 \rangle$, and are thus intersections between crystallographic planes. However, many different crystallographic planes intersect the crystal surface. So what controls the particular intersection along which the grooves form?

3.2.1.2) Periodic bond chains.

The periodic bond chains (PBC) of a crystal are crystallographic directions in which atoms are connected to each other by strong energetic bonds. Their number and orientation determine the macromorphology of a growing crystal (Hartman, 1987). They also determine the shape of dissolution pits (Heimann, 1975; Szurgot, 1995), so that the study of etch pit morphology is often used to find PBC-directions in crystals. The PBC are the direction of high surface energy where the dissolution of a non-crystallographic face starts.

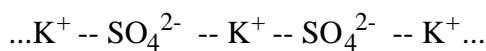
PBC-directions for a wide range of crystals are given by Kern (1955). For potassium alum, the three principal PBC are, by order of strength:

- A-PBC



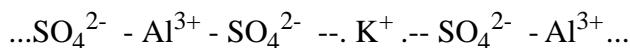
along $\langle 100 \rangle$ directions.

- B-PBC



along $\langle 110 \rangle$ directions.

- C-PBC



along $\langle 111 \rangle$ directions. The composition of the C-PBC is the same as the A-PBC, but the bonds between potassium atoms and sulphate groups are about 20% longer.

The crystallographic faces are then classified as a function of the number and strength of the PBC that are entirely contained in their plan:

- {100}: two A- and two B-PBC,
- {111}: three B-PBC,
- {110}: one A-, one B- and two C-PBC.

The most common PBC-direction on the crystal surfaces of potassium alum is thus oriented along $\langle 110 \rangle$. This explains why the B-type grooves observed on stress-free crystals are mostly oriented along $\langle 110 \rangle$ -directions.

3.2.2) Stability of stressed crystal surfaces.

3.2.2.1) Influence of the stress distribution on the surface.

The dissolution of the crystal surface along intersections between crystallographic planes, as described above (Fig. 3.12), gives the surface a "wavy" aspect (see for example Fig. 3.11). Once under stress, such a structure oriented parallel to the bulk applied stress leads to a non-homogeneous stress distribution on the surface. This stress non-homogeneity may be very easily revealed by photoelasticity experiments carried out on a Plexiglas sample with a similar geometry (Fig. 3.13). The stress is higher at concavities ("valleys") than at convexities ("crests"). This stress gradient leads to a surface instability called the Grinfeld instability (Grinfeld, 1986). The stress gradient, and hence the surface instability, then depends on the amplitude and wavelength of the wavy structure.

Let us consider a semi-circular groove of radius r on the surface of a semi-infinite isotropic plate of width d (Fig. 3.14). If we apply an uniaxial compressive stress σ_∞ on the plate at infinity, the stress will be higher at the periphery of the groove (M) than in the middle of the section MN. The ratio between the maximum compressive stress at the periphery of the groove and the compressive stress in the middle of the section MN is given by a constant k , called the factor of stress concentration. Timoshenko (1949) has shown that k ranges between 1 and 3 and increases for decreasing ratio r/d . The smaller the groove radius relatively to the width of the plate, the higher the stress heterogeneity it produces. This means that, under stress, the dissolution will be enhanced in the valleys, and a groove will grow in depth and width (so the ratio r/d will increase) to decrease the stress heterogeneity on the surface. In this way, B-type grooves (i.e. the surface energy-induced structures), may become A-type grooves (i.e. the stress-induced structures) to minimise the stress heterogeneity.

A-type grooves form always preferentially on both compressive sides of the hole, i.e. where the stress is the highest. This suggests that a "critical" stress may have to be reached for the development of A-type grooves.

3.2.2.2) Relation between A-type grooves and PBC-directions.

Although the crystal faces were not exactly parallel to either $\{110\}$, $\{111\}$ or $\{100\}$ (see Chapter 2), the orientation of the A-type grooves could always be identified with an A- or B-PBC contained in the nearest crystallographic face. As mentioned above, a crystal surface generally contains more than one PBC-direction. In all the cases however, the PBC that was oriented the most perpendicular to the bulk applied stress appeared to be the one parallel to which A-type grooves developed. This could be illustrated with experiments 76KAD16b and 77KAD17. Both stressed crystals had the same dissolving $\{110\}$ face, but the stress was applied along a $\langle 110 \rangle$ -direction for the first and along a $\langle 100 \rangle$ -direction for the second. In both cases, the A-type grooves developed roughly perpendicular to the applied stress, but along a $\langle 100 \rangle$ PBC-direction for experiment 76KAD16b and along a $\langle 110 \rangle$ PBC-direction for experiment 77KAD17. When two PBC were oriented equally favourable for the formation of the A-type grooves, because both had about the same angle with the direction of the applied stress, the resulting grooves showed a "zig-zag" shape. This could occur with two B-PBC (Fig. 3.7) or with an A- and a B-PBC.

3.2.2.3) Formation of a dissolution groove network.

In almost all of the experiments, the A-type grooves developed along a $\langle 110 \rangle$ -direction. This is due to the abundance of the B-PBC, so that for almost every crystal faces there was always one B-PBC oriented roughly perpendicular to the applied stress. In the case of experiment 76KAD16b, the only B-PBC contained on the surface was oriented roughly parallel to the bulk applied stress, while an A-PBC, along a $\langle 100 \rangle$ -direction, was oriented roughly perpendicular to it. As for all the other experiments, A-type grooves developed preferentially along the PBC the most perpendicular to the bulk applied compressive stress, in that case along an A-PBC. However, the B-PBC showed also dissolution grooves (Fig. 3.15). Development of A-type grooves along a B-PBC direction parallel to the bulk applied stress was also observed in experiment 59KAD9 (Fig. 3.9). The formation of B-type grooves parallel to the bulk applied stress, however, should not create a non-homogeneous stress distribution and the grooves should not develop into A-type grooves. Moreover, following Kern (1955), the strength of the interatomic bonds in the $\langle 110 \rangle$ -direction (B-PBC) is less than the strength of the bonds in the $\langle 100 \rangle$ -directions (A-PBC, see Paragraph 3.2.1.2). If dissolution can also be enhanced in grooves oriented parallel to the applied stress, as for both experiments described above, we should expect dissolution to take place also along the A-PBC when this is oriented parallel to the applied stress. This never happened. Hence, the $\langle 110 \rangle$ direction shows a particular behaviour under stress, and a mechanism other than the lowering of the surface energy may enhance the dissolution along this direction more than along the other directions.

We have seen in Chapter 2 that for potassium alum, each aluminium and each potassium cation is surrounded by six water molecules. After Lipson & Bevers (1935), the arrangement of six water molecules around a potassium cation is rare.

These authors have also shown that the water molecules surrounding the aluminium cations are close to each other and the bonds linking them are strong and coplanar. In contrast, the water molecules surrounding the potassium cations are far away from each other, so that their arrangement around the cations is governed by external atoms, with which bonds are weak and not all in the same plane. It could thus be that this structure is more easily affected by stressing the crystal, so that $\langle 110 \rangle$ -directions, which present the highest density of $\text{K-6H}_2\text{O}$ groups, show a stronger dissolution.

Note, however, that the development of A-type grooves parallel to the bulk applied stress direction was observed only for the experiments carried out under the highest stresses (bulk stress 3.9-4.2 MPa, corresponding to 12.5 MPa on both compressive sides of the hole), and for crystal faces oriented roughly parallel to $\{110\}$ faces. Moreover, both experiments (59KAD9 and 76KAD16b) were also the only ones for which A-type grooves also developed along C-PBC, i.e. $\langle 111 \rangle$ -directions, at $\sim 45^\circ$ to the bulk applied stress direction. This suggests that for such crystal face orientation, dissolution may be enhanced above a "critical" stress (about 3.5 MPa bulk stress) along all the PBC-directions, and this independent of their orientation on the surface. This mechanism may lead to the formation of a dissolution groove network as seen on Fig. 3.9 and lead to a subsequent decomposition of the crystal surface in a lot of small parts. This process could lead for longer experiments to a cataclastic deformation of the entire crystal.

3.2.2.4) Role of stress-trajectories.

We have seen in Paragraph 3.2.2 that dissolution under stress led to a significant roughening of the crystal surface, with the formation of valleys (concavities) and crests (convexities). In the absence of the hole or far from it, the stress gradient between valleys and crests is maximum for dissolution grooves perpendicular to the bulk applied stress direction. A-type grooves propagate laterally perpendicular to the bulk applied stress. In the vicinity of the hole, however, the stress trajectories are curved (Fig. 3.8). A-type grooves in that case still develop perpendicular to the maximum compressive stress gradient direction, i.e. perpendicular to the maximum compressive stress trajectories, and are also curved (Fig. 3.8). The PBC-direction the most perpendicular to the stress changes in that case along the perpendicular to stress trajectories (Fig. 3.16).

3.2.3) Could crystal plastic strain play a role?

Fig 3.3 and especially Fig. 3.10 show that A-type grooves are formed by joining etch pits. What is the origin of these etch pits? Is it possible that these etch pits developed at screw dislocation outcrops developed by crystal plastic deformation, i.e. could the development of dissolution grooves be due to crystal plastic deformation?

We have seen in Chapter 2 that potassium alum cannot deform plastically under room P-T conditions (Paragraph 2.1.1). The length of the stressed samples was systematically measured before and after each experiment by hand with a micrometer, with a precision of 0.1%. None of the samples was found to have deformed plastically. To test whether even smaller amount of crystal plasticity could have played a role, two key experiments were carried out:

(i) After a common experiment, a crystal that had dissolved under stress and showed abundant A-type grooves was placed back into the undersaturated solution from which it came from and held in there again, for one hour, but without load. Investigation of the surface afterwards showed that the A-type grooves had completely disappeared.

(ii) A crystal was held under stress in an approximately saturated solution for 2 hours and then taken out. No grooves had developed. The sample was placed back into the solution again and then the solution was diluted, and the crystal held in there for 24 hours, without load. Investigation of the surface afterwards showed fine B-type etch grooves, randomly distributed like on stress-free crystals, but not the wide and deep A-type grooves characteristic for crystals under stress.

The formation and development of A-type grooves is thus a purely elastic effect. The etch pits observed on Fig. 3.10 are probably the intersection points between several low index crystallographic planes along which the crystal dissolved to decrease its surface energy (see Paragraph 3.2.1.1).

3.2.4) Influence of stirring

A-type grooves mostly developed only on one frontal face (10×6 mm) of the stressed crystals, and not on the back face. This could be due to an influence of the stirrer on the evolution of the surface microstructure. For this reason, experiment 76KAD16b was carried out without stirring. A-type grooves developed on the stressed crystal as in the case of experiments carried out with stirring. The formation of the grooves on one face only is thus more probably due to an eventual non-parallelism between the top and the bottom faces of the crystals, as a consequence of which one frontal face may be more stressed than the other.

3.3) In-situ experiments.

The experimental set-up used for the experiments described above and summarised in Table 3.1 allowed the study of the grooves only after experiment. It is very important, however, to know how fast A-type grooves develop, and how stable these structures are with respect to small variations in stress. The experimental set-up discussed in Paragraph 2.5 gave the opportunity to study the formation and development of the dissolution grooves directly under the microscope. Six experiments were carried out

using this set-up, also on potassium alum single crystals. Table 3.2 gives the experimental conditions for all the in-situ experiments.

3.3.1) Experimental procedures.

The experimental vessel consisted of a 1.1 mm thin Ertalon U-shaped piece stuck between two glass plates (Den Brok et al., 1998, 1999b). For each of the experiments (see Table 3.2), a $1 \times 6 \times 8$ mm potassium alum crystal was placed in the vessel and a 1 mm thick Vanadium-steel piston applied on it. The vessel was filled with a slightly undersaturated (0.3°C) potassium alum aqueous solution with the help of a syringe. The top of the vessel was closed using silicon grease to prevent evaporation of the solution. The vessel was then mounted on an horizontal microscope, and the stress applied on the crystal with a dead weight through the piston. Distilled water could be added in the vessel through the silicon grease in order to increase the degree of undersaturation during the experiment. As a consequence of the very small volume of the vessel ($\sim 200 \text{ mm}^3$), the solution could not be stirred. The experiments were filmed with the help of a digital colour video camera connected to a computer, using the NIH-image software.

3.3.2) Experimental observations.

Fig. 3.17 shows different time sequences of the in-situ experiment ISKAL1. The bulk applied stress was held constant at 2.8 MPa, corresponding to up to 10 MPa on both compressive sides of the hole (Table 3.2). A-type grooves formed mostly at the rim of the hole and propagated outwards. Isolated A-type grooves also formed further away from the hole (arrows in Fig. 3.17). As already observed in some of the experiments carried out with the other experimental set up, the grooves developed in an orientation perpendicular to the local maximum compressive stress, especially on both compressive sides of the hole. After three days ($t = 71.25 \text{ hr}$), a fracture formed on the left side of the hole in the crystal ISKAL1. This fracture formed as a consequence of a decrease in the crystal cross section due to dissolution. This fracture event led within one hour to a 50% increase in the number of the A-type grooves. Several A-type grooves joined together while propagating. Fig. 3.18 shows such a situation. The upper groove (arrow) propagated horizontally, but after five hours it changed its direction to $\sim 30^\circ$ to move towards a lower groove, with which it joined after 15 hours. A-type grooves also moved independently of the other grooves in the vertical direction. Fig. 3.19 shows such a movement. The groove moved upwards with an average velocity of $4 \mu\text{m}\cdot\text{hr}^{-1}$. Horizontal propagation velocities up to $100 \mu\text{m}\cdot\text{hr}^{-1}$ and vertical velocities up to $10 \mu\text{m}\cdot\text{hr}^{-1}$ were observed in the other in-situ experiments.

The effect of varying the stress on the development of the A-type grooves was investigated in experiment ISKAL5. The absence of stirring of the aqueous solution resulted in an influence of gravity, and convection occurred when distilled water was

added in the vessel during the experiment. This resulted in the dissolution of the crystal at the upper part and precipitation of the dissolved material at lower part of the crystal surface. The first time sequence shown on Fig. 3.20 illustrates a situation where distilled water had just been added. A-type grooves that had formed before the addition of distilled water, were filled up and smoothed out by precipitation of material dissolved at the upper part of the crystal. By increasing at $t = t_0$ the bulk applied stress from 3 to 4.7 MPa, corresponding to about 14 MPa on both compressive sides of the hole, the grooves could be "activated" again and developed very fast on both compressive sides of the hole. At $t = t_0 + 4.5$ hr, the bulk applied stress was increased to 6.7 MPa (up to 21 MPa on the compressive sides of the hole), what led to the formation of new A-type grooves, especially on the right side of the hole. The average wavelength of the grooves decreased from $\sim 35 \mu\text{m}$ to $\sim 30 \mu\text{m}$. At $t = t_0 + 24$ hr, some grooves started developing in a direction parallel to the bulk applied stress (arrow in Fig. 3.20). A further increase in the bulk stress to 7.1 MPa (up to 23 MPa on the compressive sides of the hole) at $t = t_0 + 72$ hr caused fracturing of the crystal and further development of grooves in the direction parallel to the bulk applied stress. This led to the formation of a dissolution groove network and to a cataclastic deformation of the crystal surface. It is interesting to note that this process resulted in a decrease in the number of horizontally oriented A-type grooves. At $t = t_0 + 72$ hr, the wavelength of the grooves was $\sim 70 \mu\text{m}$.

3.3.3) Discussion of in-situ results.

The most important information obtained from the in situ experiments is that the A-type grooves did not only propagate laterally perpendicular to the maximum compressive stress direction, but could also move over the crystal surface, vertically (Fig. 3.19) or towards other grooves (Fig. 3.18). These movements suggest that the A-type groove-development was affected by local stress heterogeneities, possibly due to the presence on the surface of crystal defects or impurities. It may also suggest the influence of far field effects on the development of A-type grooves. The development of B-type grooves, which are surface energy-induced structures, in A-type grooves, which are stress-induced structures (see Paragraph 3.2.2.1), depends on the stress intensity and may need to overcome a "critical" stress value (it is why the A-type grooves develop preferentially on both compressive sides of the hole). It could be that, by dissolution of the crystal surface in the undersaturated solution, internal crystal defects came to the surface and caused a stress concentration around them, thus inducing a variation with time in the position of the sites where this "critical" stress was reached, what could be responsible of the apparent movement of the grooves. The very fast formation of new A-type grooves after fracturing of the crystal (Fig. 3.17) shows that the development of the grooves reacts very quickly to a sudden variation of the surface stress distribution.

The last time sequence from the experiment ISKAL5 shown on Fig. 3.20 shows surface structures very similar to those observed after the experiment 59KAL9 (Fig. 3.9). A-type dissolution grooves started developing parallel to the direction of the bulk applied stress at $\sigma_b = 6.7$ MPa (corresponding to 21 MPa on both sides left and right of the hole). As the crystal fractured, at $\sigma_b = 7.1$ MPa (corresponding to about 23 MPa on

both sides of the hole), this suggests that the development of A-type grooves parallel to the direction of the bulk applied stress only occurred near the limit of brittle failure strength of the crystal. Microcracking of the crystal surface may occur under such high stress conditions and lead to enhanced dissolution in directions that are no more stress-controlled. This in turn may lead to a cataclastic deformation of the crystal.

We have so far suggested that A-type grooves developed from B-type grooves, that had formed by the dissolution in the undersaturated solution of the crystal surface along PBC-directions (see Paragraph 3.2.1.1). However, A-type grooves were also observed in situ to develop in saturated solution. Experiment ISKAL4 was carried out on a crystal on which scratches were intentionally made to get a rough surface. A concavity corresponding to half a 2 mm diameter hole was made on one side of the crystal (Fig. 3.21). Once the sample was placed under stress in the saturated solution, A-type grooves developed from the scratches at the rim of the concavity, i.e. where the stress was the highest. Hence, it appeared that as soon as the crystal surface was rough, it became unstable under stress (this is the Grinfeld instability, see Paragraph 3.2.2.1) and induced the formation of A-type grooves. The undersaturation of the aqueous solution only played the role of a driving force for the roughening of the surface. When the crystal surface showed no roughness at all and was crystallographically stable (i.e. exactly parallel to a low index crystallographic plane), as was the case for the experiment ISKAL6 (Table 3.2), no dissolution grooves developed, in saturated nor in undersaturated solution.

3.4) Theoretical approach.

A very important observation is that A-type grooves only developed in the highest stressed regions of the crystals. If the crystals did not fracture, these grooves developed on both compressive sides of the hole, and nowhere else. There was no intermediate state between the fine B-type grooves observed on stress-free crystals and the wide A-type grooves observed on stressed crystals. We already suggested that the formation of A-type grooves may occur once a critical stress is reached. At this critical stress, the surface energy-induced B-type grooves caused the crystal surface to become unstable. The grooves developed in A-type grooves to reduce the non-homogeneous surface stress distribution (Timoshenko, 1949), and grew until their wavelength was in equilibrium with the aqueous solution for the local conditions of stress and surface energy on the crystal surface. What defines this equilibrium wavelength, and what defines the critical stress at which the grooves start growing? The model developed by Heidug & Leroy (1994) and Leroy & Heidug (1994) and described in Chapter 1 analyses the stability of a wavy perturbation on a stressed surface, as a function of the stress, the surface energy and the local curvature of the surface. We will in this paragraph try to apply this model to the experiments carried out in this thesis and compare the theoretical predictions to the obtained experimental results.

3.4.1) Estimation of the equilibrium configuration.

Some differences exist between the theoretical conditions considered by Heidug & Leroy (1994) and Leroy & Heidug (1994) and our experimental conditions.

Firstly, the conditions of stress we used were not hydrostatic. We had a differential stress. In their model, the applied stress is hydrostatic at infinity. However, a differential stress also exists in their model at the hole boundary, due to the difference between normal stress and tangential stress, and is written as $\sigma_{\text{diff}} = 2\sigma_{\infty} + 2p - 2\gamma/R$, where σ_{∞} is the hydrostatic stress applied at infinity, p is the fluid pressure, γ is the surface tension and R is the hole radius. In our case, the bulk stress applied on the crystal was much bigger than the fluid pressure and the surface energy term, so that we can consider $\sigma_{\text{diff}} = 2\sigma_{\infty} = 2\sigma'$, where σ' is the effective stress. Another problem is that under non-hydrostatic stress, the circular cylindrical pore geometry ceases to be an equilibrium geometry, so that the linear stability analysis used for the calculation of the equilibrium shape of the hole can not be directly applied. However, the flattening of the hole observed in our experiments was slight, with a vertical to horizontal radius ratio always around 0.9.

Secondly, their model considers the fluid phase as saturated, in equilibrium with a stress-free solid matrix. Our experiments, however, were carried out in an undersaturated solution, so that none of the solid or fluid phases were in thermodynamic equilibrium. However, this second consideration has only an effect on the chemical potential of the fluid and causes no change in the formulation of the driving force (equation 1.1), and no change in the formulation of the equilibrium wavelength (equation 1.5). The undersaturation plays in our experiments only the role of the driving force for the roughening of the crystal surface, i.e. it induces the formation of the wavy perturbation on the initial flat surface.

Finally, we need also to note in their model that the kinetics of growth and dissolution of the surface are assumed to be controlled by surface reactions. Van der Hoek et al. (1983) have shown that the dissolution of K-alum is strongly influenced by surface processes at low undersaturation (up to $\sim 2^{\circ}\text{C}$, in their case the undersaturation was obtained by increasing the solution temperature). At high undersaturation, they found that volume diffusion is the dominant process. All our experiments were carried out at an undersaturation lower than 2°C (see Table 3.1), so that the assumption of a surface reactions controlled process is valid.

Let us now estimate how the surface of the stressed crystals would evolve accordingly to the model of Heidug & Leroy (1994) and Leroy & Heidug (1994).

We have seen that as the surface of the crystals used in our experiments was unstable, the crystals dissolved along low index crystallographic faces to get a lower surface energy. This process gave to the surface a "wavy" aspect, which can be considered as the "sinusoidal disturbance" of the model. Although the exact values of some of the parameters involved are not known for K-alum, let us calculate what will be the dominant wavenumber under the stress conditions used in the experiments.

According to van der Hoek et al. (1983), the surface energy of K-alum is a little bit larger than its edge free energy, which they found to be 0.01 Pa.m. We will use the value of $\gamma = 0.05$ Pa.m calculated from the Nielsen-Söhnle empirical relationship (Nielsen & Söhnle, 1971). For the Poisson ratio, we will take the average value of $\nu = 0.25$. Under these considerations, with a pore radius $R = 0.001$ m, an effective stress $\sigma = 7.5$ MPa (corresponding to a differential stress of 15 MPa, i.e. five times the bulk applied stress, see Chapter 2) and a Young modulus $E = 20$ GPa, the equation (1.5) gives a wavenumber $\xi = 211$. Dividing the perimeter of the pore by ξ , we get the wavelength of the equilibrium configuration $\delta = 30$ μm , what means an A-type groove width of 15 μm . This value is in quite good agreement with the distance separating the A-type grooves observed on both sides of the stressed holes.

3.4.2) Influence of small variations in the parameters.

The grooves that developed on both sides of the hole in our experiments developed on a flat surface (except those that propagated into the hole), so with $R = \infty$. As the wavelength of the equilibrium configuration is obtained by dividing the perimeter of the hole by the wavenumber, the pore radius has no influence on the calculation (the surface energy term is much smaller than the effective stress). We can thus also apply the theory of Heidug & Leroy (1994) and Leroy & Heidug (1994) to flat surfaces.

Variation of the Poisson ratio causes no significant change. An increase in the surface energy from $\gamma = 0.05$ Pa.m to $\gamma = 0.08$ Pa.m increases the width of the equilibrium grooves from $\delta = 15$ μm to $\delta = 24$ μm . An increase in the value of the stress from 7.5 MPa to 10 MPa, on the contrary, decreases this wavelength from $\delta = 15$ μm to $\delta = 8$ μm . This illustrates very well the opposite effect of surface energy and stress. The surface energy always tends to flatten the surface of the sample.

3.4.3) Relation between stress and A-type groove size.

Fig. 3.22 shows the variation of the distance between A-type grooves with an estimation of the stress in the regions of the crystals where they formed. The estimation of the stress was calculated by dividing the bulk load by the section of the crystal where the grooves formed, at the end of the experiments. In spite of a wide dispersion in the data, the tendency for $\{111\}$ and $\{100\}$ faces is a decrease in the wavelength with increasing stress. This is in agreement with the model of Heidug & Leroy (1994) and Leroy & Heidug (1994). The $\{110\}$ face shows a variation of the size of the grooves with the stress that is much less pronounced than for the other faces. However, the dispersion in the data does not allow the definition of a variation trend for this face. This difference in behaviour between the $\{110\}$ face and the other two ones is also reflected in the dependence of the wavelength of the grooves with the degree of undersaturation (Fig. 3.23). The smallest grooves were also observed on this face. This

result, and the observation that the $\langle 110 \rangle$ directions seem more affected by the stress (see Paragraph 3.2.2.3), suggests an influence of the surface energy.

3.5) Conclusions.

In this chapter, the effect of an applied compressive stress on the surface microstructures of potassium alum single crystals in contact with an aqueous potassium alum solution was investigated. We found that the roughness of the crystal surface played a key role, in the way that it caused a non-homogeneous elastic strain distribution on the surface, the strain being higher in concavities than on convexities. This roughness needed to be periodic, i.e. to have a characteristic wavelength. The roughness could be induced by dissolution of the crystals in undersaturated solution along low index crystallographic faces (thus forming B-type grooves), or by intentionally made scratches on the surface. In both cases, the non-homogeneous surface stress distribution led to an enhanced dissolution in the concavities and to a subsequent increase in the wavelength of the roughness. This was characterised by the development on the crystal surface of wide and deep dissolution grooves (A-type grooves) perpendicular to the maximum compressive stress direction. The observed stress-induced evolution of the surface microstructures could be described quite accurately with the theoretical model of Heidug & Leroy (1994) and Leroy & Heidug (1994). The instability caused by the non-homogeneous surface stress distribution is corrected by the growth of the roughness until a stable wavelength is reached, for which the crystal surface is in equilibrium with the aqueous solution under the local stress conditions. This stable configuration may hold as long as the stress stays in the range given by the equations (1.6) (see Chapter 1).

We noted that A-type grooves never formed in the tension regions, i.e. above and below the hole (see Fig. 3.6, to compare with the FLAC simulation of Fig. 2.7). This may be due to the fact that the stress there is about three times lower than on both sides left and right of the hole, so that the critical stress for the development of A-type grooves is never reached there.

We also observed an influence of the surface tension on the size of the A-type grooves which, for a given degree of undersaturation, are bigger on $\{100\}$ faces than on $\{110\}$ faces (Fig. 3.22 and 3.23). This influence of crystallography on the behaviour of stressed solid-fluid interface was also observed by Ristic et al. (1997) in growth experiments. These authors found on potassium alum single crystals subjected to tensile stress in oversaturated solution that the growth rate of both $\{100\}$ and $\{110\}$ faces was strongly affected by the stress, while the one of the $\{111\}$ faces showed almost no change. We found that A-type grooves developed mostly along $\langle 110 \rangle$ crystallographic directions, although these are the most abundant low index directions.

For experiments carried out under high stress, near the brittle failure strength, A-type grooves were observed to develop along all the PBC- directions and no more only along the PBC-direction that was oriented perpendicular to the maximum compressive stress direction. This process may lead to cataclastic deformation of the crystal.

We have reported in this chapter on a strong effect of the stress on the microstructural evolution of a crystal-solution interface. The effect observed was a pure elastic effect. Now what can be the effect of stress on the dissolution rate of crystals?

experim.	orien	stress	σ_b (MPa)	σ_h (MPa)	under satura (°C)	temp. (°C)	durat (hr)	inter groove dist. (μm)	groove orient.	groove shape
60KAD10	{110}	<111>	1.2	4.7	0.5	19.7	22	28-70	B	straight
55KAD7	{110}	<100>	1.8	5	0.7	19.1	24	14-20	B	straight
50KAD2	{110}	<100>	2.2	7	1.5	35.3	14.5	26-33	B	straight
52KAD4	{110}	<100>	2.2	7	1.5	19.2	21	18-24	B	straight +ST
49KAD1	{110}	<100>	2.4	9.5	1.5	35.0	23.5	20-29	B	ST
77KAD17	{110}	<100>	2.5	9.5	0.5	20.1	19.5	41-70	B	straight
51KAD3	{110}	<100>	3	9.5	1.5	35.0	24	26-31	B	straight
56KAD8	{110}	<100>	3.2	9.5	0.5	19.5	23.5	13-23	B	ST
76KAD16	{110}	<110>	3.9	12.5	0.2	20.2	73	50-90	A(+B C)	straight
59KAD9	{110}	<110>	4.2	12.5	0.3	19.7	97	70-120	AB+2 C	catacla +ST
53KAD5	{111}	<110>	2.3	7	0.2	19.5	42.5	50-70	2B	straight
54KAD6	{111}	<111>	3.9	14	0.5	19.2	23	19-23	B	straight +ST
89KAD26	{100}	<110>	?	7.5	0.6	22.0	20	22-30	B	straight +ST
85KAD23	{100}	<110>	2.7	8	0.4	21.3	54	23-36	B	ST
82KAD22	{100}	<110>	2.7	10	0.2	20.0	164	45-70	B	ST
80KAD20	{100}	<110>	3.5	10	0.5	20.3	15.5	30-40	B	ST
79KAD19	{100}	<250>	3.6	10	0.4	20.2	22	19-44	AB	straight

Table 3.1. Experimental conditions for all the experiments carried out on potassium-alum crystals. Bulk stress and hoop stress on both sides of the hole are noted respectively as σ_b and σ_h . Crystallographic orientation of dissolving faces, direction of bulk applied stress and orientation of the grooves is deduced from the observation of fluid inclusions with negative crystal shape. A: PBC along <100>; B: PBC along <110>; C: PBC along <111>; <250>: direction between <100> and <110>. ST: maximum compressive stress trajectories.

experim.	orient	stress	σ_b (MPa)	σ_h (MPa)	under satura (°C)	temp. (°C)	durat. (hr)	inter groove dist. (μm)	groove orient.	groove shape
ISKAL1	{100}	<110>	2.8	10	0.3	21.2	95	35-65	<110>	ST
ISKAL2	{110}	<100>	2.4	10.5	1	21.5	26	80-100	<110>	straight
ISKAL3	{111}	<100>	incr. by step to 7.1	incr. by step to 21	0.3	21.2	118	30-75	<110>	straight
ISKAL4	?	?	5	5	0	21.2	17	20-25	?	straight
ISKAL5	{110}	<110>	incr. by step to 7.7	incr. by step to 23	0.3-1	23	168	30-75	<100>	straight netw.
ISKAL6	{111}	<111>	incr. by step to 12	incr. by step to 12	0.3	23	93	no groove		

Table 3.2 Experimental conditions for all the in-situ experiment on potassium alum. Bulk stress and hoop stress on both sides of the hole are noted respectively as σ_b and σ_h . Crystallographic orientation of dissolving faces, direction of bulk applied stress and orientation of the grooves are deduced with the help of fluid inclusions with negative crystal shape, except for experiment ISKAL4 for which the crystal broke accidentally.

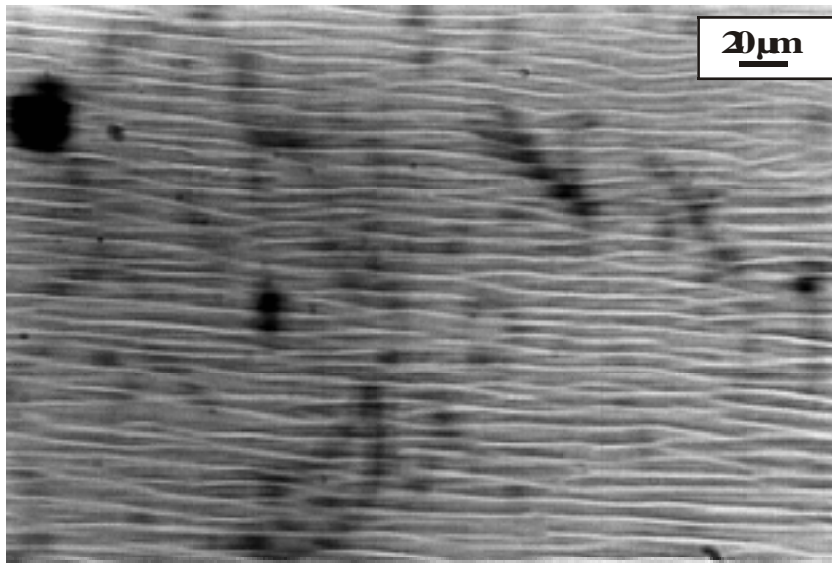


Fig. 3.1 Optical micrograph of a stress-free crystal surface oriented parallel to $\{110\}$ (to within approximately 10°) and parallel to the unloaded piston (experiment 50KAD2). The surface shows an anastomosing pattern of fine etch grooves oriented approximately parallel to $\langle 110 \rangle$ -directions. Undersaturation was 1.5 ± 0.2 °C, duration of experiment 14.5 hours.

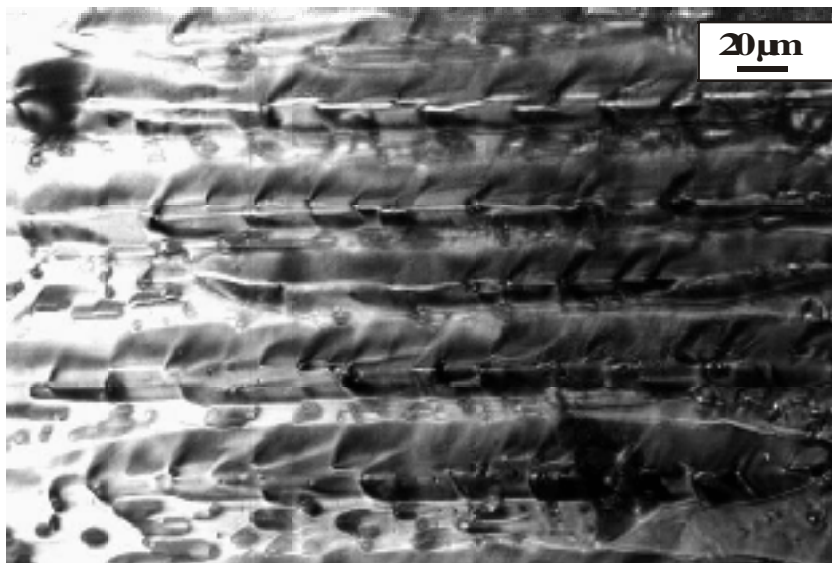


Fig. 3.3 Optical micrograph of a stressed crystal surface in experiment 50KAD2 and with the same orientation as above. The surface shows much larger etch grooves oriented approximately parallel to $\langle 110 \rangle$ -directions and perpendicular to the applied stress. Bulk stress was 2.2 ± 0.2 MPa (up to about 7 MPa around the hole) and applied vertically.

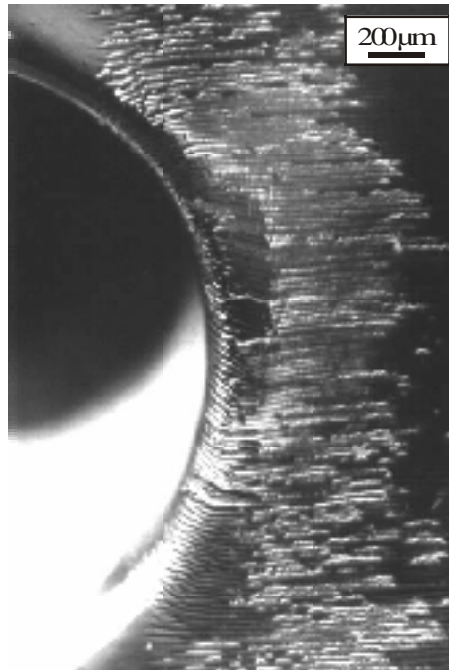


Fig. 3.2 Micrograph in reflected light showing A-type grooves on the side of the hole (experiment 52KAD4). These are parallel to each other and perpendicular to the bulk applied stress. Undersaturation was 1.5 ± 0.2 °C, bulk stress was 2.2 MPa.

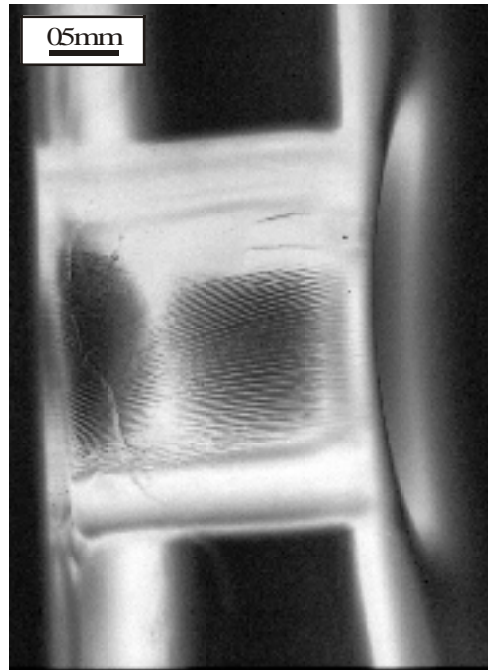


Fig. 3.4 Optical micrograph illustrating that A-type grooves also develop inside the central hole (experiment 51KAD3). Undersaturation was 1.5 ± 0.2 °C, bulk stress was 3 MPa, applied vertically.

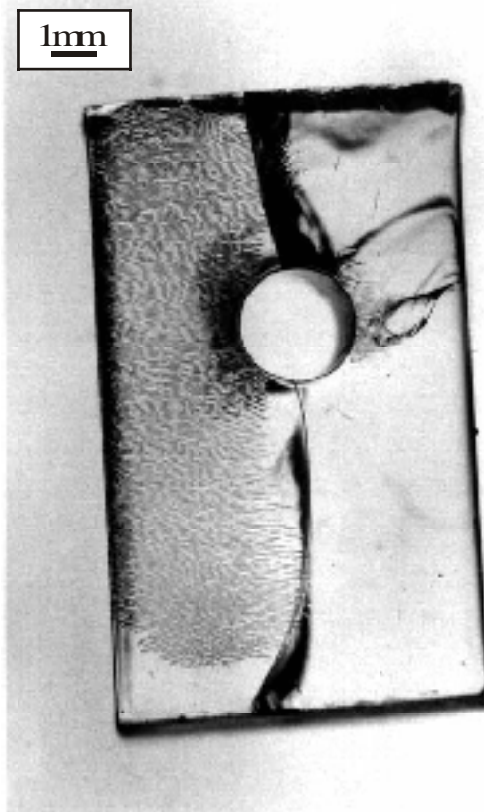


Fig. 3.5 Optical micrograph showing the entire sample 53KAD5 with faces parallel (to within 10°) to $\{111\}$. The sample fractured at the beginning of the experiment, just after loading. The left side of the fracture underwent more stress and A-type grooves developed over the entire surface. On the right side of the fracture, A-type grooves only developed in the vicinity of the hole. Undersaturation was 0.2 ± 0.2 °C. Bulk stress at the end of the experiment was 5.4 MPa on the left side of the fracture, 4 MPa on the right one.

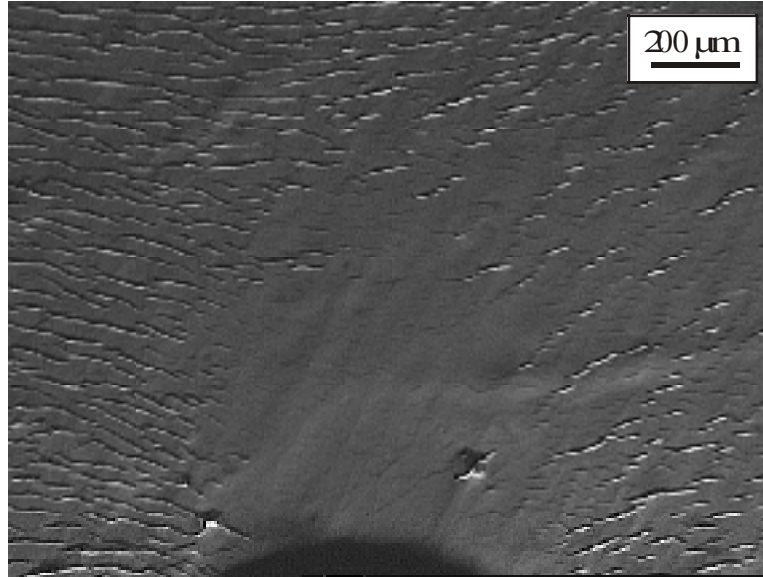


Fig. 3.6 In-situ micrograph illustrating that the tension region above the hole is free of A-type grooves, whereas these grooves have developed everywhere else on the surface. The hole was 1 ± 0.05 mm in diameter (experiment ISKAL5). Undersaturation was 0.2 ± 0.2 °C, bulk stress was 7 MPa, applied vertically.

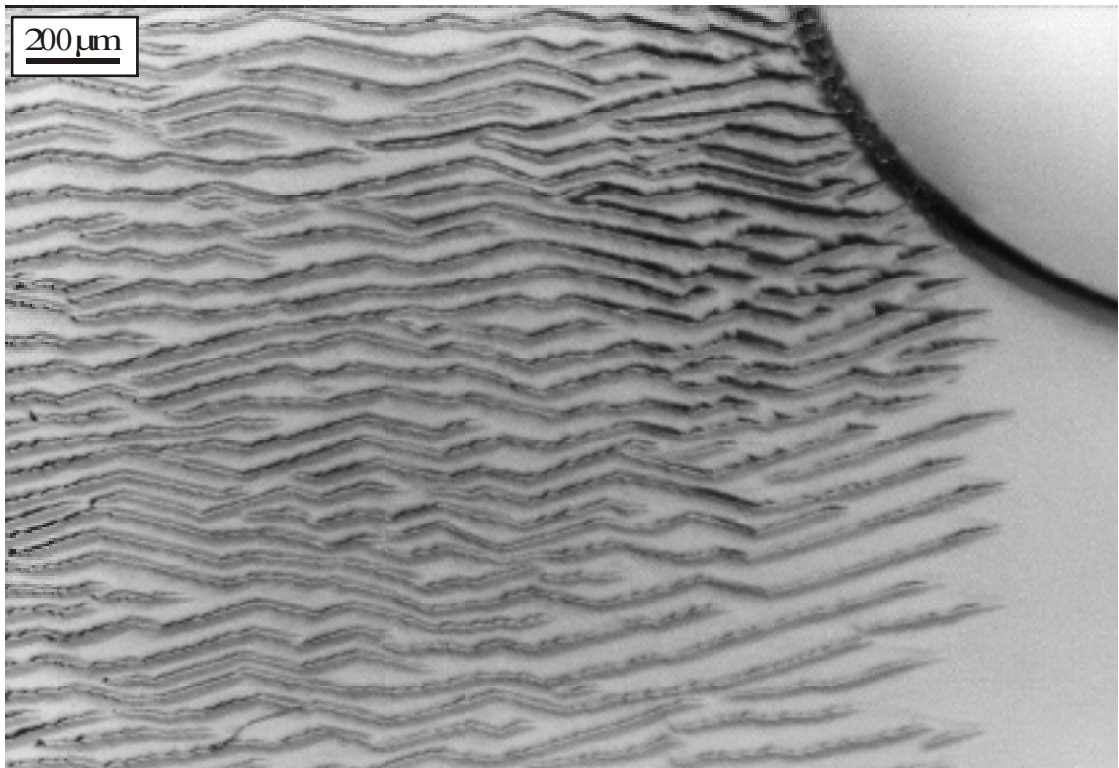


Fig. 3.7 Optical micrograph showing "zig-zag" shaped A-type grooves in the vicinity of the hole (visible in the upper right corner). Grooves are about 30 μm wide and 50-70 μm apart from each other. Undersaturation was 0.2 ± 0.2 $^{\circ}\text{C}$, bulk stress 2.3 MPa, applied vertically (experiment 53KAD5).

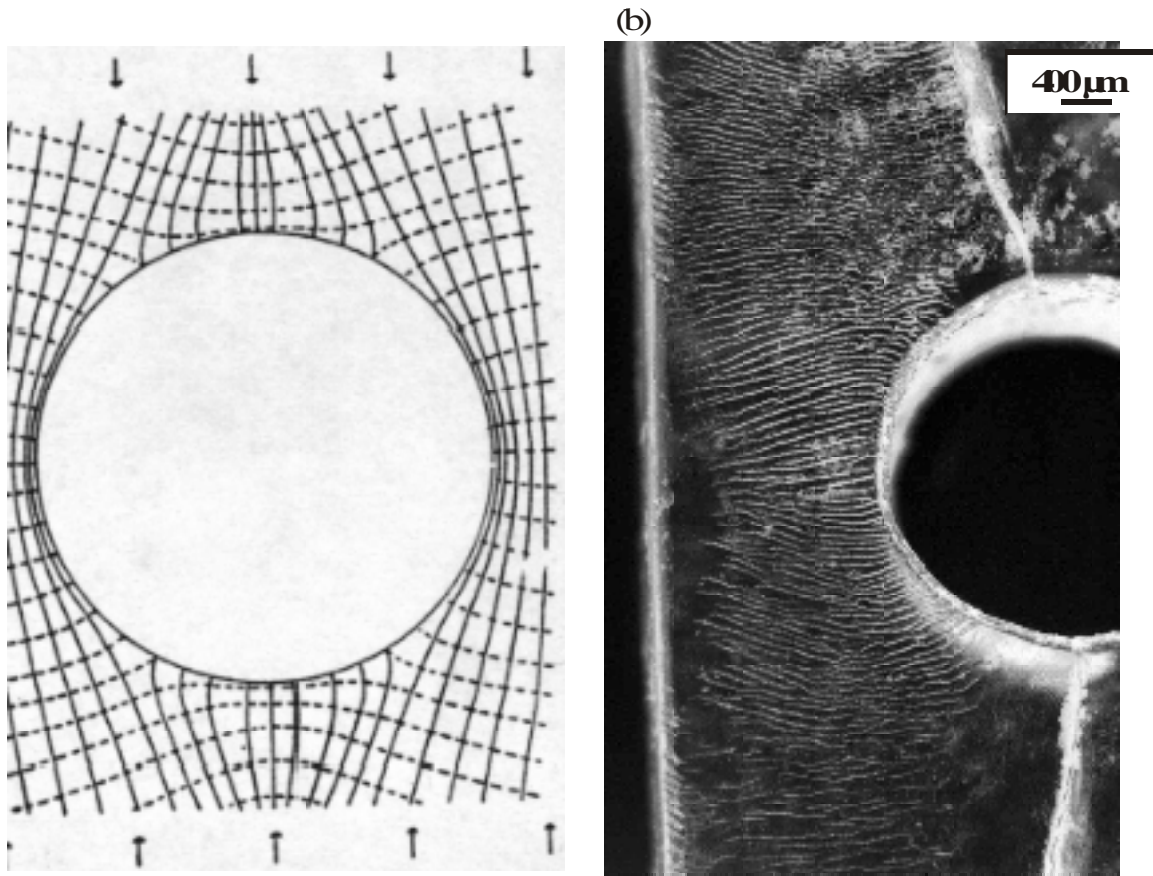


Fig. 3.8 Comparison between (a) the theoretical stress trajectories around a hole (picture copied from Jaeger, 1969) and (b) the A-type groove pattern on the side of the hole on a crystal surface oriented close to $\{100\}$ faces (experiment 82KAD22). Undersaturation was 0.2 ± 0.2 °C, bulk stress was 2.7 MPa, applied vertically.

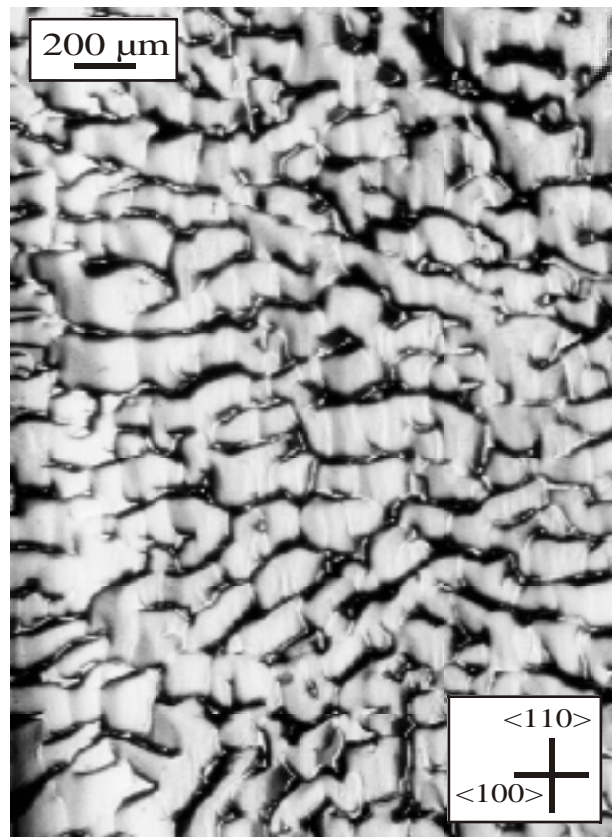


Fig. 3.9 Optical micrograph showing the cataclastic deformation of the crystal surface in the vicinity of the hole (not visible but located on the left). The surface was oriented parallel (to within 10°) to $\{110\}$ faces. A-type grooves developed preferentially perpendicular to the bulk applied stress (vertical), in that case along a $\langle 100 \rangle$ -direction, but also parallel to it (along a $\langle 110 \rangle$ -direction) and even with an angle of about 45° to it. This is probably due to the high bulk stress (4.2 MPa) used in this experiment (experiment 59KAD9). Undersaturation was 0.3 ± 0.2 °C.

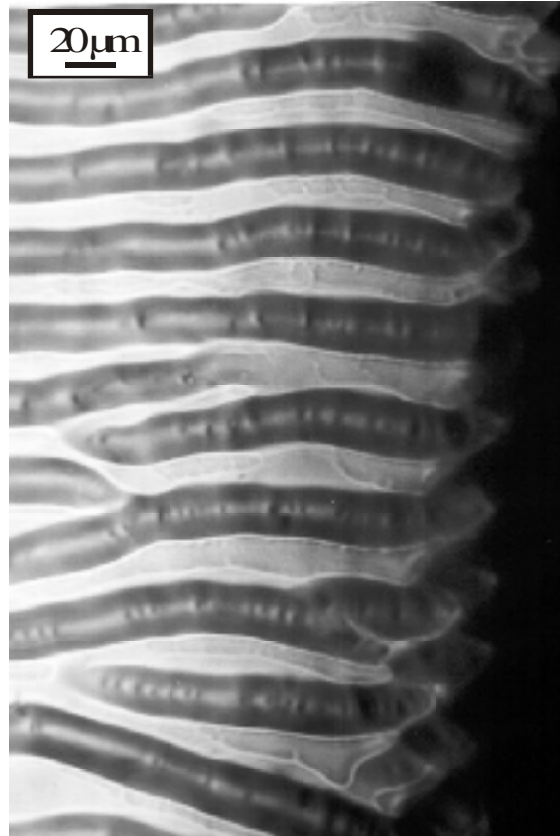


Fig. 3.10 Optical micrograph showing A-type grooves at the rim of the hole, where they form 10-40 μm deep teeth (experiment 80KAD20). Undersaturation was $0.5 \pm 0.2^\circ\text{C}$, bulk stress was 3.5 MPa, applied vertically.



Fig. 3.11 Optical micrograph showing the faceting of the A-type grooves at the rim of the hole (experiment 53KAD5). The orientation of the sample could be inferred from the facets. Undersaturation was 0.2 ± 0.2 °C, bulk stress was 4 MPa. The orientation of the face was close to $\{111\}$ faces.

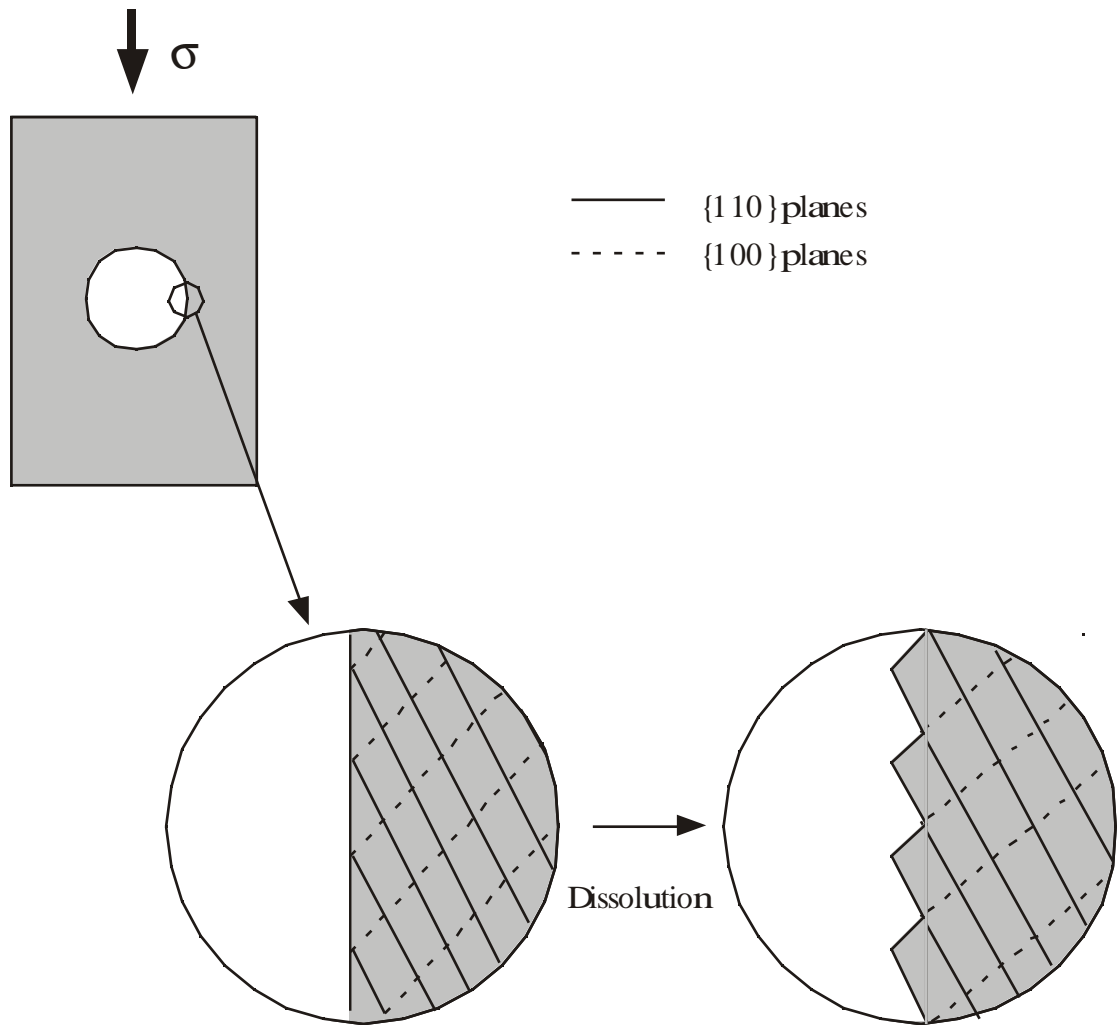


Fig. 3.12 Schematic illustration of the supposed formation of the dissolution grooves along the intersections between crystallographic planes.



Fig. 3.13 Illustration of the localisation of the elastic strain in grooves made visible by photoelasticity in a Plexiglas model about 3 x 3 x 1 cm in size. Stress was applied vertically.

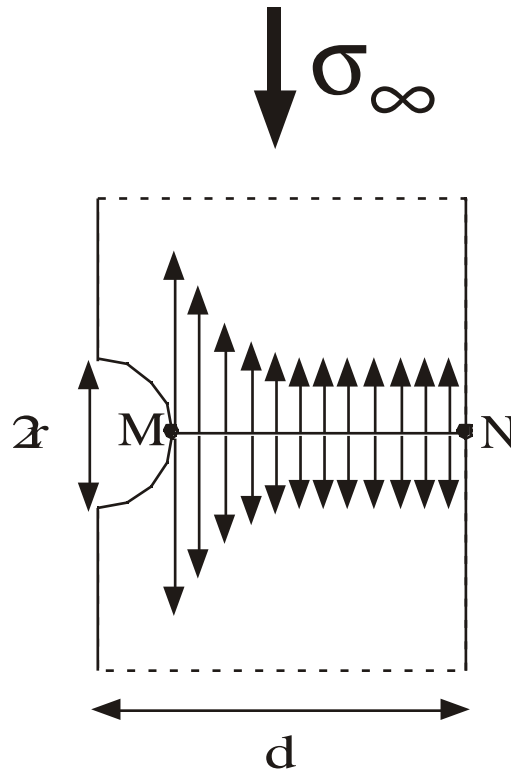


Fig. 3.14 Schematic representation of the stress distribution on a line MN on the side of a semi-circular groove in a plate submitted to uniaxial compression. The stress at point M is k times higher than in the middle of the line MN (see text).

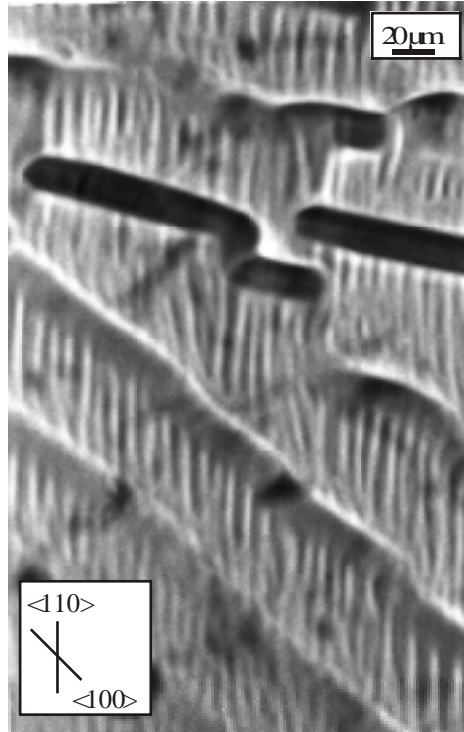


Fig. 3.15 Optical micrograph of a crystal surface oriented close to $\{110\}$ faces (experiment 76KAD16b). Bulk stress was 3.9 MPa, applied vertically. Undersaturation was 0.2 ± 0.2 °C. The large white grooves developed along a $\langle 100 \rangle$ -direction, which was for this experiment the PBC the most perpendicular to the bulk applied stress. Smaller grooves developed along a $\langle 110 \rangle$ -direction, roughly parallel to the bulk stress. The large black grooves on the left have an orientation between $\langle 100 \rangle$ and $\langle 110 \rangle$ and are oriented close to the perpendicular to the bulk applied stress.

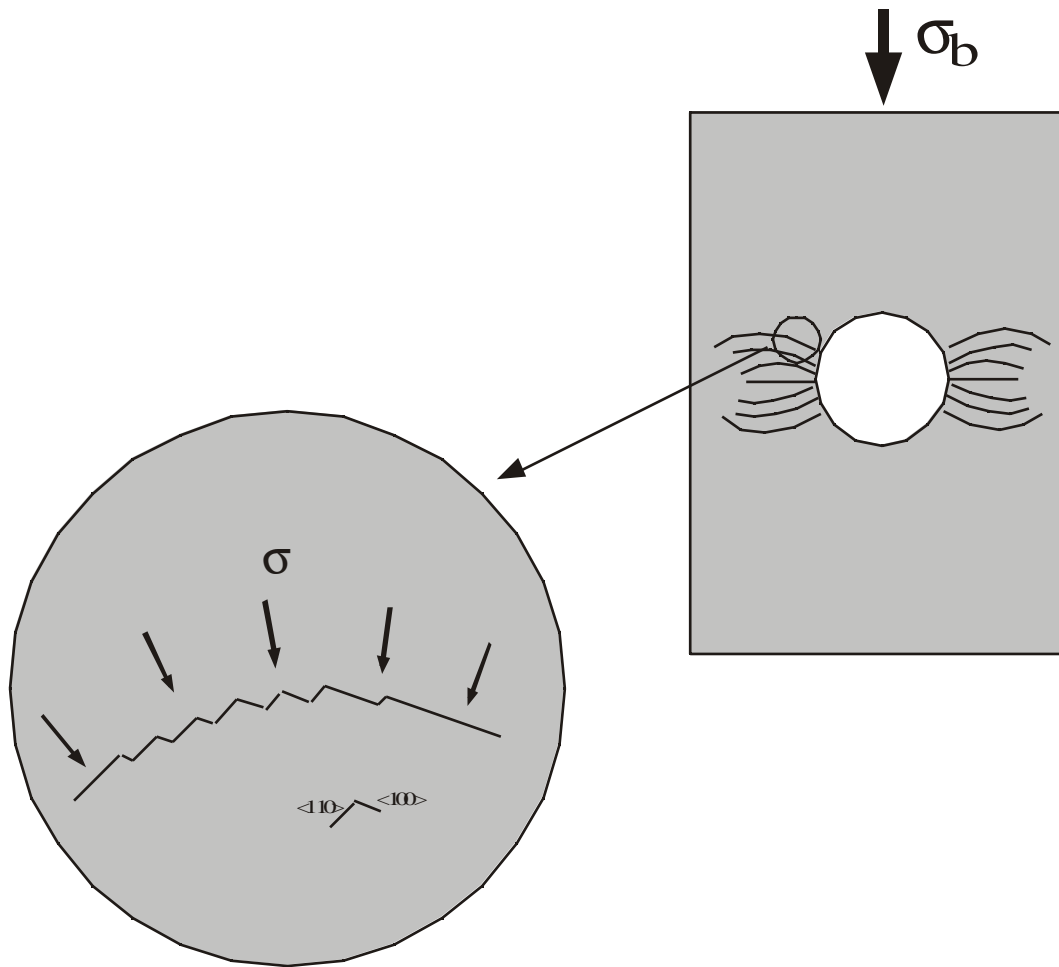
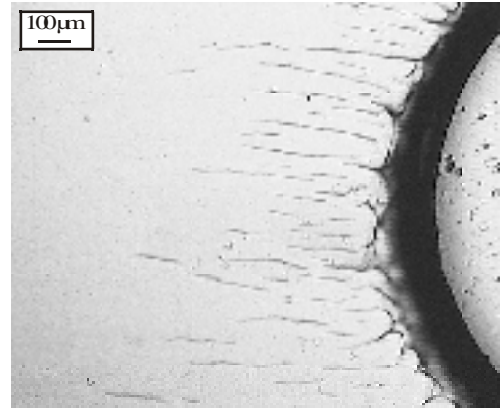


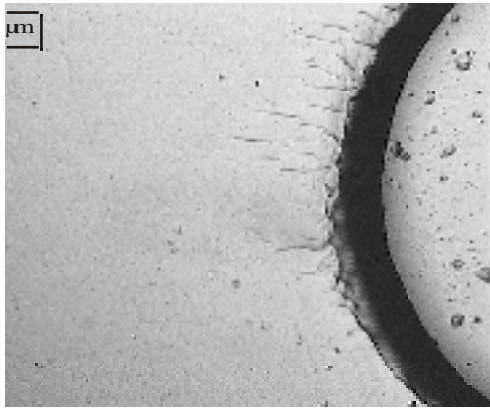
Fig. 3.16 Cartoon illustrating the curvature of a A-type groove caused by the change in the direction of maximum compressive stress on the side of the hole. The PBC (A-PBC parallel to $\langle 100 \rangle$ or B-PBC parallel to $\langle 110 \rangle$) the most perpendicular to the maximum stress direction is assumed to be the one where the dissolution is the fastest.



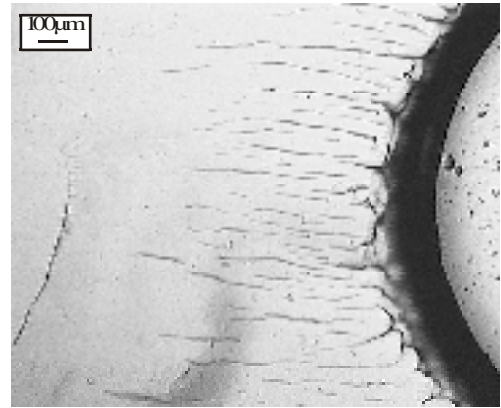
t=0



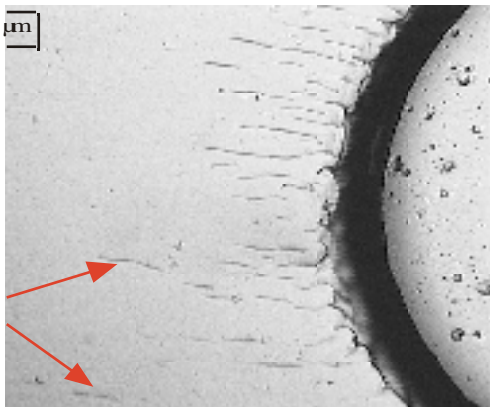
t=71.25 hr



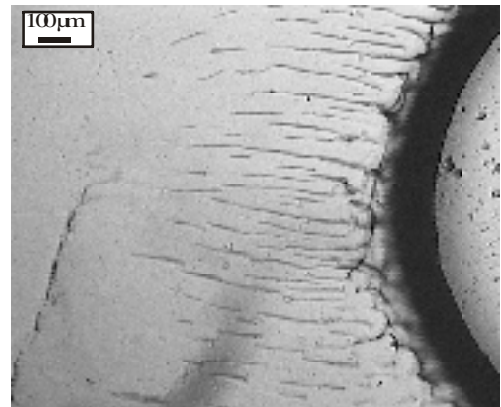
t=24 hr



t=72.5 hr



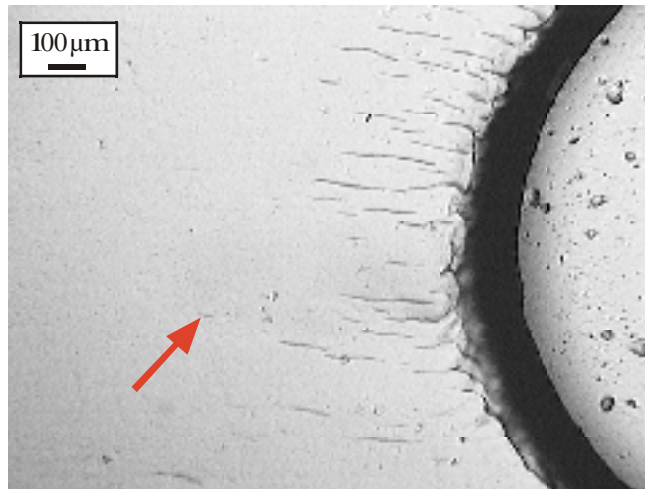
t=48 hr



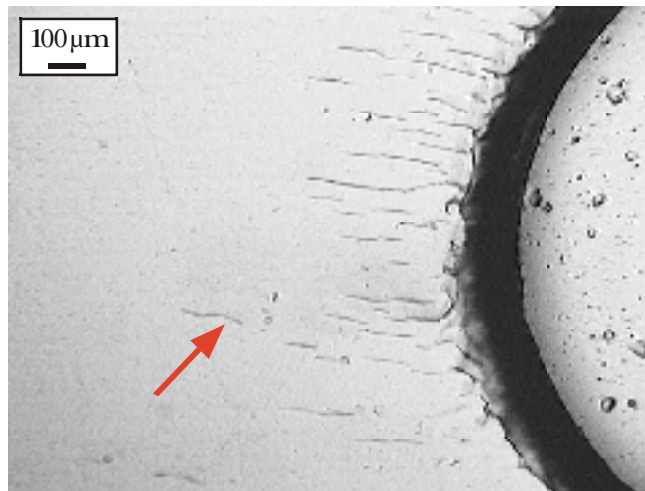
t=100 hr

Fig. 3.17 Time sequence of micrographs made in-situ, i.e. under the microscope during the experiment, showing the development of the A-type grooves on the side of the hole (experiment ISKAL1). Some isolated grooves that formed far from the hole (arrows) join together with others that propagate from the rim of the hole. Note the curvature of the originally straight grooves after development of the fracture. The bulk stress was 2.8 MPa and applied vertically.

t=38.75 hr



t=43.75 hr



t=53.75 hr

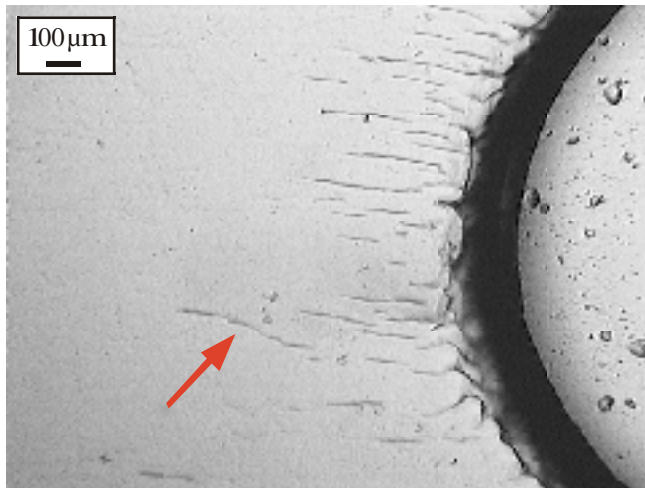
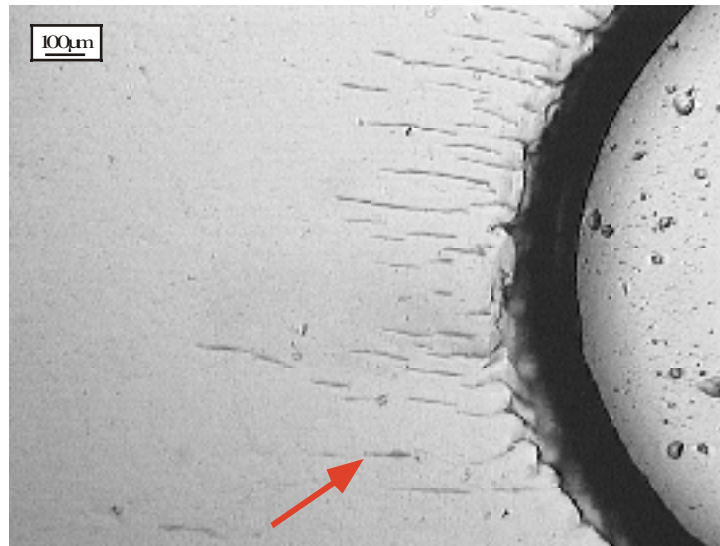
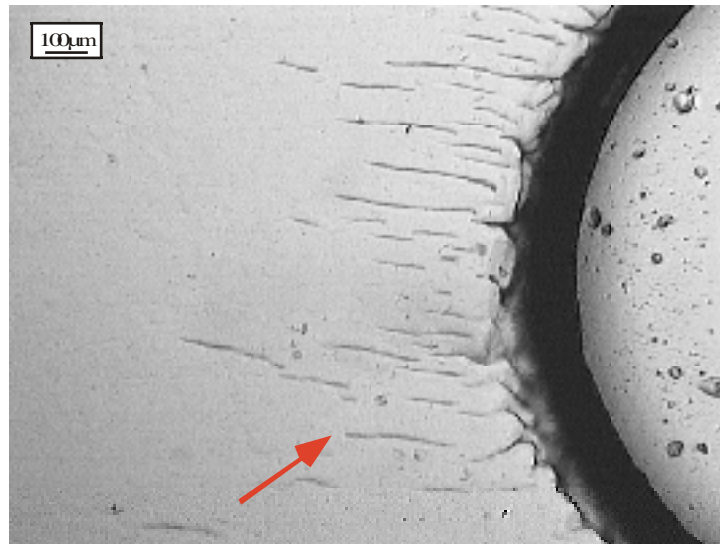


Fig. 3.18 Micrographs made in-situ showing the junction of two A-type grooves during experiment ISKAL1 (see arrow.). The bulk stress was 2.8 MPa and applied vertically.

t = 50 hr
 $\Delta y = 0 \mu\text{m}$



t = 60 hr
 $\Delta y = 47 \mu\text{m}$



t = 66.25 hr
 $\Delta y = 67 \mu\text{m}$

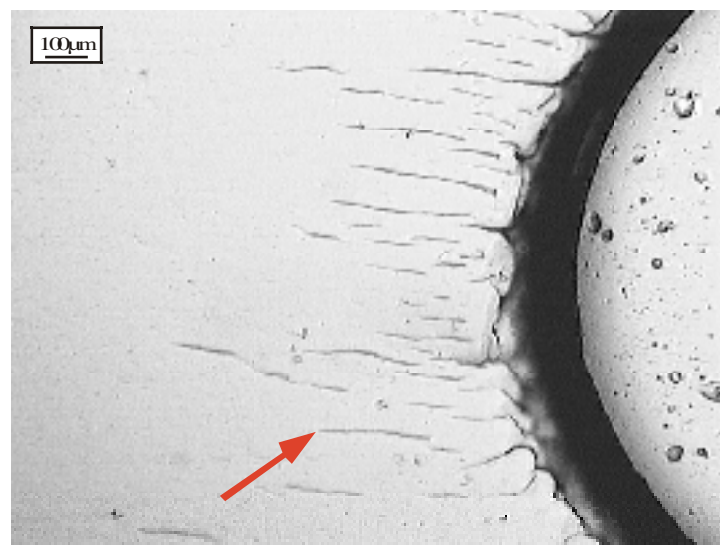
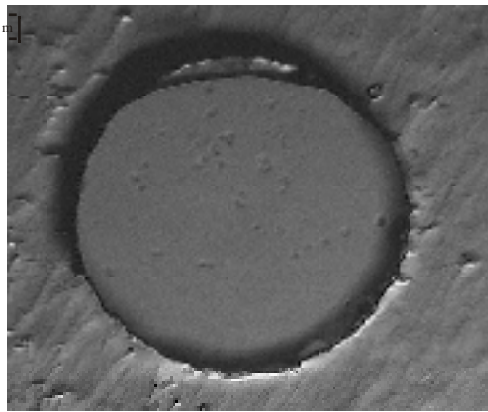
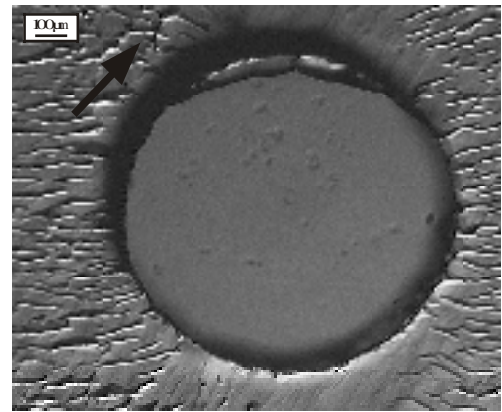


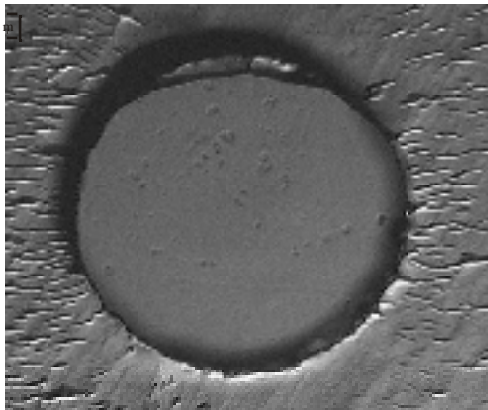
Fig. 3.19 Micrographs made in-situ showing the vertical displacement Δy from the bottom of the micrographs of a A-type groove (see arrow.) during experiment ISKAL1. The bulk stress was 2.8 MPa and applied vertically.



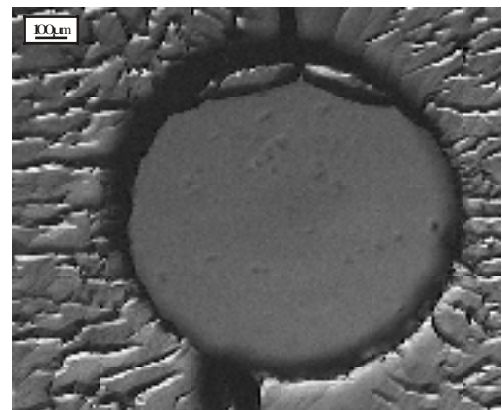
$t = t_0, \sigma_b = 3 \text{ MPa}$



$t = t_0 + 24 \text{ hr}, \sigma_b = 6.7 \text{ MPa}$



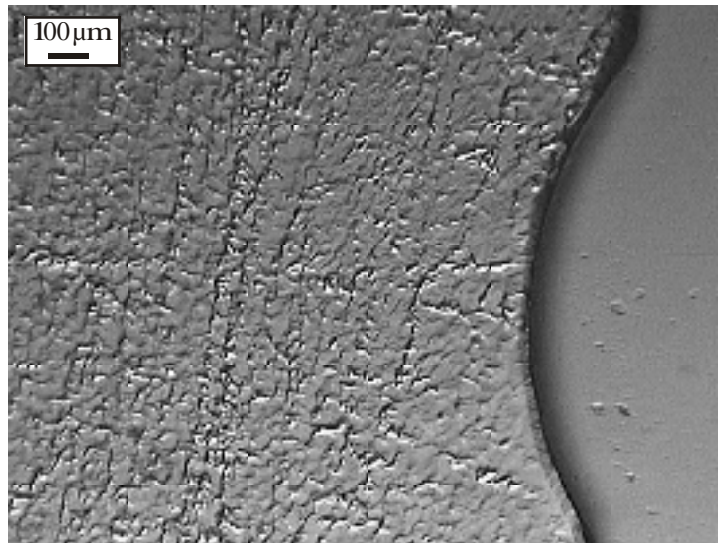
$t = t_0 + 4.5 \text{ hr}, \sigma_b = 4.7 \text{ MPa}$



$t = t_0 + 72 \text{ hr}, \sigma_b = 7.1 \text{ MPa}$

Fig. 3.20 Time sequences showing the development of the dissolution grooves on both compressive sides of the hole as a function of the bulk stress σ_b . The hole was 1 mm in diameter (experiment ISKAL5). The bulk stress was applied vertically.

t=0



t=1 hr

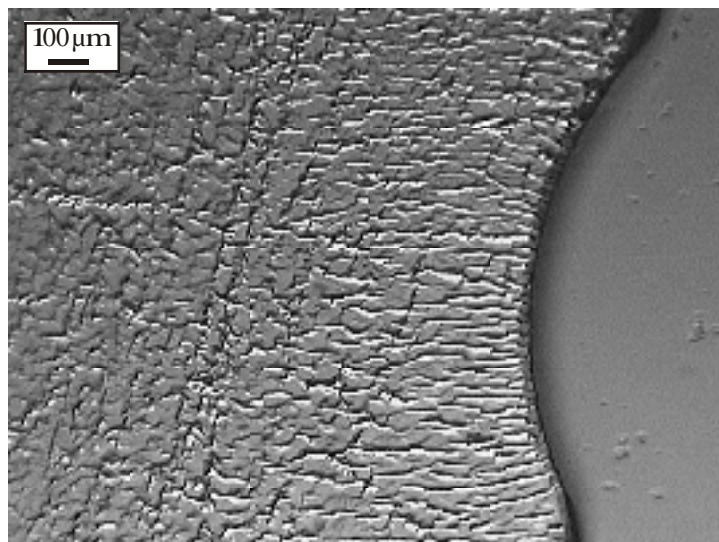


Fig. 3.21 Micrograph made in-situ showing the formation of A-type grooves from scratches intentionally made on the crystal surface (experiment ISKAL4). The grooves propagated outwards from the rim of a circular concavity on the crystal surface. The aqueous solution was saturated (± 0.1 °C). The bulk stress was 5 MPa and applied vertically.

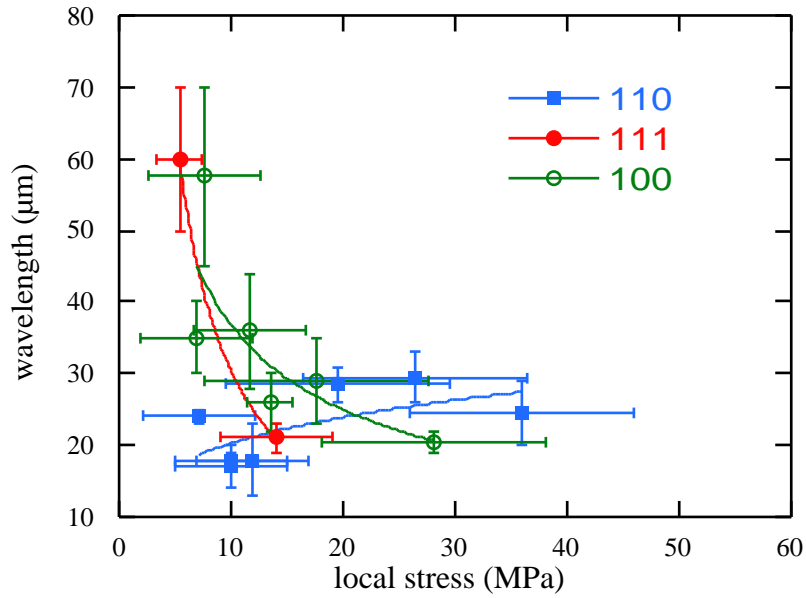


Fig. 3.22 Graph showing the wavelength of the dissolution groove pattern as a function of the calculated local stress for the {111}, {100} and {110} crystal faces.

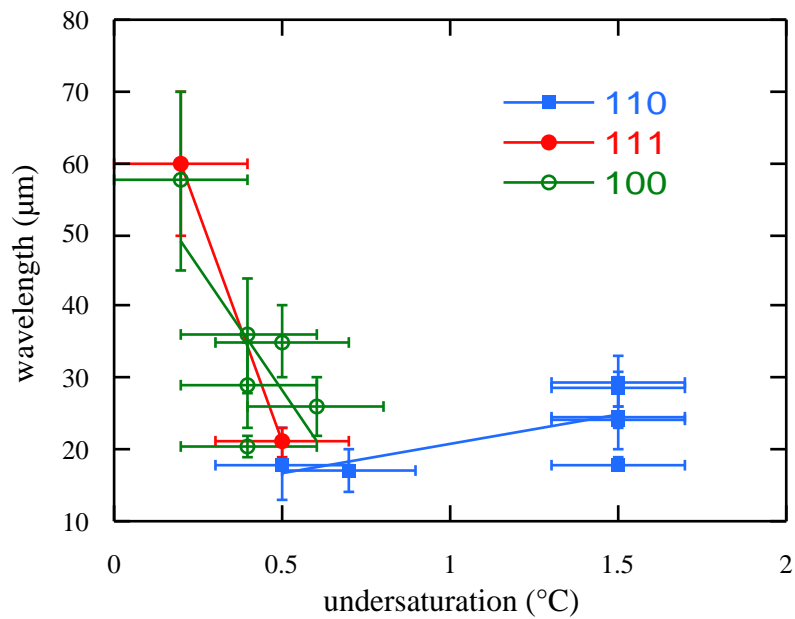


Fig. 3.23 Graph showing the wavelength of the dissolution groove pattern as a function of the degree of undersaturation for the {111}, {100} and {110} crystal faces.

Chapter 4 Dissolution rate of sodium chlorate.

We will in this chapter focus our interest on the influence of the stress on the kinetics of dissolution. The experimentally observed increase in the dissolution rate of single sodium chlorate crystals due to the applied compressive stress is one to two orders of magnitude bigger than theoretical predictions based on the bulk elastic stored energy. The cause for this increased dissolution rate is discussed and related to the results obtained in Chapter 3.

4.1) Experimental Procedures.

Samples preparation and experimental procedures are described in detail in Chapter 2. However, as the goal of the experiments presented in this section was different from the one from the former chapter, we need to mention a few important differences. Firstly, we had to take care of a possible influence of the stirring on the dissolution rate of the crystals. The two possible positions for the crystals, shown in Fig. 2.4, were noted as position A and position B.

Secondly, sodium chlorate has a solubility about 9 times higher than K-alum. The experiments were for this reason shorter to avoid the breakage of stressed crystals. Experiments ran over 2-5 hours for high undersaturations ($S \geq 0.6 \%$), and ~20 hours for low undersaturations ($S < 0.6 \%$).

At the end of each experiment, the crystals were carefully taken out of the solution, immediately washed in ethyl acetate and then dried with a cleaning tissue.

Finally, the dissolution rates were calculated by measuring under optical microscope the change in the size of the hole in the horizontal as well as in the vertical direction, and plotted as a function of the stress and undersaturation. The stress on both sides of the hole was estimated as described in Chapter 2.

4.2) Results

The dissolution rates estimated in directions parallel and perpendicular to the applied stress for stressed and stress-free crystals are given in Table 4.1. Obviously, both stressed and stress-free holes got bigger with increasing undersaturation. For almost

every experiment, the highest dissolution rates were measured in the horizontal direction. This was the case for stressed crystals as well as for stress-free ones. The average vertical to horizontal dissolution rates ratio was 0.89 for stress-free crystals and 0.87 for stressed ones. The cross section of the holes at the end of the experiments was elliptical, with the longest axis in the horizontal and the shortest in the vertical direction. Along the axis of the holes, no variation in shape was observed. Material dissolved also from the sides of the crystals (Fig. 4.1).

We found that crystals placed at position A dissolved faster than those placed at position B. This was true for stressed and stress-free crystals. The difference in dissolution rates between both positions increased with increasing undersaturation, reaching ~30% at an undersaturation of 2.4% (Fig. 4.2). For a given position and a given undersaturation, stressed crystals were found to dissolve faster than stress-free ones. This was true for the direction perpendicular, as well as for the direction parallel to the applied stress (Table 4.1). The dissolution rate increased linearly with increasing stress (Fig. 4.3). For a given position and a given stress, the stress effect on the dissolution rate increased with increasing undersaturation. The increase in dissolution rate due to a bulk stress $\sigma_b = 3.8 \pm 0.3$ MPa, corresponding to $\sigma_h = 10.5 \pm 1$ MPa on both sides of the hole, as a function of the undersaturation, is shown in Fig. 4.4. At an undersaturation of 2.4 %, the stressed crystal dissolved ~1.25 times faster than the stress-free crystal.

4.3) Discussion

The data show good agreement between the dissolution rates for the stress-free crystals and dissolution rate values on stress-free sodium chlorate crystals published in the literature (Fig. 4.5). The wide dispersion in the data from Kitamura et al. (1982) illustrates the strong dependence of the dissolution rate on experimental conditions. A slight difference between the distances from positions A and B to the stirrer, or a slight asymmetry of the paddle, may be responsible of the difference in dissolution rates between both positions observed in our experiments. Crystals placed in position A may have undergone a stronger flow than those placed in position B, and dissolved faster. For a given position, however, stressed crystals dissolved faster than stress-free ones. The increased dissolution rate due to the stress was bigger with increasing undersaturation, and varied linearly with the stress.

Theoretically, the increase in dissolution rate due to the increase in bulk stored elastic energy should be much smaller than our experimental results, and should be proportional to the square of the stress. Let us estimate how much would the dissolution rate at the compressive sides of the hole theoretically increase by increasing the stress on the crystal by 3 MPa in a solution undersaturated to 2.4% at a temperature of 23 °C?

Assuming linear elastic (i.e. hookean) behaviour, the increase in stored elastic energy $\Delta U_{\text{elastic}}$ due to increasing the differential stress by an amount of $\Delta\sigma$ is given by equation (4.1):

$$\Delta U_{\text{elastic}} = \frac{(\Delta\sigma)^2 V_m}{2E}$$

where E is the Young modulus and V_m the molar volume. For sodium chlorate, E is 43.67 GPa and V_m is $4.3 \times 10^{-5} \text{ m}^3 \cdot \text{mol}^{-1}$. For a differential stress of 3 MPa on the entire crystal, the differential stress on both compressive sides at the periphery of the hole should be ~ 15 MPa (considering a perfect symmetrical crystal), corresponding to an increase in stored elastic energy of $\sim 0.1 \text{ J} \cdot \text{mol}^{-1}$.

The driving force induced by the undersaturation is given by equation (4.2):

$$\Delta\mu = RT \ln \frac{C_0}{C}$$

where R is the gas constant, T is the absolute temperature, C is the concentration of the solution and C_0 is the saturation concentration. C , C_0 , and $S = (C_0 - C / C_0)$ were calculated using the solubility equation for sodium chlorate given in Chapter 2.

The driving force for dissolution at an undersaturation of 2.4% and a temperature of 23 °C would then correspond to $\sim 60 \text{ J} \cdot \text{mol}^{-1}$, i.e. ~ 600 times the driving force due to the elastic distortion ($\sim 0.1 \text{ J} \cdot \text{mol}^{-1}$). A driving force for dissolution of $\sim 0.1 \text{ J} \cdot \text{mol}^{-1}$ would be provided by an undersaturation of only 0.005%.

Assuming a linear variation of dissolution rate as a function of undersaturation for stress-free crystals (Fig. 4.2), a driving force of $\sim 0.1 \text{ J} \cdot \text{mol}^{-1}$ would correspond to an increase in the dissolution rate of the order of $1 \text{ mm} \cdot \text{hr}^{-1}$. Experimentally, however, the dissolution rate of a crystal submitted to a bulk stress of 3 MPa at an undersaturation of 2.4% (see Table 4.1, experiment 100CHLO20) was $162.9 \text{ } \mu\text{m} \cdot \text{hr}^{-1}$, while the dissolution rate of a stress-free crystal at the same undersaturation was $120 \text{ } \mu\text{m} \cdot \text{hr}^{-1}$. This means an increase in dissolution rate 43 times bigger than theoretically predicted. The effect of the stress on the dissolution rate for each of the experiments was found to be one to two orders of magnitude higher than theoretically predicted.

Our results do not allow to correlate the variation in stress around the hole to the observed difference between vertical and horizontal dissolution rates. Indeed, although the stressed holes are bigger, the stress-free holes showed after experiment an average degree of ellipticity equal to the stressed ones. This means that the ellipticity developed by the stressed holes is not a crystal plastic effect, because the stress-free holes show

the same shape. Moreover, the length of the crystals was measured before and after each experiment with a precision of 0.01 mm. None of the stressed samples appeared to have been shortened to within the measurement resolution. The ellipticity developed by the holes was also observed by Bosworth (1981), who attributed this effect to a stratification of the solution concentration due to gravity. This may also have happened in our experiments, due to a too slow stirring. It is thus wiser in our case to consider preferentially horizontal dissolution rates, as done in Fig. 4.2-4.5.

The increase in dissolution rate observed on the stressed crystals is then a purely elastic effect. No crystal plastic deformation occurred. This result supports the results obtained by Ristić et al. (1997b). They found that the growth rate of {100} faces of a potassium alum crystal elastically stressed in tension under 0.1 MPa and at an oversaturation of 6.47% was 1.2 times slower than when the crystal was left stress-free. The growth of some crystal faces could even be stopped by the application of a strong tensile stress. These authors suggested that elastic strain could affect the way the growth centres develop and propagate. Our results support this idea and suggest that this could be also the case for dissolution centres. This may be understood by considering that, during dissolution (or growth), the crystal surface does not stay flat but roughens. Concavities on the surface develop at sites of high surface energy, such as dislocation outcrops, impurities or fluid inclusions (for growth, convexities develop by the formation of growth hillocks). This leads for crystals placed under stress to a non-homogeneous elastic strain distribution on the surface, the strain being higher in the concavities. The results obtained in this work and described in Chapter 3 show the importance of the rugosity of a stressed crystal surface on the dissolution process. We think that due to the high elastic strain concentration, the velocity of the dissolution steps in the concavities is increased, causing an increase in the dissolution rate. With increasing undersaturation, the number of high surface energy sites activated as dissolution centres might increase, such as was experimentally demonstrated for potassium alum by Van der Hoek et al. (1983). The effect of the stress on the dissolution rate might therefore be stronger.

The observed linear dependence of the dissolution rate on the stress may be explained by considering the mobility of the dissolving particles. The velocity of a solid-fluid interface can be described as the product of two terms, the first corresponding to the kinetically driven instability term (related to the mobility), and the second corresponding to the energetically driven instability or "driving force" term (Barvosa-Carter et al., 1998). Recent studies on the behaviour of stressed interfaces between crystalline and amorphous silicon have shown that the mobility depends on the stress, such that the kinetically driven instability linearly depends on the stress (Aziz et al., 1991; Barvosa-Carter et al., 1998). The "driving force" term, on the other hand, varies as the square of the stress through the increase in the bulk stored elastic energy (equation 4.1). Yu & Suo (2000) have demonstrated theoretically that the effect of the stress on the mobility, and thus the linear dependence on stress of the surface reactions velocity, increases with increasing driving force. The strong effect of the stress on the dissolution rate observed in our experiments suggests that the occurring driving force for dissolution could be much higher than theoretically predicted and strongly affect the mobility of the dissolving particles.

4.4) Conclusion

Our results show that mechanically induced compressive elastic strain can significantly affect the dissolution rate of crystals in solution. The application of compressive stress during the dissolution of single sodium chlorate crystals increases their dissolution rate by one to two orders of magnitude more than theoretically due to the increase in bulk stored elastic energy. Now, the effect of the stress on the dissolution rate depends on the degree of undersaturation. We suggest that by increasing the degree of undersaturation, the number of surface defects activated as dissolution centres is increased, what leads to an increase in the non-homogeneity of the stress distribution on the surface. The dissolution is enhanced at the dissolution centres, where the elastic strain is the highest, and the dissolution rate of the entire crystal is increased. The linear increase of the dissolution rate with the stress is interpreted as an effect of the stress on the mobility of the dissolving particles at the interface.

experim.	S (%)	T (°C)	t (hr)	σ_b (MPa)	σ_h (MPa)	stress free R_h	stress free R_v	posit.	stress. R_h	stress. R_v	posit.
63CHLO1	2.4	19.5	4.5	3.9	10.6	84.4	84.4	B	151.1	120.0	A
93CHLO14	2.4	23.0	3.5	3.6	9.5	120.0	116.0	A	99.3	90.0	B
100CHLO20	2.4	23.0	3.5	3.0	7.8				162.9	115.7	A
99CHLO19	2.4	23.0	3.5	1.8	4.7				142.3	142.9	A
71CHLO9	1.6	19.6	4.0	4.0	11.5	57.5	37.5	B	126.2	113.7	A
104CHLO24	1.6	22.9	3.5	2.5	6.7				114.3	98.0	A
84CHLO10	1.6	21.0	2.5	2.2	6.3	94.0	82.0	A	91.2	79.2	B
90CHLO11	1.2	22.6	2.5	3.6	9.2	79.2	80.0	A	74.8	55.2	B
69CHLO7	1.1	19.5	4.5	1.5	3.9				70.0	62.2	A
64CHLO2	1.0	19.5	4.5	3.7	10.1	26.7	13.3	B	71.1	60.0	A
66CHLO4	1.0	19.5	4.5	2.6	6.7				65.6	63.3	A
98CHLO18	1.0	22.9	4.0	0.0	0.0	51.5	50.7	A			
91CHLO12	0.8	22.6	3.5	3.6	9.5	28.6	22.6	B	47.1	47.1	A
105CHLO25	0.8	22.6	4.0	3.1	8.0				46.2	36.2	A
97CHLO17	0.8	23.2	4.5	2.0	5.4	4.4	5.6	Bottom	43.3	42.2	A
67CHLO5	0.6	19.5	4.5	3.9	10.6				32.2	32.9	A
92CHLO13	0.6	22.8	21	3.9	10.3	24.8	19.8	B	31.9	27.0	A
94CHLO15	0.6	23.0	3.5	3.2	9.3	23.7	21.4	B	23.6	17.0	A
70CHLO8	0.6	19.8	4.5	1.7	5.8	20.0	20.0	A	15.6	8.9	B
65CHLO3	0.2	19.5	22.5	5.1	14.4				8.9	7.6	A
96CHLO16	0.2	23.0	16	2.0	5.2	1.2	1.2	B	1.6	1.9	A
68CHLO6	0.2	19.5	23	0.0	0.0	2.4	2.6	A			

Table 4.1 Dissolution rates in $\mu\text{m}\cdot\text{hr}^{-1}$ for each experiment estimated in the direction perpendicular to the applied stress (R_h , perpendicular to the piston for stress-free crystals), and in the direction parallel to the applied stress (R_v), as a function of undersaturation S, temperature T, duration t and stress σ . Estimations of the rates had a precision of $5 \mu\text{m}\cdot\text{hr}^{-1}$ for short experiments (duration less than 5 hours) and of $1 \mu\text{m}\cdot\text{hr}^{-1}$ for long experiments (duration ~ 20 hours). For experiment 97CHLO17, the stress-free sample lied on the bottom of the apparatus, what explains the low dissolution rate for the undersaturation used.

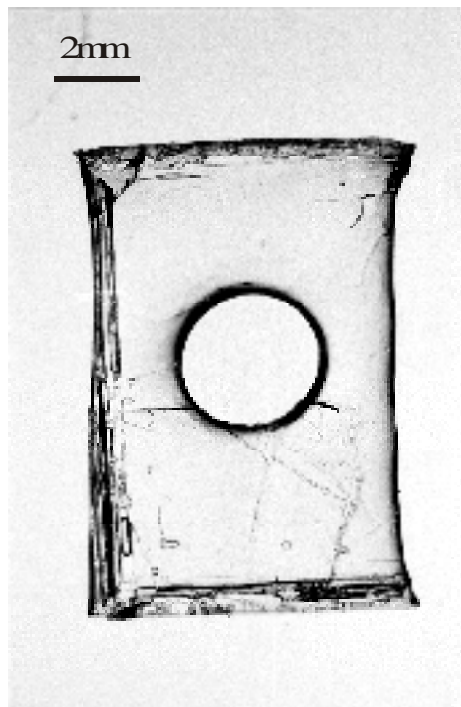


Fig. 4.1 Optical micrograph of the stressed sodium chlorate crystal 92CHLO13 after the experiment. Bulk stress was 3.9 MPa and applied vertically.

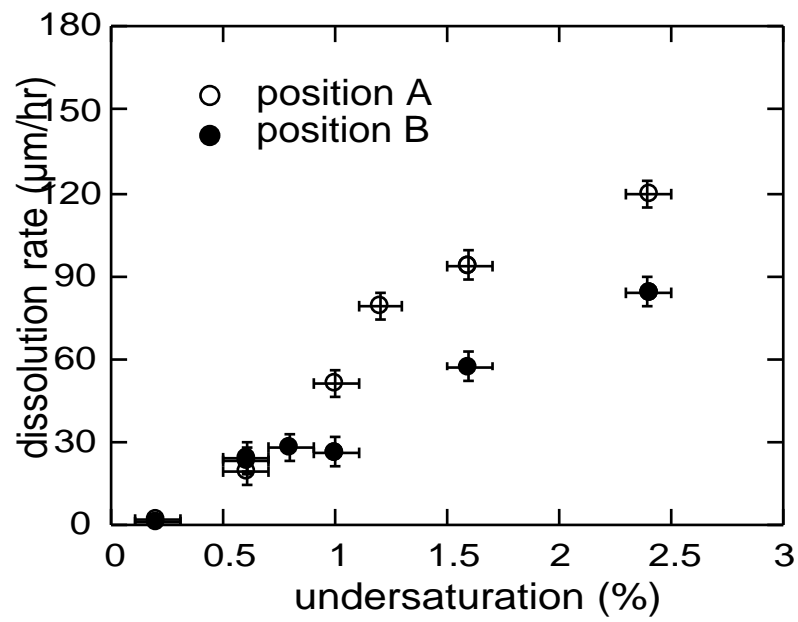


Fig. 4.2 Graph illustrating the influence of the position in the vessel of the stress-free crystals on their dissolution rate. Dissolution rates were calculated in the horizontal direction.

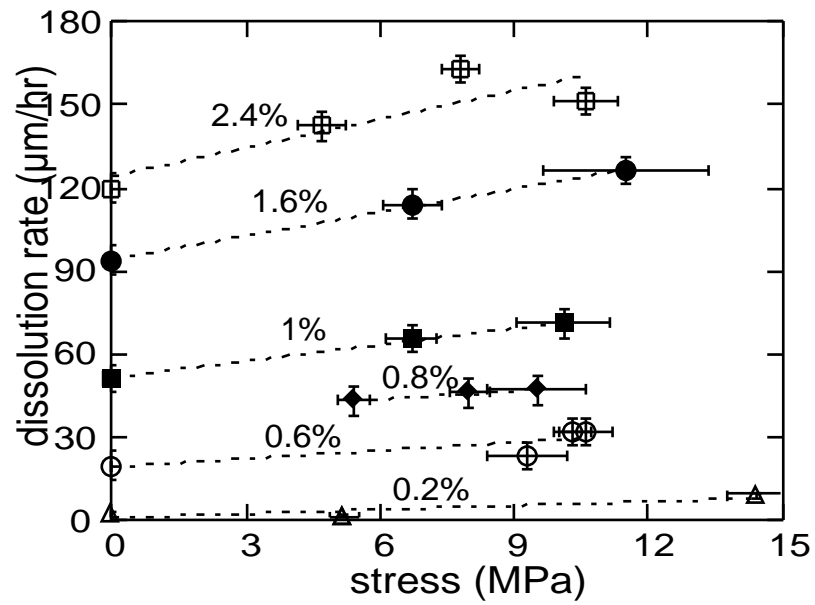


Fig. 4.3 Graph showing the dissolution rates in the horiz. direction versus the stress on both sides of the hole, for different degrees of undersaturation. All the data were obtained for crystals placed in position A.

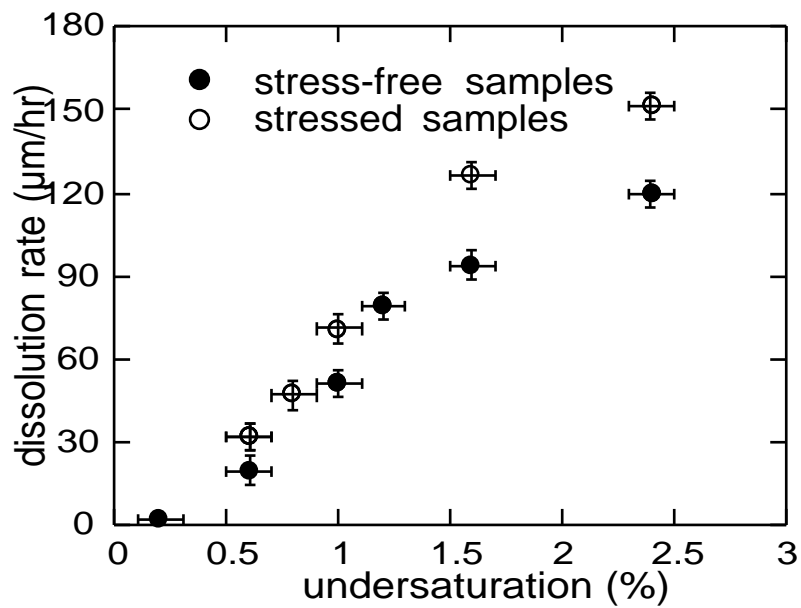


Fig. 4.4 Graph showing the effect of the application of a stress of 10.5 1 MPa on both sides of the hole on the dissolution rate in the horizontal, as a function of undersaturation. All the data were obtained for crystals placed in position A.

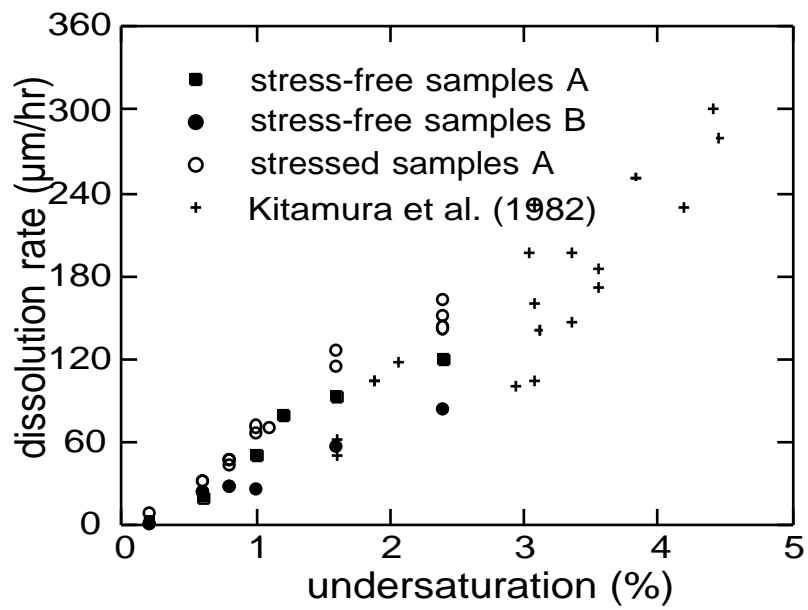


Fig. 4.5 Comparison of the dissolution rate in the horizontal direction with dissolution rate values for stress-free sodium chlorate crystals from the literature (Kitamura et al. 1982).

Chapter 5 Effect of stress on growth processes.

We have seen in chapters 3 and 4 that the dissolution processes and the dissolution rate of elastic/brittle crystals were strongly affected by the stress, and we may expect also a strong effect of the stress on the growth processes. Ristić et al. (1997b) have shown that the growth rate of potassium alum single crystals could be strongly decreased by the application of stress. They found that the growth rate of {100} faces of a potassium alum crystal stressed in tension at 0.1 MPa and at an oversaturation of 6.47% was decreased from $2.2 \mu\text{m}\cdot\text{min}^{-1}$ to $1.8 \mu\text{m}\cdot\text{min}^{-1}$. The growth of {100} and {110} faces could even be stopped by the application of a higher tensile stress. Ristić et al. (1997b) suggested that the stress could have affected the way the growth centres developed and propagated. The experimental observations we made and presented in Chapter 3 and Chapter 4 support this idea. The dissolution sites on the crystal surface caused the roughening of the surface, what led to a non-homogeneous stress distribution and an enhanced dissolution in the concavities. We present in this chapter the results of growth experiments carried out on potassium alum and potassium dihydrogen phosphate (KDP) single crystals under differential compressive stress.

5.1) Starting materials and sample preparation.

5.1.1) Potassium dihydrogen phosphate.

Potassium Dihydrogen Phosphate (KDP; KH_2PO_4), has a tetragonal symmetry, and belongs to the space group $I4_2d$ (Dam & van Enkevort, 1981). It has a solubility of $1.8 \text{ mol}\cdot\text{l}^{-1}$ water at 25°C (Gmelins Handbuch, 1970). Crystals grown in aqueous solution by slow cooling typically show four prismatic {100} faces bounded along the C-axis by two pyramidal sectors formed each by four {110} faces (Fig. 5.1). Large single KDP crystals are often tapered. In this case the transition zone between pyramidal and prismatic sectors shows intermediate higher index facets (Dam & van Enkevort, 1981). Growth of KDP crystals is characterised by a "dead area", corresponding to a range of oversaturation (from 0 to about 4°C) for which the growth rate of the prismatic faces is equal or very close to zero (Batyreva et al., 1981). In this range of oversaturation, the crystals grow only along the C-axis and develop the pyramidal sectors. KDP does not deform plastically at temperatures below 110°C . In this range of temperature, it can support about 100 MPa, a value above which it breaks (Chan Hai Guin et al., 1980).

Right-angled samples were cut from bigger KDP crystals (Fig. 5.1) grown in aqueous solution by slow cooling of the solution temperature. This operation was done using a diamond cutting machine (Isomet, Buehler) and using volatile oil (Shell S4919) as a lubricant. The samples were then polished using polishing paper (mesh sizes 600, 800, 1000 and 1200), again with volatile oil as a lubricant, to finally get crystals about $4 \times 4 \times 10$ mm in size. The polished faces of the samples were very close (to within a few degrees) to either {100}, {001} or {110} crystallographic faces. No holes were drilled in the crystals, but triangular cuts, using a razor blade (Fig. 5.2). This was done in order to increase the stress at the cuts. The stress distribution around such cuts can be very easily seen with a photoelasticity experiment carried out on a Plexiglas sample with a similar geometry (see Fig. 3.13).

5.1.2) Potassium alum.

Potassium alum ($\text{KAl}[\text{SO}_4]_2 \cdot 12\text{H}_2\text{O}$) is a cubic salt, and belongs to the space group T^h_6 . It has a solubility of 0.3 mol.l^{-1} water at 25°C (Van der Hoek et al. 1983, Ullmann Handbook 1986). Crystals have an octahedral habit typically bounded by {111}, {100} and {110} faces (Fig. 2.1). Growth of potassium alum crystals has been extensively studied. The growth rates of the three principal, low index crystallographic faces were measured (e.g. Lacmann & Tanneberger 1995, Ristić et al. 1996). The growth rate of {111} faces was found to be constant. The {110} and {100} faces, however, were characterised by a period of constant growth rate during about one hour, after which their growth rates decreased progressively (Ristić et al., 1996). For steady state growth (i.e. during the first hour), {110} faces showed the faster growth rate, followed by the {100} faces and finally the {111} faces.

Right-angled potassium alum samples, about $4 \times 4 \times 10$ mm in size, were cut from bigger, commercially available crystals (from ALVA GmbH, Germany) and prepared using the same method as for the KDP samples. One or two triangular cuts, about 1-2 mm wide and 0.5-1 mm deep, were made on at least one of the faces of each sample, as done for the KDP samples. The orientation of the potassium alum crystals were defined after each experiment with the help of the euhedral growth morphology.

5.1.3) Preparation of the saturated aqueous solutions.

Saturated solutions of potassium alum and KDP were prepared by dissolving in distilled water a slight excess quantity of crystal (potassium alum from Merck 101047 "zur analyse", KDP from 104871 "krist. reinst") for a given saturation temperature. The solution was heated for a few hours to one days to a few degrees above the saturation temperature until all the material had dissolved. The solution was then cooled down to the saturation temperature in the experimental vessel, and small crystal were submerged in it to absorb the oversaturation. The solution was left under these

conditions for a few days. Saturation was assumed to be reached when no change in the size of the small crystals could be observed.

5.2) Experimental procedures.

The experiments were carried out using the cylindrical vessel described in Chapter 2. Two crystals were used for each experiment, one stressed and the other left stress-free. Experiments were carried out at different temperatures in the range 28 to 50°C. These temperatures were provided by the circulation of oil around the cylindrical vessel. The temperature was controlled with a Haake DC5 temperature controller. Once the crystals were placed in the vessel filled with a saturated aqueous solution and one of them stressed, the temperature controller was programmed to cool down the solution temperature at a given rate, to get an oversaturation. As the crystals grew, the section of the stressed crystal supporting the load increased. The load was therefore increased by steps during the experiments to keep an approximately constant stress. Stresses, temperatures and cooling are given for all the experiments in Table 5.1.

At the end of the experiments, the crystals were taken out of the solution and immediately dried using a cleaning tissue. The length of the stressed samples was then measured by hand with a micrometer, with a precision of 0.1%. The crystals were then glued in araldite. Once the glue had dried, the crystals were cut in their middle using volatile oil as lubricant. They were then polished to finally get thin sections.

5.3) Results.

Measurement of the length of the stressed crystals before and after each of the experiments revealed that none of the samples had deformed plastically within the measurement resolution (0.1% strain). The experiment GRW4 was carried out on potassium alum crystals on which two triangular cuts had been made on one face (Table 5.1). Fig. 5.3 shows a thin section of the stressed crystal after the experiment. The original crystal (seed) appears on the micrograph as a black rectangle, due to the fracturing of the seed by increasing the stress during the experiment. The crystal face where no cuts were present (right side of the seed on Fig. 5.3) grew parallel to the seed. Different growth stages due to the incorporation of fluid inclusions on the surface during the experiment were separated by parallel alignment of fluid inclusions. The left side of the crystal, where the two cuts had been made, showed a completely different morphology. The cuts did not heal during the growth process, and became even bigger. The upper cut was at the end of the experiment about 3.5-4 mm wide and 2.5-3 mm deep, i.e. two to three times bigger than at the beginning of the experiment. Average growth rates measured at points A, B, C and D (Fig. 5.3) under the microscope at the end of the experiment ranged from 275 $\mu\text{m}\cdot\text{hr}^{-1}$ in B to 425 $\mu\text{m}\cdot\text{hr}^{-1}$ in C, i.e. the growth rate in the middle of the upper cut was about 1.5 times slower than between the cuts. On the crystal left stress-free, the cuts were completely healed during the

experiment. The same result was obtained with the experiment GRW12, again using potassium alum with two artificial cuts on one face. Fig. 5.4 shows the stressed crystal after the experiment. The crystal developed on the right side in three parts separated by the two cuts. In this experiment, however, the stressed crystal developed in two parts on the left side, although no cut had been made on this side. The stress-free crystal of experiment GRW12 did not show such a morphology but a typical octahedral habit. For both the experiments GRW4 and GRW12, the compressive stress applied on the stressed crystals was increased by steps during the experiments to keep it constant at 10 MPa. Cuts made on one face of potassium alum crystals stressed under less than 10 MPa (experiments GRW3 and GRW6, see Table 5.1) were healed during growth.

The experiment GRW17 was carried out on KDP crystals, the long axis of which was oriented along to the C-axis. The four free-faces were thus parallel (to within a few degrees) to prismatic $\{100\}$ faces. Cuts (one or two) were made on each face of the crystals. The oversaturation at the end of the experiment was 3.5°C . However, none of the four prismatic faces of the crystals grew. Growth only occurred along the C-axis, parallel to the $[001]$ direction. This growth caused the healing of the cuts, on the stress-free crystal as well as on the stressed crystal (Fig. 5.5). By removing the load (quasi instantaneously) at the end of the experiment, fractures formed in the stressed crystal in the middle of the cuts, in the newly grown material (Fig. 5.6). Such unloading fractures were observed in all the growth experiments. The fractures developed always only in the newly grown material and never in the original crystal seed. Experiment GRW2 was carried out on potassium alum crystals without cuts on their faces. The unloading fracture developed in the stressed crystal exactly in the middle of the newly grown material, and did not propagate into the seed (Fig. 5.7). The unloading fractures developed for all the experiments perpendicular to the bulk applied stress.

5.4) Discussion.

After examination of the euhedral growth morphology of the potassium crystals at the end of the experiment GRW4, a thin section was cut in the middle of the crystals parallel to a $\{110\}$ crystallographic plane (Fig. 5.3). The vertical direction, which was the direction of the bulk applied compressive stress, was oriented parallel to a $\langle 110 \rangle$ direction, while the horizontal direction (the direction of growth on the thin section) was parallel to a $\langle 100 \rangle$ direction. The two cuts made on one side of the stress-free crystal had disappeared during the experiment. Considering the growth rates of the different faces in the first hour of the experiment (Paragraph 5.1.2), we can conclude that the cuts on the stress-free crystal were quickly healed by the growth of the $\{110\}$ faces, parallel to the loading direction, and of the $\{100\}$ faces, perpendicular to the loading direction, which had the faster growth rates. The cuts that had been made on the stressed crystal, however, had increased in size. This means that the growth at the beginning of the experiment was faster parallel to the sides of the cuts, which were parallel to $\{111\}$ faces. In other words, the growth rate of the $\{111\}$ faces was already at the beginning of the experiment higher than the growth rates of $\{100\}$ and $\{110\}$ faces. Hence, we can suggest that the growth mechanisms of both $\{100\}$ and $\{110\}$ faces were much more affected by the high stress concentration in the cuts than the $\{111\}$ faces (Fig. 3.13). The growth in the horizontal direction, parallel to the $\{100\}$

faces, was 1.5 times slower in the middle of the upper cut (point B on Fig. 5.3) than between the cuts (point C on Fig. 5.3). This result is consistent with the results obtained by Ristić et al. (1997b). They found that, under a tensile stress of the order of 0.1 MPa, the growth rates of both {100} and {110} faces of potassium alum crystals were 1.2 times smaller than when the crystals were left stress-free, while the growth rate of {111} faces remained approximately constant. However, Ristić et al. (1997b) found an effect of the stress on the growth rate of {100} faces of the same order than our observations with a stress 100 times smaller than in our case. Asymmetry between the effect of tensile and compressive stress was also observed by Aziz et al. (1991), although in their case the effect of compressive stress on the growth rate of crystalline from amorphous silicon was greater than the effect of tensile stress. Finally, cuts made on crystals stressed under a bulk stress smaller than 10 MPa healed during the experiment. This result suggests that a "critical" stress may have to be reached to affect significantly the growth mechanisms operating on {100} and {110} faces. Formation of growth hillocks on the crystal surface induced the roughening of the surface. This, independently from the cuts, led to a non-homogeneous stress distribution on the crystal surface, the stress being higher between the hillocks than on the hillocks. This stress distribution may have caused the surface to become unstable over a critical stress, as we suggested in Chapter 3, and may have slowed down the growth steps between the hillocks, what in turn may have caused a decrease in the growth rate.

The KDP crystals used for the experiment GRW17 had four prismatic faces. None of the prismatic faces grew, although the solution was oversaturated (3.5 °C cooling in 30.5 hours). This is explained by the occurrence of the "dead area" for {100} faces for oversaturation degrees up to 4°C (Batyreva et al., 1981, see Paragraph 5.1.2). Growth only occurred along the C-axis, parallel to the [001] direction, and caused the healing of the cuts, on the stress-free crystal as well as on the stressed crystal. The velocity with which the cuts were healed was not measured during the experiment, so that the effect of the stress on the growth rate of {001} KDP faces could not be quantitatively established. By removing the load, the seed which was elastically compressed relaxed and recovered its original length. The new material that had grown in the cuts followed this relaxation and fractured, perpendicular to the bulk applied stress direction. This means that during the unloading the newly grown material was stretched in tension, and that before the unloading it was stress-free. Hence, we can conclude that the growth in the cuts of the stressed crystal occurred stress-free, at least after the growth of the first atomic layers during which stresses due to misfits between the seed and the newly grown material may occur (the so called capping process). The same conclusion can be drawn for the stressed potassium alum crystal of the experiment GRW2. No cut was made on the crystal surface. By removing the load on the seed, the newly grown material underwent a tension and fractured exactly in the middle, perpendicular to the tensile stress direction.

5.5) Conclusion.

We have demonstrated in this chapter that mechanically induced compressive elastic strain can strongly affect the growth mechanisms of potassium alum single crystal. We found that the growth rates of {100} and {110} faces were significantly decreased by

compressive stress, in agreement with the observations made by Ristić et al. (1997b) under tensile stress. We suggest that the non-homogeneous elastic strain distribution on the surface of the stressed crystals decreased the growth step velocity between the growth hillocks, i.e. where the strain was the highest. This in turn caused a decrease in the growth rate. This interpretation is consistent with the suggestions made in Chapter 3 and Chapter 4, and reflects the importance that the roughness of the crystal surface may have on the growth and dissolution processes. We also showed that the overgrowth on the crystal seed occurred stress-free, at least after the formation of the first atomic layers.

experim.	crystals	geometry	duration (hr)	sat. temp. (°C)	cooling (°C)	bulk stress at begin (MPa)	bulk stress at end (MPa)
GRW2	K-alum	no cut	15.5	47	3	9.4	?
GRW3	K-alum	1 cut on 1 face	14	47	3	8.0	?
GRW4	K-alum	2 cuts on 1 face	15	47	7	10.0	10
GRW6	K-alum	2 cuts on 1 face	8	47	4	6.0	6
GRW7	K-alum	no cut	4	50	4	10.0	10
GRW12	K-alum	2 cuts on 1 face	43.5	50	3	10.0	10
GRW14	KDP 2 {100} and 2 {001} faces.	no cut	113	42.5	1 in first half, 14 in second half of exp.	15.0	9
GRW15	KDP 2 {100} and 2 {001} faces.	2 cuts on each face	45.5	42.5	4 in first half, 10 in second half of exp.	14.0	14
GRW17	KDP 4 {100} faces	1 or 2 cuts on each face	30.5	28	3.5	10.0	20
GRW18	KDP 4 {100} faces	2 cuts on each face	144	28	0	20.0	24
GRW19	KDP 2 {100} and 2 {110} faces	no cut	1007	29	0.5	18.5	15
GRW21	KDP 2 {100} and 2 {001} faces	2 cuts on each edge	48	30	2	15.0	12.5
GRW22	KDP 2 {100} and 2 {001} faces	2 cuts on 1 {001} face	96.5	30	2	20.0	12.5
GRW23	KDP 2 {100} and 2 {001} faces	no cut	65	28	1.5	8.5	8.5

Table 5.1 Experimental conditions for the growth experiments. In all the experiments (except GRW2 and GRW3), the bulk stress was increased in steps during the experiments. The saturation temperature is the temperature of the aqueous solution at the beginning of the experiment. The cooling corresponds to the decrease in solution temperature during the experiments.

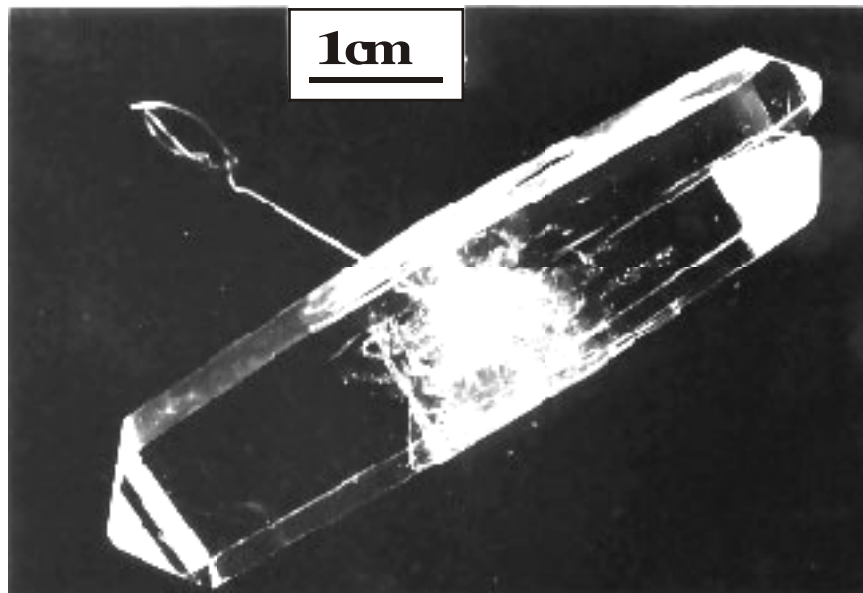


Fig. 5.1 Typical habit of a KDP crystal grown by slow cooling in an aqueous solution. The white zone in the crystal centre corresponds to the capping region, during which a lot of fluid inclusions are formed. Note the tapering of the prismatic faces.

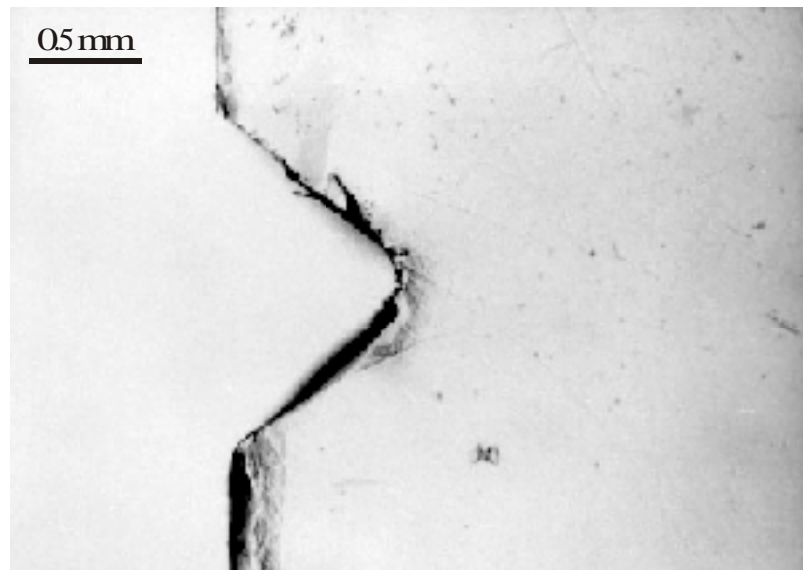


Fig. 5.2 Optical micrograph showing the cut made with a razor blade in the side of the K-alum crystal GRW3 (seen on the right side of the micrograph). The stress distribution around such a cut was visualised by photoelasticity on a Plexiglas sample with the same geometry (Fig. 3.14).

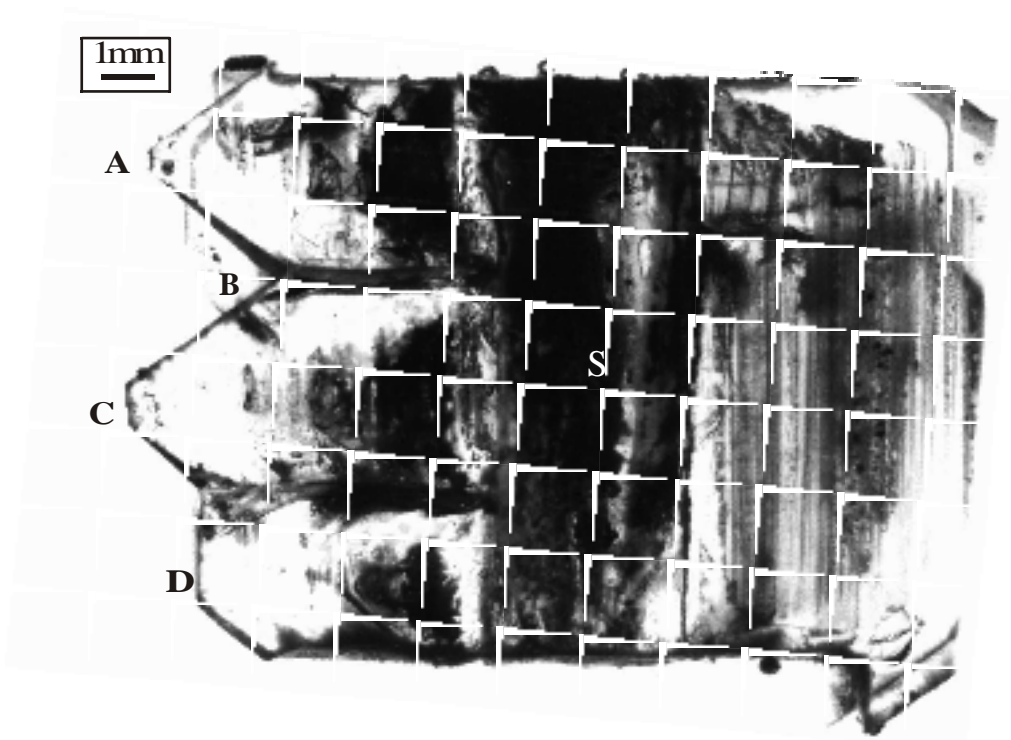


Fig. 5.3 Optical micrograph of a thin section of the stressed K-alum crystal GRW4. The bulk stress was applied vertically. The crystal seed *S* appears as a black rectangular, due to abundant fracturing of the seed under stress during the experiment. Two cuts were made in the left side of the crystal, and none in the right side. The crystal grew on the left side in three different parts separated by the cuts, whereas it grew in only one part on the right side. The black regions visible in each of the three parts on the left side of the seed correspond to the first stage of growth, i.e. the capping process due to a slight misfit between the polished crystal face and the crystallographically oriented new material. Average growth rates were calculated at points A, B, C and D.

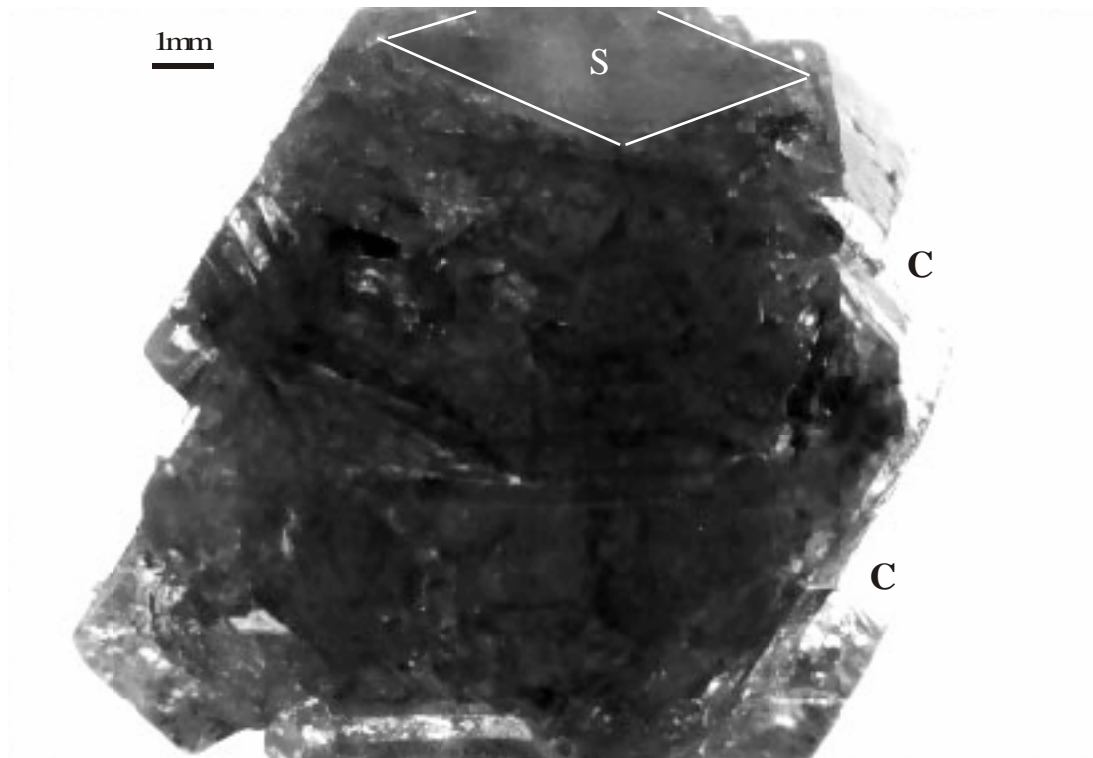


Fig. 5.4 Optical micrograph of the stressed K-alum sample GRW12 after experiment. The top of the crystal seed (S) is delimited by the white lines. Two cuts were made on the right side of the seed and remained at the end of the experiment (C). The stress was applied vertically.

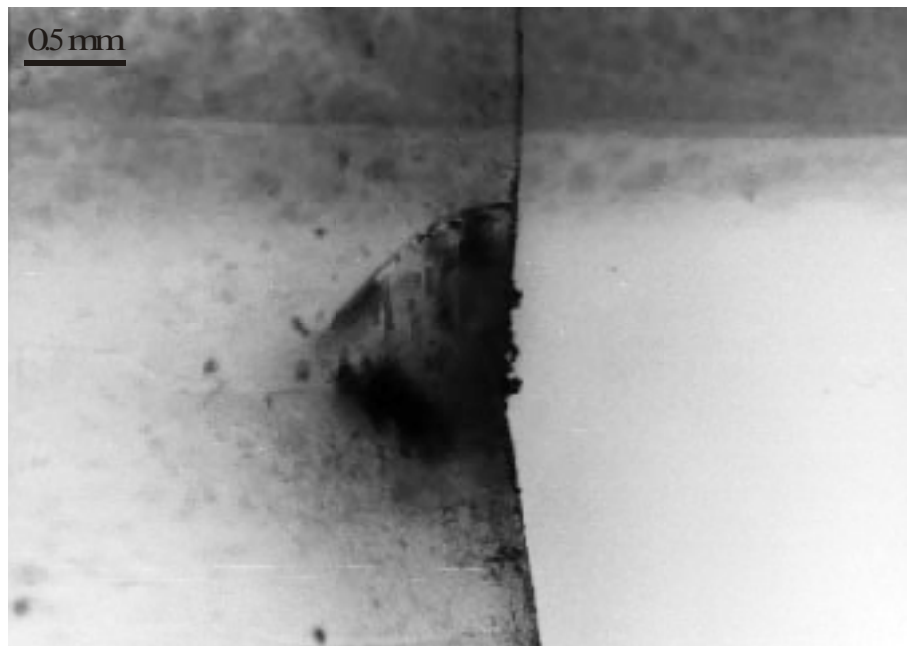


Fig. 5.5 Optical micrograph of the stress-free KDP crystal GRW17 (left side of the micrograph). The oversaturation at the end of the experiment was 3.5°C and growth only occurred vertically (see text), along the C-axis, and healed the cut.

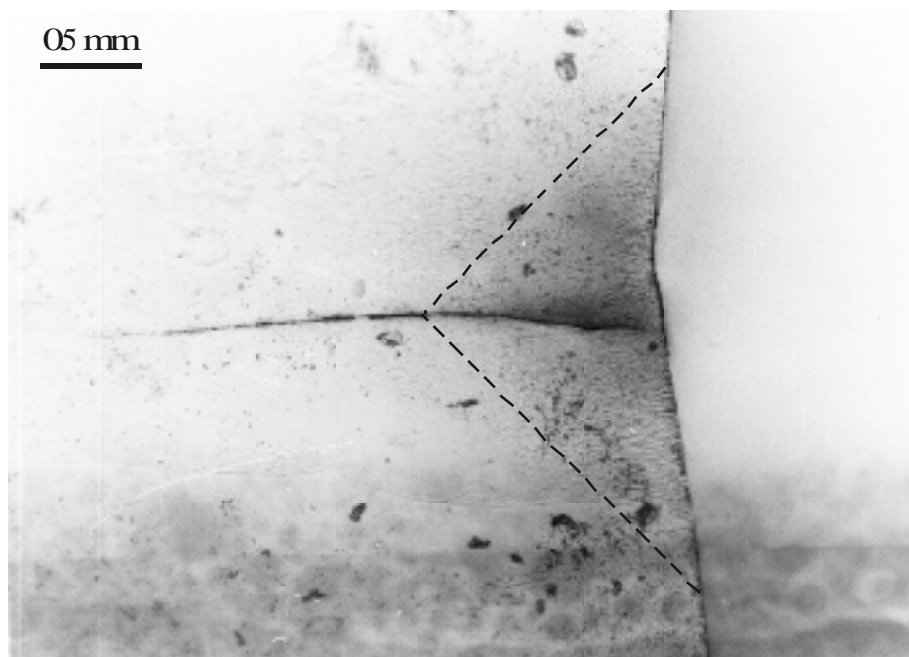


Fig. 5.6 Optical micrograph of the stressed KDP crystal GRW17. The dashed lines define a darker region which corresponds to the original cut. The crystal grew in the cut, vertically, along the C-axis. The bulk stress at the end of the experiment was 20 MPa, and was applied vertically. The unloading fracture developed in the middle of the newly grown material.

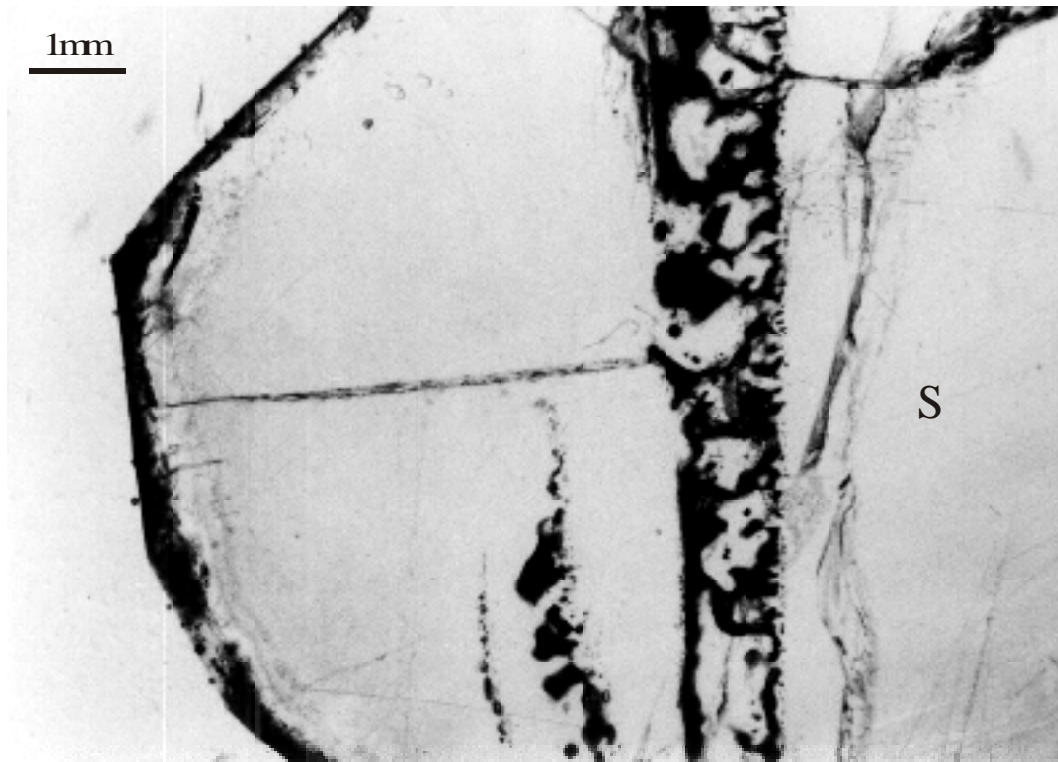


Fig. 5.7 Optical micrograph of a thin section of the stressed K-alum crystal GRW2, showing the unloading fracture that formed in the middle of the newly grown material. The bulk stress was applied vertically. Abundant fluid inclusions developed during the capping stage of the growth process. They form a wide black boundary between the seed (S) and the newly grown material.

Chapter 6 Summary and conclusions.

This PhD thesis has been undertaken with the goal to investigate the role of mechanically induced elastic strain on pressure solution processes. At geological realistic stresses, differences in elastic strain energy are much smaller than differences in crystal plastic strain energy or differences in grain boundary surface normal stress and, for this reason, are commonly neglected as a possible driving force for pressure solution (Paterson, 1973; Shimizu, 1995). The experiments on the effect of mechanically induced elastic strain on the dissolution and growth mechanisms in aqueous solution were carried out on elastic/brittle crystals of potassium alum, sodium chlorate and potassium dihydrogen phosphate (KDP). These crystals were used as analogues to rock-forming minerals such as quartz to make experimental investigation on the effect of elastic strain easier with low P-T conditions. It was found that, in contrast to what is commonly thought, mechanically induced elastic strain can strongly affect the dissolution and growth behaviour of crystals in aqueous solution, much stronger than theoretically expected on the basis of the increase in bulk stored elastic strain energy. The following observations were made:

1) The microstructure of stressed potassium alum crystal surfaces was strongly affected by the elastic strain if the surfaces were rough. This roughness was caused by surface energy-controlled dissolution, along periodic bond chain (PBC) directions, in the slightly undersaturated solution, and consisted of fine etch grooves (referred to in this thesis as B-type grooves). It only occurred if the crystal surfaces were slightly misoriented with respect to low index crystallographic faces (Herring, 1951). This roughness was mathematically described as a geometrical sinusoidal perturbation, with a characteristic wavelength, on an initially flat surface. For a crystal surface under differential stress, this perturbation led to a strongly non-homogeneous elastic strain distribution on the surface. The elastic strain was high in concavities ("valleys"), and small on convexities ("crests", see Fig. 3.13). Above a critical stress, the stress gradient between the crests and the valleys led to the instability of the crystal surface (the so called Grinfeld instability, Grinfeld 1986). The dissolution in the valleys was strongly enhanced and a new steady state structure developed, characterised by wide and deep dissolution grooves (further referred to as A-type grooves), oriented perpendicular to the bulk applied stress. The grooves grew until an equilibrium wavelength was reached. This equilibrium wavelength appeared to be a function of the local surface stress, of the surface energy and of the degree of undersaturation. For potassium alum, the equilibrium wavelength ranged from 20 to 80 μm , and decreased with increasing stress and increasing undersaturation. This microstructural evolution of a stressed crystal surface in contact with an aqueous solution was consistent with the theoretical model from Heidug & Leroy (1994) and Leroy & Heidug (1994).

A-type grooves developed always perpendicular to the local maximum compressive stress trajectories on the crystal surface, i.e. perpendicular to the direction of the

maximum compressive stress gradient between the crests and the valleys. The grooves were straight far from the central hole, and curved near the hole. However, when the crystals were stressed near their brittle failure strength, A-type grooves developed in several other directions as well (may be due to the formation of microfractures), even in an orientation parallel to the direction of the maximum compressive stress. In some experiments, this led to the formation of a network of dissolution grooves and to a decomposition of the crystal surface in many small parts. It was assumed that for longer experiments this process could have led to cataclastic deformation of the entire crystal. In all experiments, the orientation of the A- as well as B-type grooves was also crystallographically controlled, i.e. the grooves developed parallel to the PBC-directions of the crystal. The PBC-direction the most perpendicular to the local maximum compressive stress trajectories was the one along which the grooves preferentially developed.

A-type grooves were also observed to develop on the surfaces of stressed crystals held in saturated solution when scratches were intentionally made on the crystal surface. On the contrary, such grooves were never observed on perfectly flat, original low index crystal surfaces.

2) The dissolution of sodium chlorate single crystals appeared to be strongly enhanced by the stress. The faces of the crystals were parallel (to within a few degrees) to low index crystallographic planes, and no optically visible dissolution grooves developed. However, the dissolution rate of the stressed crystals was increased by one to two orders of magnitude more than expected on the basis of the increase in bulk stored elastic energy. The dissolution rate of the stressed crystals increased linearly with increasing stress. The increased dissolution rate was higher with increasing undersaturation. It was suggested that a non-homogeneous stress distribution developed around dissolution pits formed at high surface energy sites on the crystal surface (for example at screw dislocation outcrops or around impurities, i.e. where the dissolution preferentially occurred). The high elastic strain at the dissolution pits would have led to an increase in the velocity of the dissolution steps, what in turn caused an increased surface dissolution rate. The higher the undersaturation, the higher the number of structural surface defects that were activated as dissolution centres, as was demonstrated for potassium alum by Van der Hoek et al. (1983). Therefore the effect of the stress on the dissolution rate was increased with increasing undersaturation. The linear dependence of the dissolution rate on the stress was interpreted as due to a stress-dependent mobility of the dissolving particles (Barvosa-Carter et al., 1998).

3) The growth rate of both {100} and {110} faces of potassium alum crystals was strongly decreased under compressive stress. This result was consistent with the observations made by Ristić et al. (1997b) who observed a decrease in the growth rate of these faces on crystals stressed in tension. It was suggested that a non-homogeneous elastic strain distribution would develop on the crystal surface due to the formation of growth hillocks. This could have led to a decrease in the velocity of the growth steps between the hillocks, i.e. where the elastic strain was the highest. This in turn would have led to the observed decrease of the growth rates.

It appears from these different observations that the influence of the elastic strain on the behaviour of stressed crystals in solution strongly depends on the roughness of the crystal surface. This roughness leads to a non-homogeneous elastic strain distribution on the crystal surface. The surface is no more in equilibrium with the aqueous solution, and the dissolution is enhanced where the elastic strain concentration is the highest, i.e. in the concavities of the surface.

For a periodic roughness, caused for example by a surface energy-induced dissolution (see point 1 above), the non-homogeneous elastic strain distribution causes the development of a the solid/fluid interface microstructure completely different of that of a stress-free interface, with a strong increase in the amplitude and wavelength of the roughness. One may expect such a stress-induced microstructural evolution also to occur on rock-forming minerals in contact with an undersaturated fluid. For example, for a typical rock-forming mineral such as quartz, solving equation (1.5) with a Young modulus $E \sim 50$ GPa, a surface energy $\gamma \sim 0.5$ Pa.m and a Poisson ratio $\nu = 0.25$ would give an equilibrium wavelength of $17 \mu\text{m}$ for an effective stress $\sigma = 50$ MPa, and of $4 \mu\text{m}$ for an effective stress $\sigma = 100$ MPa. Such a roughness would be able to significantly affect the diffusion of the dissolving material along the mineral/fluid interface. The observations on potassium alum crystals (see again point 1 above) were made on free crystal surfaces oriented parallel to the bulk applied stress direction, i.e. surfaces for which only tangential stresses and no normal stresses play a role. Geological situations of high tangential stresses may be found for example in shear zones, where the migration of over- or undersaturated fluids through rocks may cause the roughening of the surfaces of the minerals, and hence induce a strong effect of the stress on the surface microstructures. The observations made on potassium alum are thus of prime important for the understanding of pressure solution mechanisms, particularly for the island-channel grain boundary model (Raj, 1982; Spiers & Schutjens, 1990; Gratz, 1991). The observation of grooves moving over the surface shows that the position of islands and channels may change in time, depending on the evolution of the surface stress distribution. A dynamic island-channel model was already suggested (e.g. Spiers & Schutjens, 1990) but never actually observed. Development of periodic wide and deep dissolution grooves on the surfaces of minerals may lead to an increase in the permeability of the rocks by increasing the channel/island area ratio at grain boundaries, and hence to an increase in the effective diffusion rate of the dissolved material along the grain boundaries. This would lead to an increased pressure solution rate. The crystallographic orientation of the grooves, the dependence of the size of the equilibrium wavelength of the surface roughness on the crystallographic orientation suggest that pressure solution might depend on the crystallographic orientation, as was already suggested by Den Brok (1998).

For a non periodic roughness, caused by preferential dissolution at screw dislocation outcrops or at structural surface defects, or caused by the development of growth hillocks, the non-homogeneous elastic strain distribution affects the propagation of the dissolution or growth steps. The strong increase in the dissolution rate of sodium chlorate crystals with increasing stress and the decrease in the growth rate of $\{110\}$ and $\{100\}$ faces of potassium alum crystals (see points 2 and 3 above) may strongly affect pressure solution rate, especially when new grains with well formed crystallographic surfaces developed, for example, along grain boundaries by cataclastic deformation of

older grains and may be present along grain boundaries. Formation of new grains with well formed crystallographic surfaces was observed following the cataclastic deformation of sodium chlorate aggregates.

The experimental effect of the elastic strain observed in this thesis may have serious consequences for the understanding of dissolution and growth processes in natural rocks, notably under metamorphic conditions where interstitial fluids may readily be over- or undersaturated with respect to the neighbouring mineral phases. This effect appears much too strong to be neglected in modelling pressure solution phenomena. The recent progresses made in non-equilibrium thermodynamics applied to geological problems (Heidug & Leroy, 1994; Leroy & Heidug, 1994; Yang & Srolovitz, 1994) gives the necessary tools to incorporate the effect of elastic strain energy in the modelling of pressure solution mechanisms. However, a more systematic confrontation between theoretical models and experimental observations is needed in order to quantify more precisely the influence of the elastic strain. An accurate relation between the equilibrium wavelength of the dissolution grooves and the stress may, for example, help in determining paleo-stress.

References

Aziz,M.J., Sabin,P.C. and Lu,G.Q.(1991): The activation strain tensor: non-hydrostatic stress effects on crystal growth kinetics. *Phys. Rev. B* 44, p. 9812-9816

Barvosa-Carter,W., Aziz,M.J., Gray,L.J. and Kaplan,T.(1998): Kinetically driven growth instability in stressed solids. *Phys. Rev. Lett.* 81[7], p. 1445-1448

Batyreva,I.A., Bespalov,V.I., Bredikhin,V.I., Galushkina,G.L., Ershov,V.P., Katsman,V.I., Kuznetsov,S.P., Lavrov,L.A., Novikov,M.A. and Shvetsova,N.R.(1981): Growth and investigation of optical single crystals for high power laser systems. *J. Cryst. Growth* 52, p. 832-836

Bosworth,W.(1981): Strain-induced preferential dissolution of halite. *Tektonophysics*, 78, p. 509-525

Buckley,H.E.(1958): *Crystal growth*. 4th edition. John Wiley & Sons, inc. New York

Chan Hai Guin, Katrich,M.D., Savinkov,A.I., and Shaskolskaya,M.P.(1980): Plastic strain and dislocation structure of the KDP group crystals. *Kristall und technik* 15, p. 479-488

Correns,C.W.(1949): Growth and dissolution of crystals under linear pressure. *Discuss.Faraday Soc.*, 5, p. 267-271

Dam,B. and van Enckevort,W.J.P.(1981): On the formation of etch grooves around stress fields due to inhomogeneous impurity distribution in KH_2PO_4 single crystals. *J. Cryst. Growth* 51, p. 607-623

De Meer,S. and Spiers,C.J.(1995): Creep of wet gypsum aggregates under hydrostatic loading conditions. *Tectonophysics* 245, p. 171-183

De Meer,S. and Spiers,C.J.(1999): Influence of pore-fluid salinity on pressure solution creep in gypsum. *Tectonophysics* 308, p. 311-330

Den Brok,S.W.J.(1992): An experimental investigation into the effect of water on the ductile behaviour of quartz rocks. *Geologica Ultraiectina* 95, 178pp.

Den Brok,S.W.J.(1998): Effect of microcracking on pressure solution strain rate: The Gratz grain-boundary model. *Geology* 26 [10], p. 915-918

Den Brok,S.W.J., Zahid,M. and Passchier,C.W.(1998): Cataclastic solution creep of very soluble brittle salt as a rock analog. *Earth Planet. Sci. Lett.* 163, p. 83-95

Den Brok,S.W.J., Zahid,M. and Passchier,C.W.(1999a): Pressure solution compaction of NaClO₃ and implications for pressure solution in NaCl. *Tectonophysics* 307, p. 297-312

Den Brok,S.W.J., Zahid,M. and Passchier,C.W.(1999b): Stress induced grain boundary migration in very soluble brittle salt. *J. Struct. Geol.* 21, p. 147-151

Den Brok,S.W.J. and Melisa,G.(1999): Pressure solution indentation experiments on K-Alum crystals. Abstract volume of the International conference on "Deformation Mechanisms, Rheology and Microstructures" held in Neustadt an der Weinstrasse, Germany, 22-24 March

Den Brok,S.W.J. and Melisa,G.(2000): An experimental example of chemical reaction driven solution transfer creep. Abstract for EGS XXV General Assembly, Nice, France, 25-29 April

Elias,B.P. and Hajash,A.Jr.(1992): Changes in quartz solubility and porosity due to effective stress: an experimental investigation of pressure solution. *Geology* 20, p. 451-454

Elliot,D.(1973): Diffusion flow laws in metamorphic rocks. Bull. Geol. Soc. Am. 84, p. 2645-64

Engelder,T.(1982): A natural example of the simultaneous operation of free-face dissolution and pressure-solution. Geochim. Cosmochim. Acta 46, p. 69-74

Gal,D. and Nur,A.(1998): Elastic strain energy as a control in the evolution of asymmetric pressure-solution contacts. Geology 26(7), p. 663-665

Gal,D., Nur,A. and Aharonov,E.(1998): Stability analysis of a pressure-solution surface. Geophys. Res. Lett. 25(8), p. 1237-1240

Gibbs,J.W.(1878): On the equilibrium of heterogeneous substances. Trans. Conn. Acad. 3, p.343-524 (Reprinted in The Scientific Papers of J. Willard Gibbs, vol.1, Longmans, Green, Toronto, Ont. 1906; reprinted by Dover, Mineola, N.Y., 1961)

Gmelins Handbuch der anorganischen Chemie (1970), 8 Aufl., Systemnr. 21

Weinheim/Bergstr. (sodium chlorate)

Gmelins Handbuch der anorganischen Chemie (1970), 8 Aufl., Systemnr. 22

Weinheim/Bergstr. (KDP)

Gmelins Handbuch der anorganischen Chemie (1970), 8 Aufl., Systemnr. 35

Weinheim/Bergstr. (potassium alum)

Gratier,J.P.(1993): Experimental pressure solution of halite by an indenter technique. Geophys. Res. Lett. 20(15), p. 1647-1650

Gratier,J.P. and Guiguet,R.(1986): Experimental pressure solution-deposition on quartz grains: the crucial effect of the nature of the fluid. J. Struct. Geol. 8, p. 845-856

Gratz,A.J.(1991): Solution-transfer compaction of quartzites: Progress toward a rate law. *Geology* 19, p. 901-904

Grinfel'd,M.A.(1986): Instability of the separation boundary between a non-hydrostatically stressed elastic body and a melt. *Sov. Phys. Dokl.* 31 [10], p. 831-834

Guzzetta,G.(1984): Kinematics of stylolite formation and physics of the pressure-solution process. *Tectonophysics* 101, p. 383-394

Hartman,P.(1987): Modern PBC theory. In *Morphology of crystals*, Terrapub, Tokyo

Haussühl,S.(1961): Kristallographie der Alaune I. *Z. Kristall.*, 116, p. 371-405

Heidug,W.K. and Leroy,Y.M.(1994): Geometrical evolution of stressed and curved solid-fluid phase boundaries. 1. Transformation kinetics. *J. Geophys. Res.* 99(B1), p. 505-515

Heimann,R.B.(1975): *Auflösung von Kristallen*. Springer-Verlag publications

Herring,C.(1951): Some theorems on the free energies of crystal surfaces. *Phys. Rev.* 82(1), p. 87-93

Hickman,S.H. and Evans,B.(1991): Experimental pressure solution in halite: the effect of grain/interphase boundary structure. *J. Geol.Soc.London* 148, p. 549-560

Jaeger, J. C.(1969): *Elasticity, Fracture and Flow*, Chapman and Hall,

London, 268 p.

Kamb,W.B.(1959): Theory of preferred orientation developed by crystallization under stress. *J. Geol.* 67, p. 153-170

Kern,R.(1955): Influence du milieu de croissance sur la correspondance entre morphologie et structure cristalline. Interaction du cristal et du solvant, résultats expérimentaux (II). Bull. soc. franc. miner. cryst. 78, p. 497-520

Kitamura,M., Kouchi,A., Hosoya,S. and Sunagawa,I.(1982): Growth and dissolution of NaClO₃ crystal in aqueous solution. Mineral. J. 11(3), p. 119-137

Lacmann,R. and Tanneberger,U.(1995): Growth rate dispersion of single potassium alum crystals. J. Cryst. Growth 147, p. 194-199

Lehner,F.K. and Bataille,J.(1984): Nonequilibrium thermodynamics of pressure solution. Pure Appl. Geophys. 122, p. 53-85

Lehner,F.K.(1995): A model of intergranular pressure solution in open systems. Tectonophysics 245, p. 153-170

Leroy,Y.M. and Heidug,W.K.(1994): Geometrical evolution of stressed and curved solid-fluid phase boundaries. 2. Stability of cylindrical pores. J. Geophys. Res. 99(B1), p. 517-530

Lipson,H. and Beevers,C.A.(1935): The crystal structure of the alums. Proc.Roy.Soc., A148, p. 664-680

Lipson,H.(1935): The relations between the alum structures. Proc.Roy.Soc., A151, p.347-356

Martin,B., Röller,K. and Stöckhert,B.(1999): Low-stress pressure solution experiments on halite single crystals. Tectonophysics 308, p. 299-310

Nielsen,A.E. and Söhnle,O.(1971): Interfacial tensions electrolyte crystal-aqueous solution from nucleation data. J. Cryst. Growth 11, p. 233-242

Ostapenko,G.T.(1968): Recrystallization of minerals under stress. Geochemistry Intern. 6, p. 183-186

Ostapenko,G.T.(1975): Theories of local and absolute chemicals potential, their experimental testing and application of the phase rule to the systems with nonhydrostatically stressed solid phases. *Geochemistry Intern.*, p. 126-135

Passchier,C.W. and Trouw,R.A.J.(1996): *Microtectonics*, Springer Verlag, Berlin

Paterson,M.S.(1973): Nonhydrostatic thermodynamics and its geological applications. *Rev. Geophys. Space Phys.* 11, p. 355-389

Raj,R.(1982): Creep in polycrystalline aggregates by matter transport through a liquid phase. *J. Geophys. Res.* 87(B6), p. 4731-4739

Raj,R. and Chyung,C.K.(1981): Solution precipitation creep in glass ceramics. *Acta Metall.* 29, p. 159-166

Riecke,E.(1912): Zur Erniedrigung des Schmelzpunktes durch einseitigen Zug oder Druck, *Zentralbl. Mineral. Geol. Palaeontol.* Teil 3, p. 97-104

Ristic,R.I., Sherwood,J.N. and Shripathi,T.(1997b): The influence of tensile strain on the growth of crystals of potash alum and sodium nitrate. *J. cryst. growth* 179, p. 194-204

Ristic,R.I., Shekunov,B. and Sherwood,J.N.(1996): Long and short period growth rate variations in potash alum crystals. *J. Cryst. Growth* 160, p. 330-336

Ristic,R.I., Shekunov,B.Y. and Sherwood,J.N.(1997a): The influence of synchrotron radiation-induced strain on the growth and dissolution of brittle and ductile materials. *J. cryst. growth* 179, p. 205-212

Ristic,R.I., Sherwood,J.N. and Wojciechowski,K.(1993): Morphology and growth kinetics of large sodium chlorate crystals grown in the presence and absence of sodium dithionate impurity. *J. Phys. Chem.* 97(41), p. 10774-10782

Robin,P.Y.F.(1978): Pressure solution at grain to grain contacts. *Geochim. Cosmochim. Acta* 42[9], p. 1383-1398

Russel,G.A.(1935): Crystal growth and solution under local stress. *Amer.Mineral.*, 20, p. 733-737

Rutter,E.H.(1976): The kinetics of rock deformation by pressure solution. *Phil. Trans. R. Soc. London A283*, p. 203-219

Rutter,E.H.(1983): Pressure solution in Nature, theory and experiment. *J. Geol. Soc. London* 140, p. 725-740

Rutter,E.H. and Wanten,P.H. (2000): Experimental study of the compaction of phyllosilicate-bearing sand at elevated temperature and with controlled pore water pressure. *J. Sedim. Res. A* 70 [1], p. 107-116

Schubnikow,A. and Brunowsky,B.(1931): Über die Natur der Vizinalflächen des Oktaeders des Aluminiumalauns: *Z. Kristall. Mineral.* 77, p. 337-352

Schutjens,P.M.T.M.(1991): Experimental compaction of quartz sand at low effective stress and temperature conditions. *J. Geol. Soc. London* 148, p. 527-539

Schwarz,S. and Stöckhert,B.(1996): Pressure solution in siliclastic HP-LT metamorphic rocks-constraints on the state of the stress in deep levels of accretionary complexes. *Tectonophysics* 255, p. 203-209

Shimizu,I.(1995): Kinetics of pressure solution creep in quartz: theoretical considerations. *Tectonophysics* 245, p. 121-134

Sorby,J.C.(1863): Über Kalkstein-Geschiebe mit Eindrucken. *Neues Jahrb. Mineral. Geol. Palaeontol.*, p. 801-807

Spiers,C.J., Urai,J.L., Lister,G.S., Boland,J.N. and Zwart,H.J.(1986): The influence of fluid-rock interaction on the rheology of salt rock. EUR 10399 EN, Office for Official Publications of the European Communities, Luxembourg

Spiers,C.J. and Schutjens,P.M.T.M.(1990): Densification of crystalline aggregates by fluid-phase diffusional creep. In: D.J. Barber and P.G. Meredith (Editors), Deformation processes in minerals, ceramics and rocks. Unwin Hyman, London, Chapter 12, p. 334-353

Spiers,C.J. and Brzesowsky,R.H.(1993): Densification behaviour of wet granular salt: theory versus experiment. Seventh symposium on salt 1, p. 83-92

Sprunt,E.S. and Nur,A.(1977a): Destruction of porosity through pressure solution. Geophysics 42, p. 726-741

Sprunt,E.S. and Nur,A.(1977b): Experimental study of the effects of stress on solution rate. J. Geophys. Res. 82(20), p. 3013-3022

Srolovitz,D.J.(1989): On the stability of surfaces of stressed solids. Acta Metall. 37, p. 621-625

Szurgot,M.(1995): Chiral etch pits on sodium chlorate crystals. Cryst. Res. Technol. 30, p. 621-628

Tada,R. and Siever,R.(1986): Experimental knife-edge pressure solution of halite. Geochim. Cosmochim. Acta 50, p. 29-36

Tada,R. and Siever,R.(1989): Pressure solution during diagenesis. Ann. Rev. of Earth and Planet. Sci. 17, p. 89-118

Thompson,J.(1862): On crystallization and liquefaction, as influenced by stresses tending to change of form in the crystals. Proc. Roy. Soc. London 11, p. 473-481

Timoshenko,S.P.(1949): Strength of materials PartII. Advanced theory and problems. 2nd ed., D. van Nostrand Company, inc., p. 319-320 (pp.510)

Timoshenko,S.P. and Goodier,J.N.(1970): Theory of elasticity. 3rd ed., McGraw-Hill, New York

Ullmann's encyclopedia of industrial chemistry (1985), 5th edition, Vol. A1

Urai,J.L., Spiers,C.J., Zwart,H.J. and Lister, G.S.(1986): Weakening of rock salt by water during long-term creep. Nature 324, p. 554-557

Van der Hoek,B., van Enckevort,W.J.P. and van der Linden,W.H.(1983): Dissolution kinetics and etch pit studies of potassium aluminium sulphate. J. Cryst. Growth 61, p. 181-193

Viswanathan,R.(1966): Elastic constants of sodium chlorate single crystals by pulse-echo method. J. Appl. Phys. 37, p. 884-888

Weyl,P.K.(1959): Pressure solution and the force of crystallisation. A phenomenological theory. J. Geophys. Res. 64, p. 2001-2025

Wilke,K.Th.(1988): Kristall Züchtung. New edition by Bohm,J. Verlag Harri Deutsch publications, Frankfurt/Main

Yang, W.H. and Srolovitz,D.J.(1994): Surface morphology evolution in stressed solids: surface diffusion controlled crack initiation. J. Mech. Phys. Solids 42, p. 1551-1574

Yu,H.H. and Suo,Z.(2000): Stress-dependent surface reactions and implications for a stress measurement technique. J. Appl. Phys. 87[3], p. 1211-1218

Appendix 1.

Detailed drawings of the cylindrical vessel used in the experiments. The scale of all the drawings is 1:2.

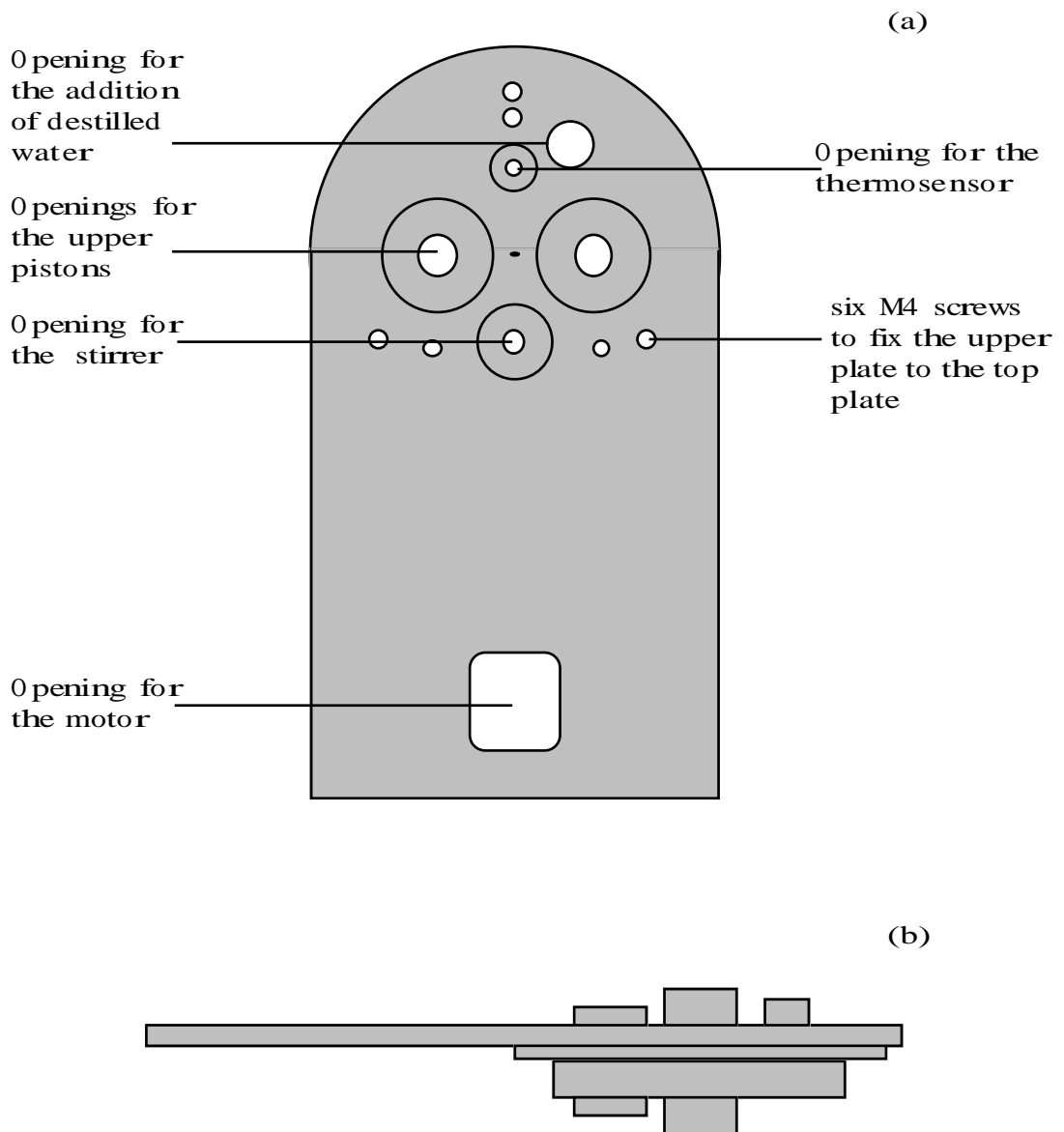
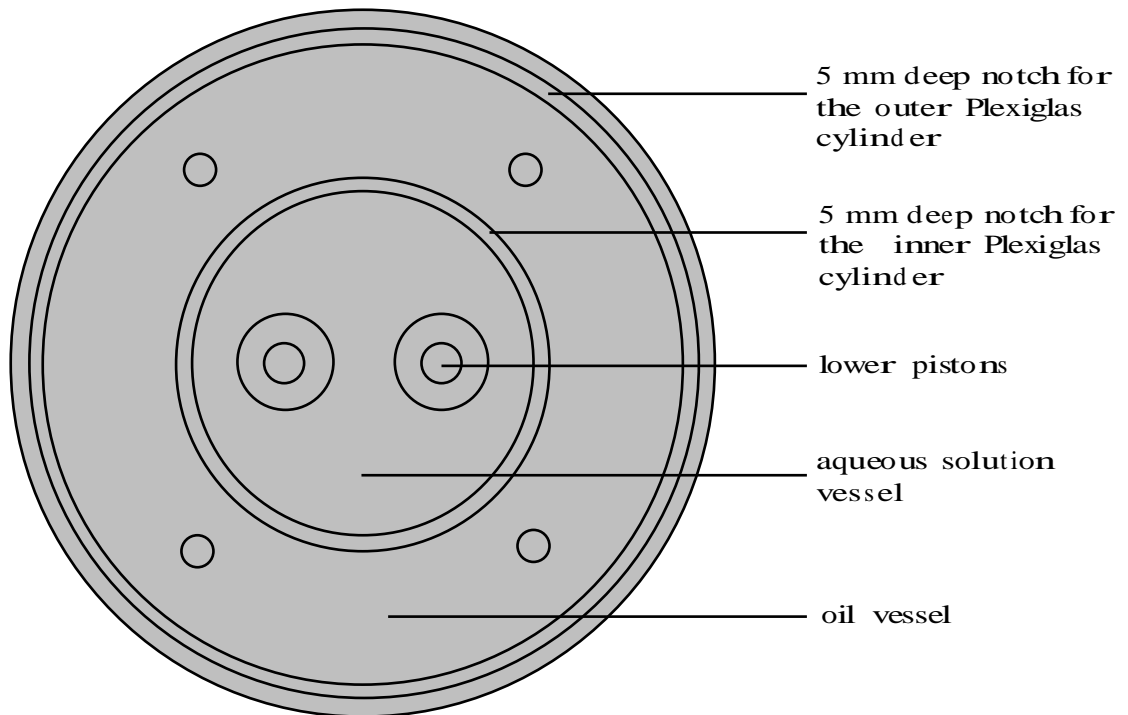


Fig. A1.1 Front view (a) and side view (b) of the upper plate closing the cylindrical vessel.

(a)



(b)

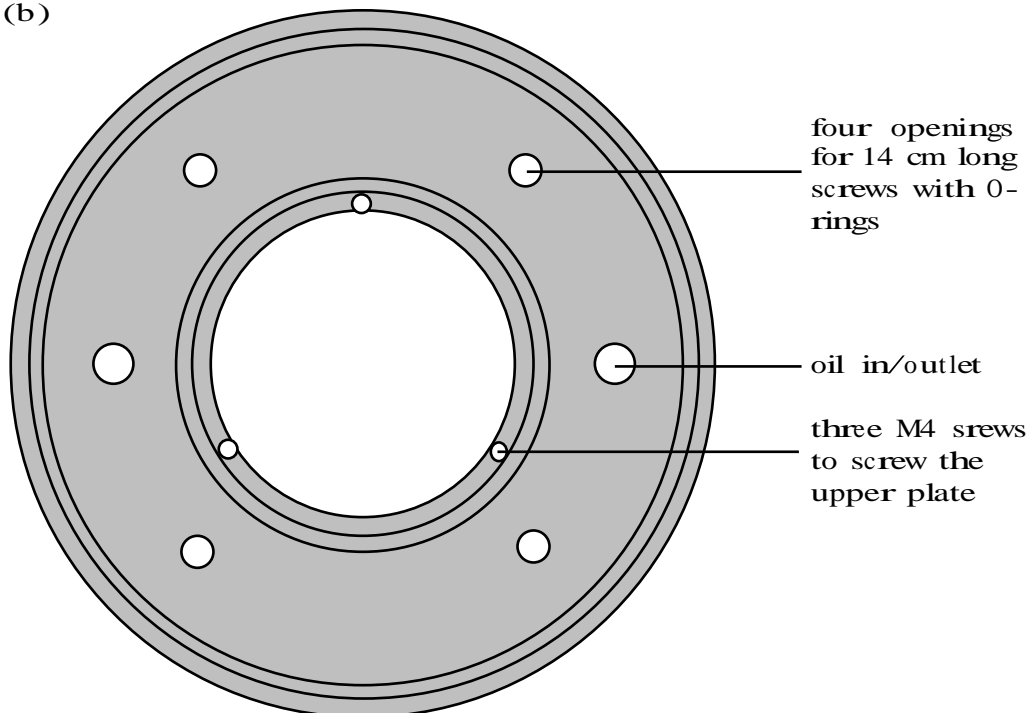


Fig. A1.2 Bottom(a) and top (b) plates of the cylindrical vessel. The Plexiglas cylinders were 12 cm high.

Lebenslauf

Name: Jacques MOREL

Wohnort: 129, route de la Pointe de Moustierlin

F-29170 Fouesnant, Frankreich

Staatsangehörigkeit: französisch

21/09/74 geboren in Quimper, département Finistère, Frankreich

06/1991 Baccalauréat C (Mathématiques et Physique), Quimper

06/1993 DEUG A (Mathématiques, Physiques et Informatiques) option
physique, Université de Bretagne Occidentale, Brest, Frankreich

06/1994 Licence de physique, Université de Bretagne Occidentale, Brest,
Frankreich

06/1995 Maîtrise de physique, Université de Bretagne Occidentale, Brest,
Frankreich

06/1996 DEA Physique et Chimie de la Terre, EOPG Strasbourg, Frankreich

11/1996-11/2000 Doktorarbeit in Geologie, Institut für Geowissenschaften, Johannes
Gutenberg-Universität Mainz, Deutschland

